A two-dimensional finite element analysis of a ceramic dental implant placed in a canine mandible

by

Cathleen Jeanne McMahon

A Thesis Submitted to the

Graduate Faculty in Partial Fulfillment of the

Requirements for the Degree of

MASTER OF SCIENCE

Interdepartmental Program: Biomedical Engineering
Major: Biomedical Engineering

Iowa State University
Ames, Iowa

1994

This work is dedicated to my husband,

Bernard Gerard McMahon,

with much love, gratitude and appreciation

TABLE OF CONTENTS

INTRODUCTION

Approximately 125 million people in the United States are missing some of their teeth; nearly 42% of those over age sixty-five are totally edentulous (Schnitman, 1993). Efforts to replace missing teeth typically involve the use of full or partial dentures. Dentures, however, are known to cause a continuous resorption of the underlying bone while restoring only 25% of the patient's normal masticatory function (Niznick, 1985). The use of dental implants has been investigated for many years as a potentially superior method of tooth replacement which can dramatically improve the patient's oral health and quality of life. The development of the Branemark implant system in the late 1960's, with its extensive documentation and 10 to 15 year implant lifetimes, moved dental implantology into the realm of standard dental practice (Branemark, 1977; Zarb, 1983; Branemark et al., 1985). The use of dental implants increased 73% between 1986 and 1990 with 435,685 implants placed in 1990 (Stillman and Douglass, 1993).

Dental implants are intended for permanent use. According to Albrekttson and Sennerby (1991), however, many popular implant systems are not sufficiently reliable over a five year period. Implant failure, which typically involves the loss of prosthesis function and associated pain at the implant site, is usually caused by severe bone resorption surrounding the implant surfaces (Ko et al., 1992). Dental implants are predominantly manufactured from titanium-based alloys, but it is generally held that the use of a bioactive ceramic material could improve implant longevity (Marquis, 1993). This is primarily because bioactive ceramics are composed of calcium and phosphate which are the major constituents of bone. They are not only much more biocompatible than metals; they also form a chemical bond with bone and seem to induce quicker bone healing (Yukna, 1991). Calcium phosphate bioceramics, however, are inherently weak in tension and tend to degrade *in vivo* which further weakens them (Ducheyne and McGuckin, Jr., 1990).

Dr. Thomas McGee at Iowa State University has developed a composite material termed osteoceramic, which combines a calcium phosphate bioactive ceramic with an inert ceramic, magnesium alumina spinel. Osteoceramic is extremely biocompatible, forms a chemical bond with the surrounding bone, and its strength does not degrade *in vivo* (Tweden, 1987). While the osteoceramic is stronger in tension than either of its components, it is questionable whether its tensile strength (σ_t ~ 70 MPa) is adequate for use as a dental implant.

This study uses finite element analysis (FEA) of a two-dimensional (2-D), plane strain finite element model (FEM) to determine the stresses and strains in an osteoceramic dental implant and its surrounding bone. The finite element method is a computerized numerical technique of stress analysis which has been used in dental research since the early 1970's (Farah et al., 1973). Finite element analysis has been used with two-dimensional (2-D), axisymmetric, and three-dimensional (3-D) finite element models to determine the stresses and strains in natural teeth, dental implants and their surrounding bone (Craig, 1986).

In a previous study (Niederauer, 1990), osteoceramic composite dental implants were placed in the premolar region of 10 dogs. In this study, a 2-D finite element model (FEM) was created from a scanned image of the central slice of one of the implants retrieved by Niederauer (1990). Numerous finite element analyses were performed throughout this study based upon this original FEM, as well as variations of this model.

Specifically, this study was composed of three separate investigations. The objective of investigation #1 was to estimate the magnitude and location of the maximum tensile stresses that an osteoceramic dental implant might experience in response to typical physiological loads. Investigation #2 explored the effects of three simple design modifications upon the stresses and strains in the implant and the surrounding bone in comparison to the osteoceramic dental implant design that was used in the previous study (Niederauer, 1990). The objective of investigation #3 was to determine the effect of cancellous bone modeling upon finite element analysis results. All finite element analyses of dental implants model the cancellous bone surrounding the implant as if it were a homogeneous material, but it is actually inhomogenous (Brunski, 1992). Three cancellous bone models were created, and finite element analysis results from each model were evaluated and compared to one another.

LITERATURE REVIEW

The literature review begins with an in-depth presentation of the physical and mechanical properties of bone. The composition, organization, material and strength properties of bone and how it adapts to mechanical loading and in the presence of a dental implant will be presented. The second portion of the literature review pertains to the subject of dental implants. This section begins with a review of the anatomy and biomechanics of a natural tooth and is followed by an overview of the general principles associated with the design of dental implants. The types of implants currently used, the success rates, and the factors that contribute to the fate of endosseous dental implants are then discussed. The last portion of the literature review is concerned with the method of analysis used in this study to determine the stresses and strains in a dental implant and surrounding bone. Finite element analysis theory is presented and is followed by a description of the finite element process. Current practices and assumptions made in the creation of finite element models are then discussed in addition to some of the results obtained in previous studies associated with finite element analyses of dental implants.

Bone

A dental implant can perform the normal chewing, grinding and stress transfer functions of a missing tooth only if it is firmly fixed within the bone of the mandible or maxilla. Initially, the success of a dental implant depends on how the bone responds to both the surgical implantation procedure and the artificial implant material. Assuming that this response is positive, the bone and implant will become either mechanically or chemically bonded to form an interface that is strong enough to withstand physiological loading. Bone adjacent to the implant, however, must not be subjected to stresses or strains that are too large (Imamura et al., 1990) or too small (Smith et al., 1976; Goodship et al., 1979; Lanyon et al., 1982; Rubin and Lanyon, 1985; Meade, 1989; Jee and Li, 1990) because the bone will "dissolve" or resorb in response and disrupt the interfacial bond. Due to the importance of bone in determining the fate of a dental implant, this section of the literature review presents an extensive overview of bone including its composition, organization, mechanical properties, and adaptation characteristics.

Bone composition

Bone is a highly ordered, living, connective tissue. It is composed of specialized cells embedded within an extracellular matrix. The three cell types unique to bone tissue, which make up approximately 2% of its total weight, are osteoblasts, osteocytes and osteoclasts. Osteoblasts, which tend to be organized as a continuous layer of cells lining the bone tissue, synthesize the organic portion of the bone matrix and store the inorganic materials used in mineralization (van Mullem and Maltha, 1984). Osteocytes are osteoblasts that have become encased in their own mineralized secretions. Osteocytes have cellular processes which extend to, and are in contact with, other bone cells via channels called cannaliculi. The osteocytes coordinate the maintenance of the bone matrix, synthesize organic materials at a much slower rate than osteoblasts, and are also capable of removing matrix to maintain blood calcium levels (Banks, 1986). Osteoclasts are multinucleated giant cells which dissolve bone mineral and digest organic matrix. They are continually active, motile cells, which are found in areas where bone resorption takes place (van Mullem and Maltha, 1983).

Extracellular bone matrix is a viscous, gel-like substance containing water and various organic and inorganic constituents which account for approximately 10%, 30%, and 60% of the total bone weight, respectively (van Mullem and Maltha, 1983). Factors such as age, species, health, bone type and configuration, however, all influence the exact compositions of these components (Banks, 1986). Collagen, which is a strong but flexible structural protein, comprises approximately 90% of the organic matrix. The remaining 10% is an amorphous ground substance containing water, polysaccharide/protein complexes and numerous organic factors related to cell and matrix maturation and matrix mineralization (Roberts et al., 1987). The inorganic or mineral phase of bone consists primarily of hydroxyapatite crystal, $Ca_5(PO_4)_3OH$, which organizes along collagen fibrils during mineralization. Initial mineralization involves about one half of the mineral-holding capacity of bone, and 100% mineralization may be achieved within one year (Banks, 1986).

Bone organization

The primary constituents of bone tissue, as described above, may be combined in two different ways to form two types of osseous tissue. The first type is called woven, immature or primary bone, while the second tissue type is referred to as lamellar bone. These tissues can be further categorized according to their morphological configurations as cortical or cancellous bone.

Tissue types

Woven bone Woven bone is characterized by rapid growth (30-50 μm/day), high cellularity, low mineral content, random collagen fiber orientation and minimal strength (Roberts et al., 1987). Woven bone is usually a temporary tissue that exists primarily in fetal bone and at repair and pathological sites in adult bone (Bourne, 1956). Some woven bone persists in the adult skeleton in areas such as tooth sockets and near cranial sutures and sites of tendon and ligament attachments (Junqueira and Carneiro, 1983). An important feature of woven bone is that, unlike lamellar bone, it can form *de novo* which means that it doesn't require any pre-existing osseous or cartilaginous surface. Primary bone offers mechanical support during development and repair until it is slowly replaced by lamellar or mature bone.

Lamellar bone The second type of osseous tissue produced by bone cells, which is predominant in the adult skeleton, is called lamellar or mature bone. Lamellar bone is a secondary or replacement tissue that is densely mineralized and highly organized. It forms slowly (~6 μm/day) on pre-existing bony or cartilaginous surfaces (Roberts et al., 1987). Collagen and its associated minerals are organized in sheets or lamellae that are approximately 3-7 μm in width (Junqueira,1983). Lacunas containing osteocytes are distributed in an ordered manner between, and sometimes within, these lamellae. Collagen fibrils tend to lie within the plane of each lamellae in a generalized preferred direction that varies from 0 to 90 degrees between successive lamellae. A ring of interlamellar bone about .1 μm thick, which has a high mineral content and little collagen, is thought to separate adjacent lamellae (Currey, 1984). Lamellar bone is much stronger than woven bone.

Morphological configurations The next level of organization describes the arrangement of osseous tissue into two distinct morphological configurations. These configurations, illustrated in Figure 1, are referred to as cancellous (spongy or trabecular) bone, and compact or cortical bone. They are macroscopic in nature and are classified according to the degree of porosity present within the bone tissue (Banks, 1986).

Cortical bone Cortical bone is dense and contains pores which are not visible to the naked eye. These pores contain osteocytes, osteocytic processes, capillaries and resorption sites (Currey, 1984). Compact bone forms the outer shell of all bones and is usually composed of lamellar bone that is arranged into concentric, interstitial or circumferential lamellar patterns (Bourne, 1956). Concentrically arranged lamellae form primary or

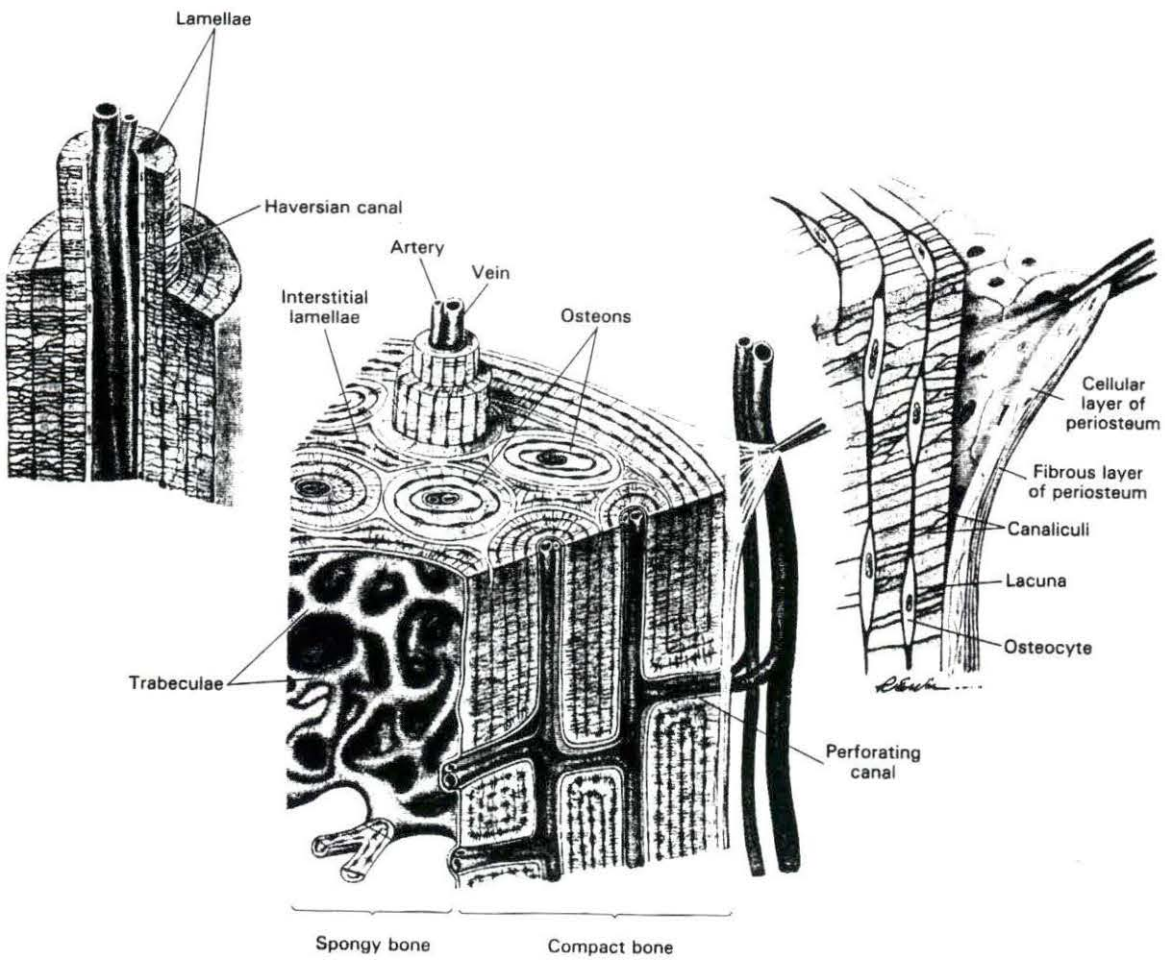

Figure 1. Morphological configurations of bone tissue (Martini, 1989)

secondary osteons (Haversian systems) that are approximately 200 μm in diameter and 1 to 2 cm long (Cowin, 1991). Primary osteons form at the periosteal surfaces as small cylinders containing just a few lamellae that surround an osteonal canal which contains blood vessels, vasomotor nerves and endosteal cells. Secondary osteons may be formed around any pre-existing vascularized tunnel such as the osteonal canal of a primary osteon (Banks, 1986). This tunnel is expanded by osteoclastic erosion until the cavity approaches a diameter of approximately 100 μm. The walls of the cavity are then made smooth, and bone is deposited on the internal surface in concentric lamellae (Currey, 1984). Unlike primary osteons, secondary osteons contain cement lines that are 1 to 5 μm thick and separate the osteon from the rest of the matrix. Cement lines are indicative of the point where resorption stops and osteoblast bone formation begins (Martin and Burr, 1989). The existence of these cement lines, coupled with the fact that secondary osteons have larger vascular channels than primary osteons, indicates that secondary osteons may be mechanically weaker than primary osteons (Currey, 1984; Martin and Burr, 1989). Secondary osteons are continually destroyed (resorbed) and rebuilt during growth and the normal maintenance of adult bone (Junqueira, 1983). Interstitial lamellae are located in the angular spaces that occur between osteons and usually consist of remnants of old, eroded Haversian systems (Bourne, 1956). Circumferential lamellae occur at the free surfaces of compact bone where Haversian systems give way to lamellae that conform to the surfaces of the bone. Figure 2 illustrates all three lamellar patterns.

Cancellous bone Cancellous bone is a highly porous material with pores that are visible to the naked eye. Adult cancellous bone material is usually composed of primary lamellar bone or secondary osteon bone fragments that are arranged in a three dimensional lattice (Currey, 1984). This lattice is composed of spicules or trabeculae that are actually avascular plates and/or rods of bone material (Banks, 1986). The spicules are short and often supported by transverse struts so that the risk of buckling is minimized (Currey, 1984). Trabeculae are efficient in resisting compression, and they tend to allign themselves along lines of stress (Banks, 1986). Spongy bone is usually contained within cortical bone shells, and the struts transfer stress from one part of the cortical shell to another.

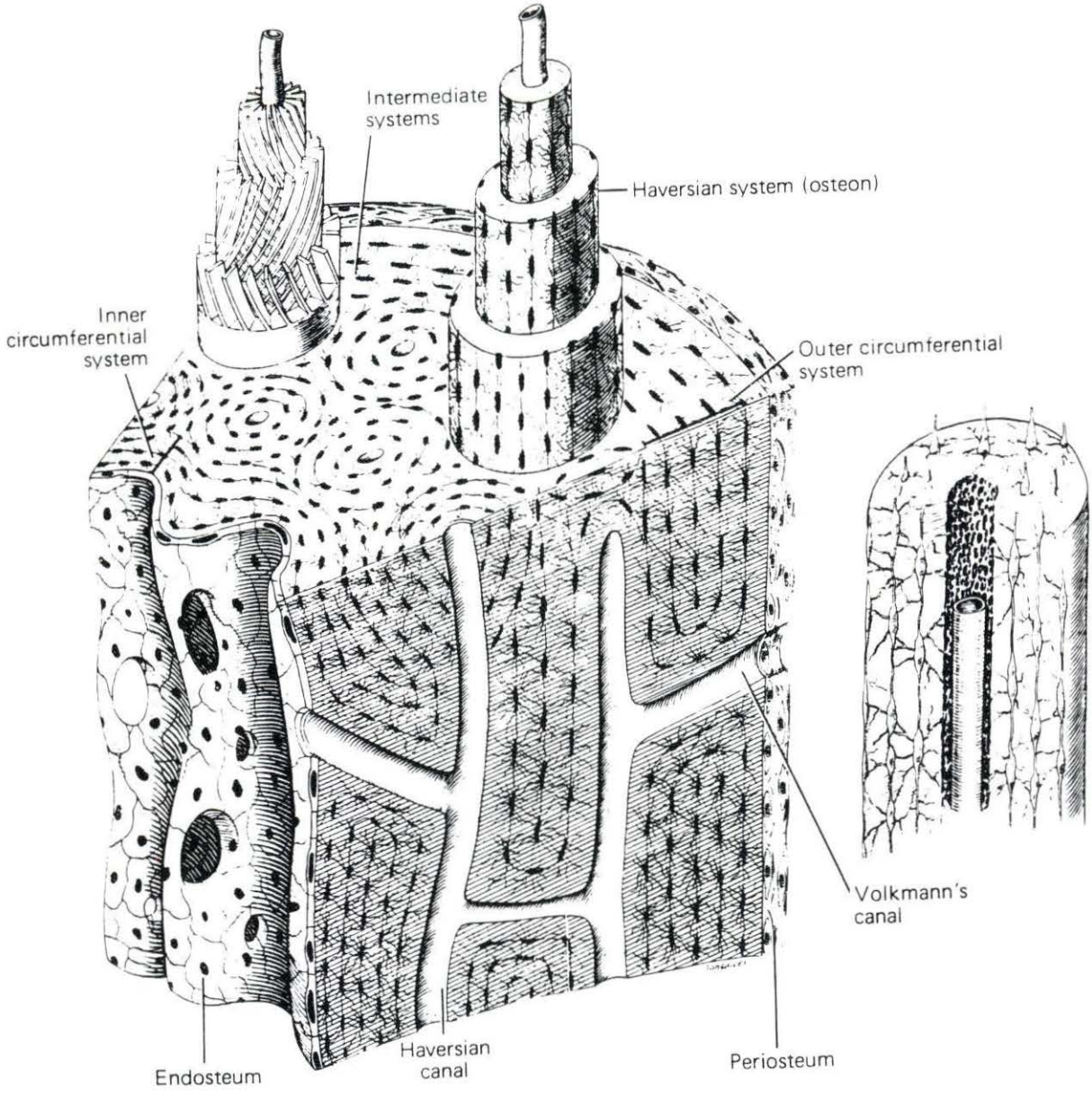

Figure 2. Typical section of compact bone from a diaphysis (Junqueira and Carneiro, 1983)

Mechanical properties of cortical bone

Materials that have elastic properties which do not vary with respect to direction are classified, in terms of their symmetry, as isotropic. They are fully characterized by the determination of only two independent quantities, such as the modulus of elasticity (E) and Poisson's ratio (ν). The modulus of elasticity is defined as the slope of the linear portion of a curve in which the stress (σ) applied to a test specimen is plotted versus the strain (ε) experienced in response. Strain, which is usually measured in microstrain (i.e., 10^{-6} mm/mm), is defined as the fractional change in dimension experienced by a loaded structure. The larger the modulus of elasticity is, the stiffer the response of the material to an applied load. Poisson's ratio is the ratio of the strain perpendicular to the direction of loading to the strain parallel to the loading direction.

Since the elastic properties of bone tissue vary with direction, bone is not isotropic, but rather, it is classified as an anisotropic, nonhomgeneous, slightly nonlinear, viscoelastic material (Cowin et al., 1987). Most studies that analyze the stress and strain properties of bone make the assumption that it is linearly elastic with the constitutive equation

$$\mathbf{T}_{ij} = \mathbf{C}_{ijkl}\mathbf{E}_{kl} \qquad (1)$$

where:

$\mathbf{T}_{ij}$ = stress tensor,

$\mathbf{E}_{kl}$= infinitesimal strain tensor,

$\mathbf{C}_{ijkl}$ = elasticity tensor.

The assumption of linear elasticity is thought to be valid because physiologic loads tend to fall within the range where bone behaves very similarly to a typical, linear elastic material (Currey, 1984). Table 1 shows an equivalent, single-index notation that is often used to describe an equivalent, but more manageable, constitutive equation

$$\mathbf{s}_i = \mathbf{C}_{ij}\mathbf{e}_j \qquad (2)$$

where $\mathbf{C}_{ij}$ is known as the stiffness matrix.

Table 1. Equivalent notations for stress and strain (Cowin, Van Buskirk and Ashman, 1987)

Stresses	Strains
$s_1=T_{11}$	$e_1 = E_{11}$
$s_2 = T_{22}$	$e_2 = E_{22}$
$s_3 = T_{33}$	$e_3 = E_{33}$
$s_4 = T_{23} = T_{32}$	$e_4 = 2E_{33} = 2E_{32}$
$s_5 = T_{13} = T_{31}$	$e_5 = 2E_{13} = 2E_{31}$
$s_6 = T_{12} = T_{21}$	$e_6 = 2E_{12} = 2E_{21}$

Material symmetry The most general type of symmetry that has been assigned to bone tissue is that of orthotropy in which the material and mechanical properties vary in each of three mutually perpendicular directions. Katz and coworkers (Yoon and Katz, 1976, 1979; Katz, 1980) suggest that cortical lamellar bone is orthotropic, but that cortical Haversian bone has a greater degree of symmetry, that of transverse isotropy, due to its osteonal microstucture. Ashman et al. (1984) have done extensive work using ultrasonic testing to determine the elastic constants of both cortical and trabecular bone. They consider all cortical bone to be orthotropic because they feel that it is often difficult to differentiate between lamellar and Haversian bone or some combination of the two. They also assert that it is fairly rare to find bone that exhibits the hexagonal close packing that is necessary to exhibit transversely isotropic behavior. If bone is assumed to be orthotropic, then the

following represents the stiffness matrix:

$$[c_{ij}] = \begin{vmatrix} c_{11} & c_{12} & c_{13} & 0 & 0 & 0 \\ c_{12} & c_{22} & c_{23} & 0 & 0 & 0 \\ c_{13} & c_{23} & c_{33} & 0 & 0 & 0 \\ 0 & 0 & 0 & c_{44} & 0 & 0 \\ 0 & 0 & 0 & 0 & c_{55} & 0 \\ 0 & 0 & 0 & 0 & 0 & c_{66} \end{vmatrix} \qquad (3)$$

Of the twelve non-zero components, only nine are independent.

Many researchers assume the symmetry of cortical bone to be transversely isotropic (Lang, 1970; Reilly and Burstein, 1975; Yoon and Katz, 1976). A transversely isotropic material has similar elastic properties in two directions which are significantly different from those in the third orthogonal direction. The plane of isotropy is taken to be the transverse or y-z plane in long bone. This is generally perpendicular to the long or x axis of the osteons (Figure 3). The unique direction is along the x or longitudinal axis of the bone. According to Reilly et al. (1974), in each type of cortical bone architecture, the principle direction of the osteons is along the bone axis so that the stiffness is always greatest in the longitudinal direction while the elastic properties in the transverse or y-z plane are fairly isotropic and very different from those in the longitudinal plane (Keaveny and Hayes, 1993). Reilly et al. (1974) also reported that the elastic properties of cortical bone were similar for both tension and compression. A transversely isotropic material has 12 non-zero components, of which only five are independent, since $C_{11} = C_{22}$, $C_{13} = C_{23}$, $C_{44} = C_{55}$ and $C_{66} = 1/2(C_{11}-C_{12})$.

Technical constants The stiffness coefficients of cortical bone as described above are directly proportional to the technical constants, E, G, and ν. The magnitude of one of these technical constants, the modulus of elasticity, E, depends upon the precise nature of the bone and its microstructure and normally ranges from 7-30 GPa for the longitudinal orientation (E_3) of mature compact bone in the wet condition (Bonfield and Grynpas, 1977). Table 3 lists the technical constants for human and canine bone as determined by various researchers.

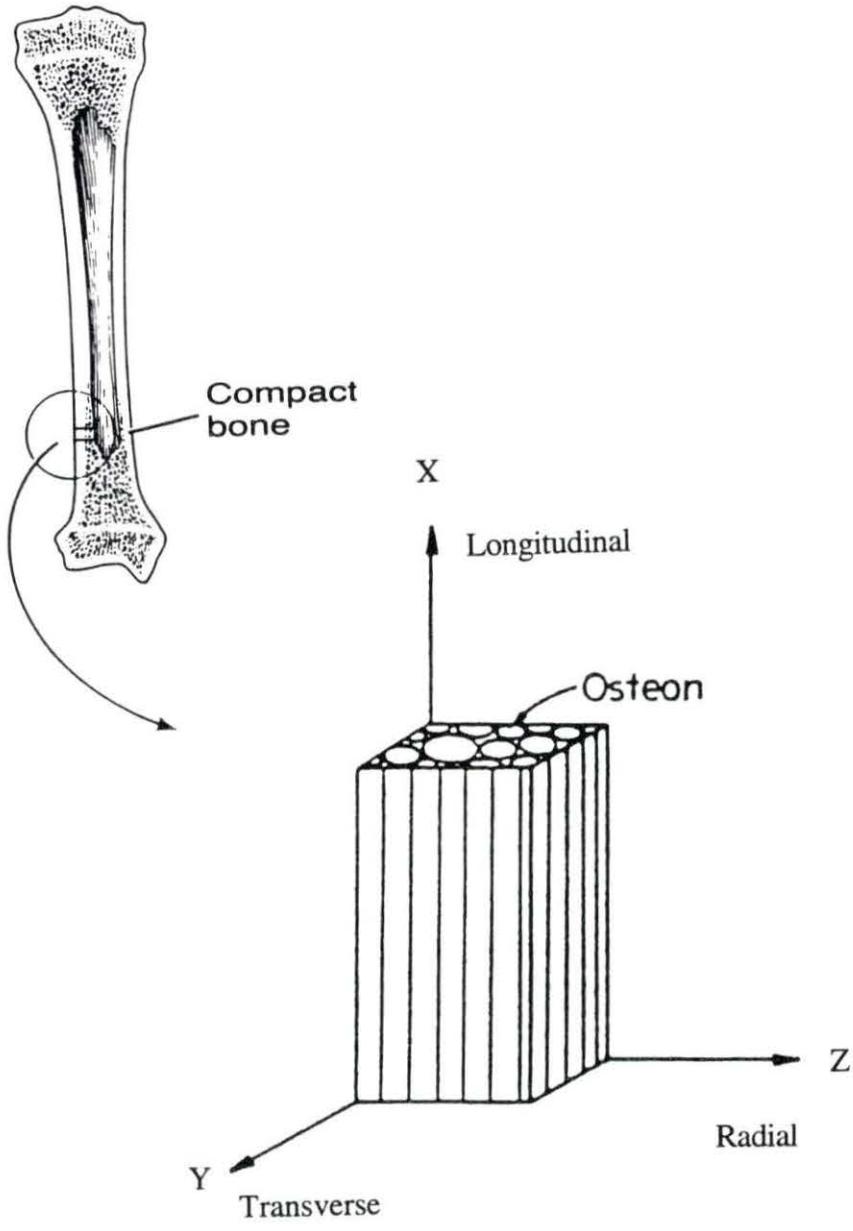

Figure 3. Typical long bone configuration which shows the orientation of the osteons relative to the long or x axis of the whole bone

Table 2. Technical constants for human and canine bone

Group	**Reilly and Burstein (1975)**	**Knets et al. (1977)**	**Ashman et al. (1984)**	**Ashman et al. (1984)**	**Ashman and van Buskirk (1987)**	**Ashman et al. (1985)**
Bone	Femur	Tibia	Femur	Femur	Mandible	Mandible
Species	Human	Human	Human	Canine	Human	Canine
E_1[a] (GPa)	11.5	6.91	12.0	12.8	10.8	7.39
E_2 (GPa)	11.5	8.51	13.4	15.6	13.3	7.39
E_3 (GPa)	17.0	18.4	20.0	20.1	19.4	7.39
G_{12} (GPa)	3.6	2.41	4.53	4.68	3.81	2.63
G_{13} (GPa)	3.3	3.56	5.61	5.68	4.12	2.63
G_{23} (GPa)	3.6	4.91	6.23	6.67	4.63	2.63
ν_{12}	0.58	0.49	0.376	0.282	0.309	0.403
ν_{13}	0.31	0.12	0.222	0.289	0.249	0.403
ν_{23}	0.31	0.14	0.235	0.265	0.224	0.403
ν_{21}	0.58	0.62	0.422	0.366	0.381	0.403
ν_{31}	0.46	0.32	0.371	0.454	0.445	0.403
ν_{32}	0.46	0.31	0.350	0.341	0.328	0.403

[a] The 1-direction is radial (Z), the 2-direction is transverse (Y), and the 3-direction is axial (X).

Stress-strain curve The elastic properties of bone are often determined by mechanical testing. A load is applied to bone either perpendicular to (transverse plane) or parallel to (longitudinal plane) the long axis of a bone of a known cross-sectional area. The deformation of the bone is measured and the stress applied to the bone (force/area) is plotted versus the resultant strain. Stress-strain curves yield some very important information regarding the mechanical performance of the material of interest in the plane of the applied load. Figure 4 shows two typical stress-strain curves for human cortical bone subjected to uniaxial, monotonic, tensile and compressive mechanical testing in the longitudinal plane.

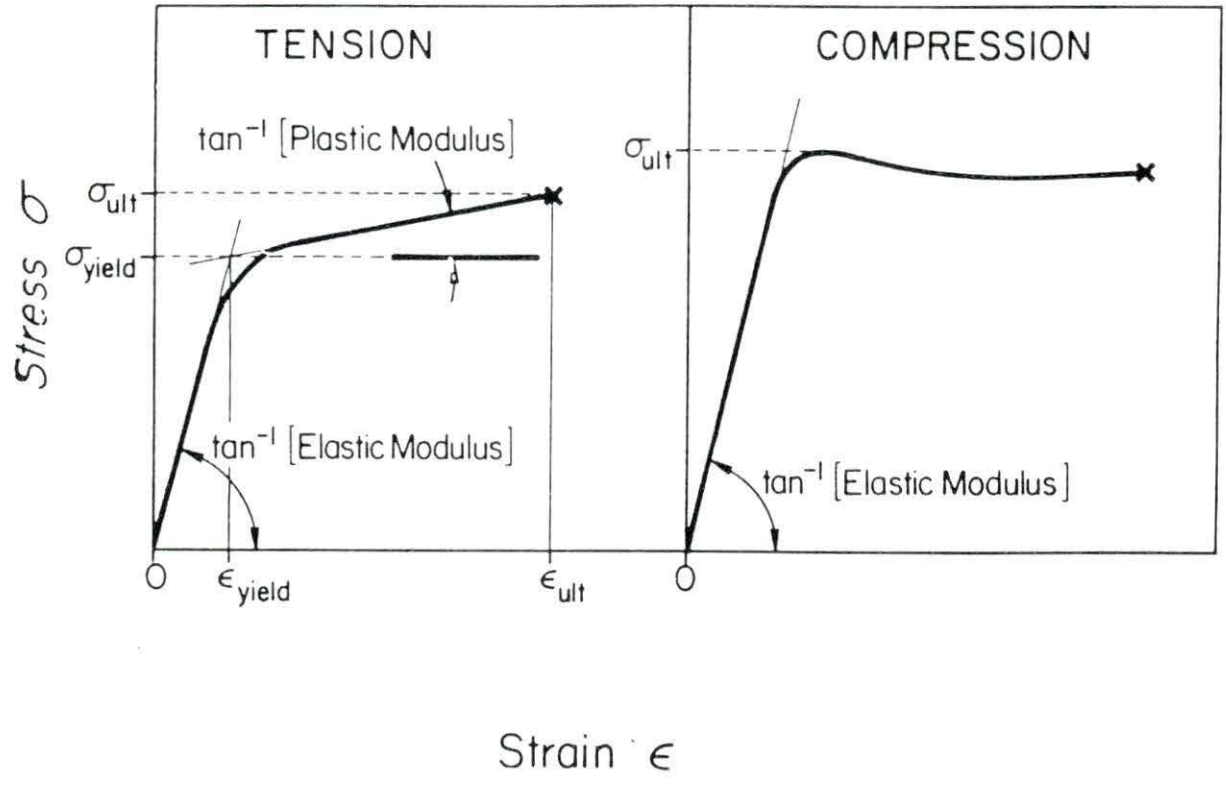

Figure 4. Stylized stress-strain curves for human cortical bone specimens tested in tension and compression (Carter and Spengler, 1978)

Each of the curves in Figure 4 has an initial elastic region that is nearly linear, and its slope determines the modulus of elasticity in the plane of the applied load. The point where the curve deviates from a straight line indicates the yield point of the material in question. Since a material such as bone does not exhibit an abrupt deviation from the straight line portion of the curve, the yield stress and strain are defined as the point where a line drawn parallel to, and 0.2% offset from, the straight line portion of the curve intersects the curve itself. The portion of each curve between the yield point and the ultimate failure point (point x) represents nonelastic or plastic deformation that "reflects diffuse, irreversible microdamage introduced throughout the bone structure" (Carter and Wright, 1986). The curves in Figure 5 illustrate that cortical bone is stronger in compression and in the longitudinal direction. Note that during both compression and tensile testing, yield strengths are approximately equal to their respective ultimate strengths. This means that if a bone is loaded close to its yield point that it is close to fracture and will undergo a relatively large deformation just before fracture (Keaveny and Hayes, 1993a).

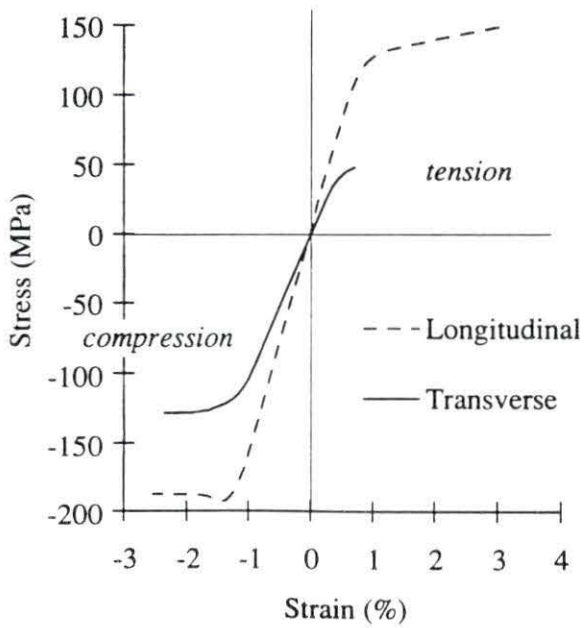

Figure 5. Stress-strain plots for human cortical bone for tensile and compressive loading in both the longitudinal and transverse loading directions (Gibson and Ashby, 1988)

Cortical bone can act in a relatively ductile or brittle fashion depending on the loading direction and whether tension or compression is applied. The total energy per unit volume absorbed by a material upon loading is equal to the total area under the stress-strain curve. For both compressive and tensile loading in the long direction, cortical bone is a tough or ductile material since it can absorb substantial energy before fracture occurs. Also, bone is tougher under compression than tension. Thus bone has a lower resistance to loading that causes tensile stresses in the transverse plane (Keaveny and Hayes, 1993a). For transverse loading, bone is also tougher in compression than in tension. In tension it acts as a relatively brittle material.

Reilly and Burstein (1975) studied the relative contributions of collagen and mineral to the elastic properties of bovine Haversian cortical bone and suggested that the mineral contributes the major proportion of the tensile strength, but the magnitude of the plastic modulus is due to the properties of collagen which also contributes slightly to the tensile strength of bone. They also found that the degree of mineralization has a strong influence on the strength and modulus, but it has little influence on the yield strain. This seems to confirm the belief of Currey (1970) that tissue yield strain might be the most valuable quantity in determining bone tissue yielding.

Strength The uniaxial strength of cortical bone depends upon both the direction of loading and whether the loading is tensile, compressive, or torsional (Cezayirlioglu et al., 1985; Pope and Outwater, 1974; Reilly and Burstein, 1975). Figure 5 shows stress-strain plots for human cortical bone subjected to tensile or compressive loading in the longitudinal or transverse planes. Table 3 lists the ultimate strengths of human femoral cortical bone as determined by Reilly and Burstein (1975). It is important to remember that the information in Figure 5 and Table 3 relates the strength of cortical bone subjected to uniaxial loading only.

Carter and Hayes (1976b, 1977c) found that the elastic modulus and compressive strength of bone were strongly related to the strain rate ($d\varepsilon/dt$) raised to the 0.06 power. Carter and Caler (1983) reported that the ultimate tensile strength of bone was related to the strain rate in the following manner:

$$\sigma = 147\ d\varepsilon/dt^{\,0.055}\ \text{MPa} \qquad (4)$$

Table 3. Ultimate strength properties of human cortical femoral bone (Reilly and Burstein, 1975)

Longitudinal (MPa)	Tension	133
	Compression	193
Transverse (MPa)	Tension	51
	Compression	133
Shear (MPa)	-----	68

In vivo, bone often experiences complex, multiaxial loading. It is important, therefore, to experimentally determine the strength of bone when it is exposed to this type of loading. A mathematical expression, or failure criterion, can then be determined for predicting the failure of bone for any combination of loads. A generalized failure criterion called the Tsai-Wu criterion (Tsai and Wu, 1971) has been applied in a simplified form (assuming transverse isotropy) by Cezayirlioglu et al. (1985) and Reilly and Burstein (1975) to cortical bone. This criterion accounts for both the anisotropy and the different strengths of bone in compression and tension. Application of the Tsai-Wu criterion by Cezayirlioglu et al. (1985) indicates that the tensile and compressive strengths of cortical bone are reduced as shear stresses from torsional loads are applied.

Cortical bone is mainly subjected to repetitive, low magnitude forces that impart stresses within the bone that are generally smaller than those that would cause fracture during monotonic loading. Cyclic loading of bone sometimes causes microstructural damage. If damage does occur and accumulates over time, then the strength of the bone is compromised (Carter and Hayes, 1977b). The resultant mechanical properties of bone subjected to this type of loading are referred to as the fatigue properties of bone. It is believed that bone remodeling, which occurs continually, may repair the microcracks that do occur in vivo from the cyclic loading of bones that occurs during daily activity (Burr et al., 1985; Burr and

Stafford, 1990; Frost, 1960). According to Carter et al. (1981), the fatigue life of bone is correlated with the difference between maximum and minimum strain values of the applied cyclic strain. The greater the strain range associated with a particular loading is, the fewer cycles it takes for fatigue damage to occur, and, conversely, the smaller the strain range is, the greater the fatigue life. Fatigue life of cortical bone was found to decrease by a factor of 3 when temperature was increased from 21° C to 45° C (Carter and Hayes, 1976a). Schaffler et al. (1989) found fatigue damage increases with increasing strain rate, and Caler and Carter (1989) reported that the fatigue life for cortical bone loaded in uniaxial compression is greater than when it is loaded in uniaxial tension. Cortical bone has a fatigue mechanism similar to that of oriented, short-fibered, composite materials which involves crack initiation, propagation and final fracture (Carter and Hayes, 1977a; Martin and Burr, 1989; Wright and Hayes, 1976a). Lacunae and canaliculi may act as crack initiators because they represent areas of local stress concentrations. This implies that cracks are started easily in bone (Keaveny and Hayes, 1993). These cracks may induce bone remodeling which results in repaired cracks and a decrease in local stress concentrations (Burstein et al. 1972a).

Viscoelasticity A material is viscoelastic if any of its mechanical properties are time dependent. The mechanical properties of bone are affected by how fast (strain rate) and how long (creep) loads are applied.

Strain rate Typical physiological strain rates encountered in vivo are .001 s^{-1} for a slow walk, .01 s^{-1} during a brisk walk and .03 s^{-1} during a slow run (Lanyon et al., 1975, 1981, 1982; Nunamaker et al., 1990; O'Connor et al., 1982; Robertson and Smith, 1978). Strain rate typically increases as activity becomes more strenuous. Figure 6 shows the effect of strain rate upon the material and strength properties of cortical bone. This graph demonstrates that the modulus of elasticity of cortical bone increases with increasing strain rate, but that for the range of typical daily activity (.001 s^{-1} to .01 s^{-1}) E doesn't change appreciably (Crowninshield and Pope, 1974; McElhaney, 1966; Wright and Hayes, 1976b). Figure 6 also shows that cortical bone exhibits a ductile to brittle transition as strain rate increases, but that in the normal physiological range (< 0.1 s^{-1}) ductility increases. Finally, Figure 6 shows that the yield and ultimate strength of cortical bone increases with increasing strain rate which means that cortical bone is stronger during more strenuous activity.

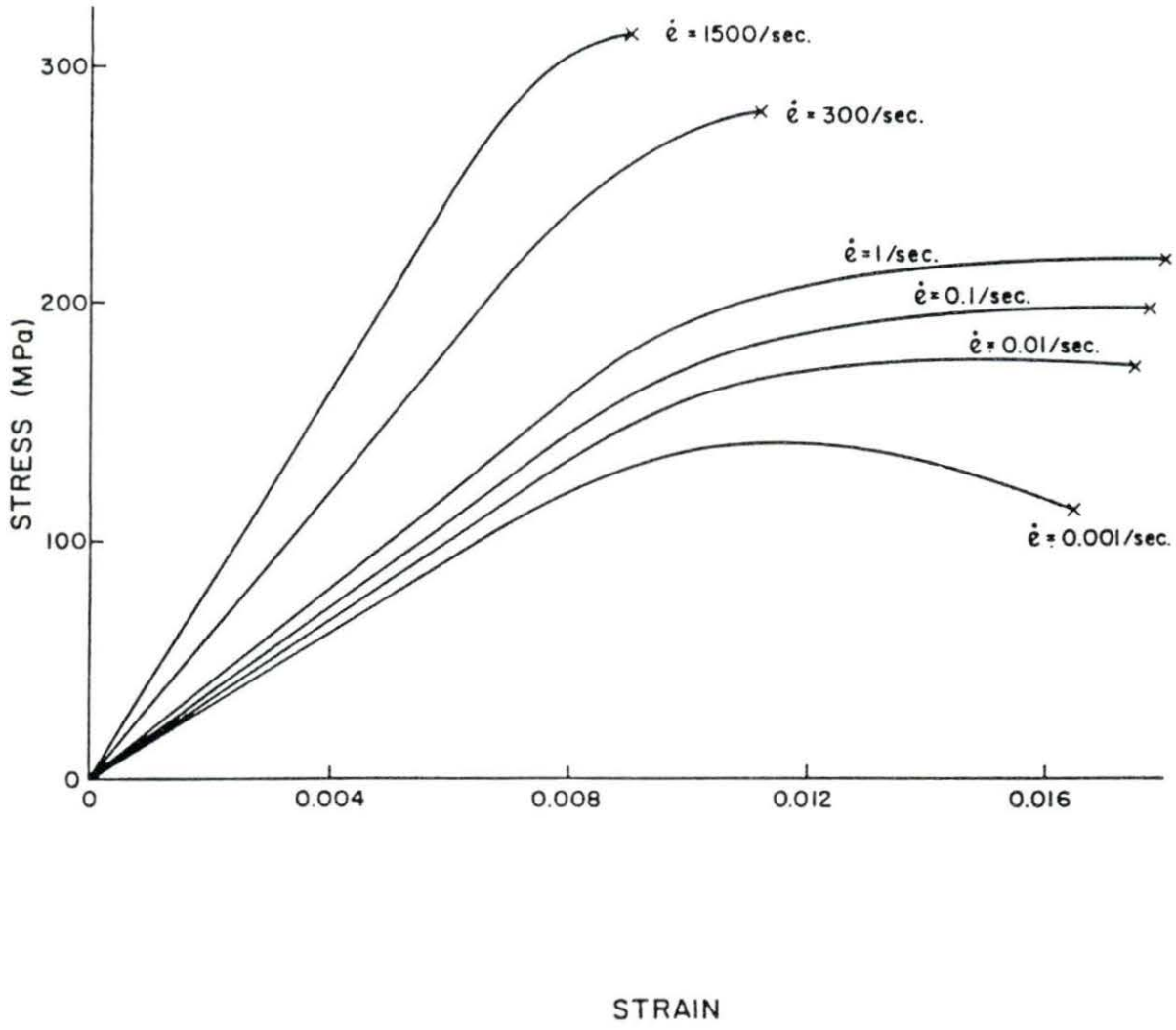

Figure 6. An illustration of the strain rate dependence of the stress-strain curve (McElhaney, 1966)

Creep Cortical bone also exhibits creep behavior because it continues to deform when subjected to a constant stress for an extended period of time (Caler and Carter, 1989; Carter and Caler, 1983; 1985; Fondrk et al., 1988). This means that, if cortical bone is loaded for enough time, creep fractures may occur even though the stress level may be well below the yield and ultimate strengths. Figure 7 indicates that the time necessary to cause creep fracture decreases with increasing stress and that the resistance to creep fracture is greater when bone is subjected to compression versus tension (Caler and Carter, 1989). If creep occurs without fracture, the bone experiences permanent deformation upon unloading (Fondrk et al., 1988).

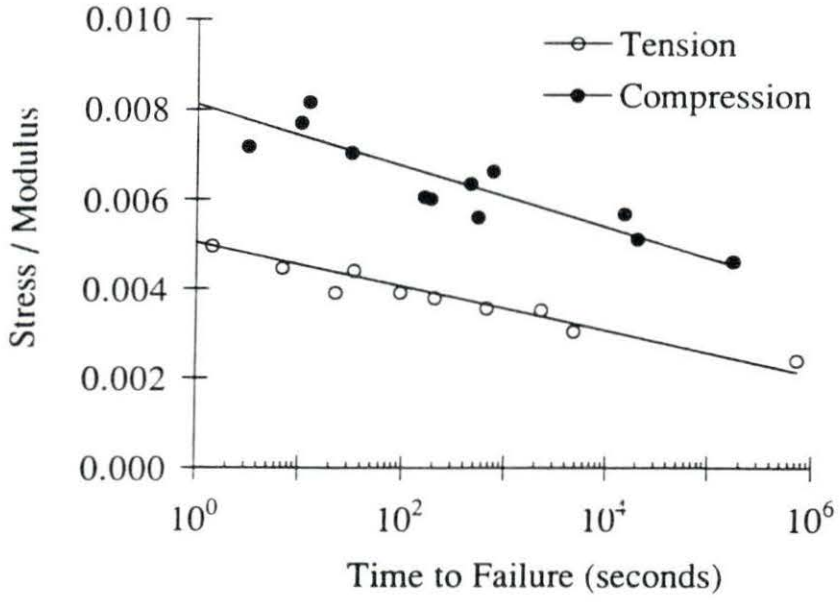

Figure 7. Creep fracture stress for human cortical bone in tension and compression as a function of the time to failure (Caler and Carter, 1989)

Figure 8 shows that, if the applied stress is greater than a threshold value of about 70 MPa or 55% of its ultimate strength (of human cortical bone subjected to tensile longitudinal loading), the rate and magnitude of permanent deformation increases substantially (Fondrk et al., 1988).

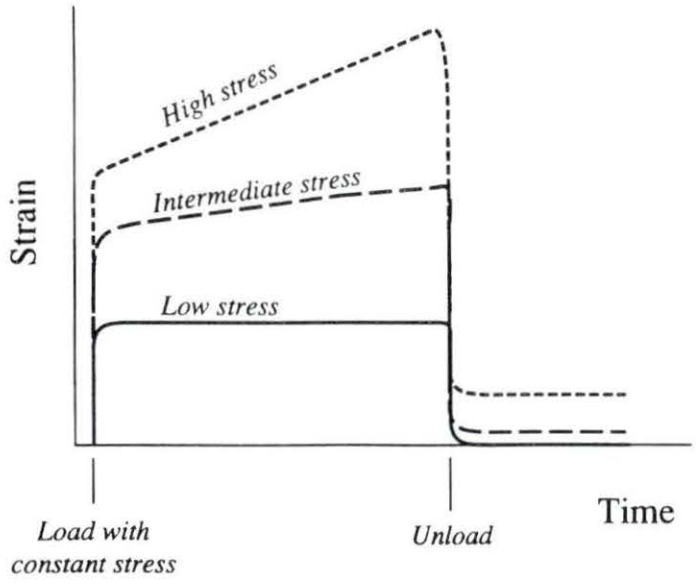

Figure 8. Typical stress-time curves, illustrating the viscoplastic behavior of human cortical bone (Fondrk et al., 1988)

Mechanical properties of trabecular bone

Trabecular bone material In 1892, Wolff suggested that cortical bone is just a more dense cancellous bone (Cowin, 1989). This is certainly a reasonable assumption because, looking at Table 4, it is obvious that the chemical composition of both types of bone are very similar. The major difference between the two types of bone is that the water fraction is greater and the ash fraction is less for trabecular bone than for cortical bone.

Table 4. Results of hydrated bone assays for trabecular and cortical bone for four species (Gong et al., 1964)

Species	Specific Gravity	Water fraction vol%	Ash fraction vol%	Organic fraction vol%	Volatile inorganic fraction vol%
Trabecular bone (vertebral bone)					
Human being	1.92	27.0	33.9	34.9	4.2
Monkey	1.89	27.1	32.9	36.1	4.0
Cow	1.93	28.1	33.5	34.2	4.2
Dog	1.91	28.8	32.6	34.5	4.2
Cortical Bone (tibial and femoral bone)					
Human being	1.99	23.9	37.7	33.8	4.6
Monkey	2.04	23.7	38.2	33.7	4.7
Cow	2.00	25.2	36.6	33.6	4.6
Dog	2.00	22.3	36.8	36.3	4.6

Research by Carter and Hayes (1976b, 1977c) and Keller et al. (1990) indirectly supports Wolff's hypothesis, but others report that the elastic properties of individual trabeculae are less than those of cortical bone (Rho et al., 1993; Ashman and Rho, 1988; Choi et al., 1989, 1991; Ku et al., 1987; Kuhn et al., 1989; Mente and Lewis, 1987; Townsend et al., 1975). An emerging consensus seems to be that the modulus of elasticity of trabecular bone tissue is approximately 20-30% less than that of cortical bone tissue (Keaveny and Hayes, 1993). This variation is thought to arise from slight differences in the mineralization and microstructure between the two materials (Choi, 1990; Hodgskinson and Currey, 1989). Rho et al. (1993), in surveying the literature, found that the various measurements and estimates of the modulus of elasticity of trabecular bone material ranged from 0.76 to 20 GPa. They evaluated the weaknesses in the various procedures used to determine these values and whether these weaknesses would overestimate or underestimate the actual values. They concluded that the modulus of elasticity of trabecular bone material is probably closer to the upper end of the range of values determined from bending tests (3.2 to

7.8 GPa) and the lower end of the range of values determined by tensile testing (8.7-12.7 GPa).

Bulk trabecular bone Trabecular bone material properties are usually measured from bulk trabecular bone test specimens that contain many trabeculae (Martin, 1991). It is assumed that the resultant macroscopically determined material properties combine the mechanical effects of variations in the trabecular architecture with those in the real bone material properties (Martin, 1991). The material properties of bulk cancellous bone can vary considerably depending upon the anatomic location, age, the species and state of health of the bone specimen (Rho et al., 1993). The variables which explain the greatest amount of variation in the material properties of bulk cancellous bone are porosity, mineralization, apparent density, and bone architecture.

Porosity Porosity is the fraction of the bulk bone volume (intertrabecular spaces plus bone material) that is occupied by the intertrabecular spaces or pores that are filled with soft tissue. Since the stiffness and strength of these marrow spaces is much less than that of the bone material itself, it makes sense that as the porosity of the bulk material increases, its strength and stiffness decrease.

Mineralization The degree of mineralization of a given bone is the mass of the mineral portion of the solid bone matrix divided by the combined mass of the organic and mineral components. Mineralization is largely governed by rates of bone modeling and remodeling since new bone takes about six months to reach full mineralization (Martin, 1991). Currey (1969 a,b) and Burstein et al. (1975) determined that the mechanical properties of bone are very sensitive to the degree of mineralization of the bone matrix with either a linear or exponential increase in bone stiffness with increasing mineralization. More recent experiments, however, have determined that bone strength is not related to mineralization in any strong, positive way (Currey, 1990) or that there is even a negative correlation between mineralization and strength (Martin and Ishida, 1989; Martin, 1990).

Apparent density Apparent or bulk density refers to the mass of the bone material divided by the total volume of the specimen which includes any voids. Apparent density, then, is a function of both porosity and the degree of mineralization. Ashman and Rho (1988) found that apparent density of trabecular bone ranges from 100 kg/m^3 to 1000 kg/m^3 as compared to its real density (mass of bone material /volume occupied by bone only) which ranges from approximately 1600-1900 kg/m^3. Carter and Hayes (1977b) showed that the

compressive strength (σ_{cf}) and the elastic modulus (E) of bone (combination cortical and trabecular) were related to the square and cube, respectively, of the apparent density, d(g/cc):

$$\sigma_{cf} = 68r^{.06}d^2 \text{ (MPa)} \qquad (5)$$

$$E = 3790r^{.06}d^3 \text{ (GPa)} \qquad (6)$$

where r = strain rate (s^{-1}). Studies which used only cancellous bone specimens found that both σ_{cf} and E correlate better with d^2 than d^3 (Rice et al., 1988; Bensusan et al.,1983; Ashman and Rho, 1988). Gibson and Ashby (1988) may have resolved this disagreement when they analyzed trabecular bone as if it were an industrial porous foam. They found that for open-celled porous structures (analogous to less dense trabecular bone) E is proportional to d^2; but that for closed-cell structures (analogous to dense trabecular or cortical bone) E varies with d^3. These results may explain that Carter and Hayes' (1977b) results ($E \propto d^3$) were correct because they pooled results from both cancellous and cortical bone while the other studies determined their results ($E \propto d^2$) from trabecular bone specimens only. Typically, differences in apparent density can explain approximately 60-80% of the variation observed in measurements of the modulus of elasticity of cancellous bone (Keaveny and Hayes, 1993b).

Cancellous bone architecture Trabecular architecture can be described as a combination of rod-rod, rod-plate, and plate-plate cellular structures in which rods are thin trabeculae and plates are thicker trabeculae (Keaveny and Hayes, 1993a). The type, size and orientation of these basic cellular structures can substantially influence the magnitudes and anisotropy of the macroscopically measured material properties of cancellous bone (Brown and Ferguson, 1980; Ducheyne et al., 1977; Evans, 1973; Galante et al., 1970; Goldstein et al., 1983; Hvid and Hansen, 1985; Jensen et al., 1991; Mosekilde and Mosekilde, 1988; Mosekilde et al., 1985; Townsend et al., 1975). Cancellous bone, in some anatomic sites such as the proximal humerus, is nearly isotropic, but in other sites such as the lumbar spine, it is highly anisotropic (Keaveny and Hayes, 1993a). While cortical bone anisotropy is primarily determined by osteonal orientation, the anisotropy of cancellous bone is dominated by the orientation of the trabecular struts. It is currently very difficult to correlate the trabecular architecture to the elastic constants of the anisotropic material. Cowin (1985, 1986) devised a complex mathematical formulation that uses stereological principles to describe the relationship between the stiffness of cancellous bone and its apparent density

and trabecular orientation. Turner et al. (1990) provided experimental evidence which indicates that Cowin's theory accounts for approximately 72-94% of the variability in the elastic constants for cancellous bone. It is not presently possible to apply this mathematical formulation to the cancellous bone of the mandible (Ashman, 1992; Turner, 1992).

Stress-strain curve

Figure 9 shows stress-strain curves for trabecular bone of two different apparent densities subjected to uniaxial compression (Carter and Hayes, 1977c; Gibson, 1985). Note that the elastic and post-yield behavior is dependent upon the apparent density of the specimen.

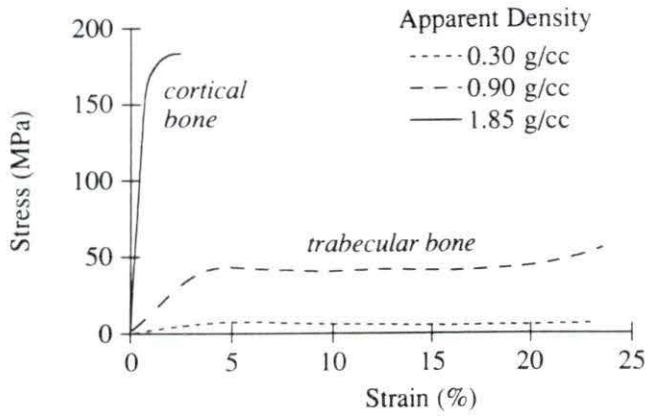

Figure 9. Examples of typical compressive stress-strain behavior of cortical bone and trabecular bone of two different apparent densities (Keaveny and Hayes, 1993a)

The stress-strain curves of the trabecular bone show an initial, almost linear, elastic region where the trabecular struts bend and compress as the bulk tissue is compressed. Failure occurs when some struts fracture, and/or some struts buckle (Ducheyne et al., 1977; Eurell and Kazarian, 1982; Gibson and Ashby, 1988; Hayes and Carter, 1976; Townsend et al., 1975; Turner, 1989). As the strain continues to increase, broken struts begin to fill

intertrabecular pores causing a final increase in stiffness as shown in the latter portion of the curve.

The post-yield behavior of cancellous bone when subjected to tensile loading, as shown by the stress-strain curve in Figure 10, is very different than its compressive behavior (Carter et al., 1980; Kaplan et al., 1985; Stone et al., 1983). Failure occurs by fracture of individual struts and leads eventually to complete fracture since the unfractured struts must carry an increasing amount of load due to the failure of neighboring struts.

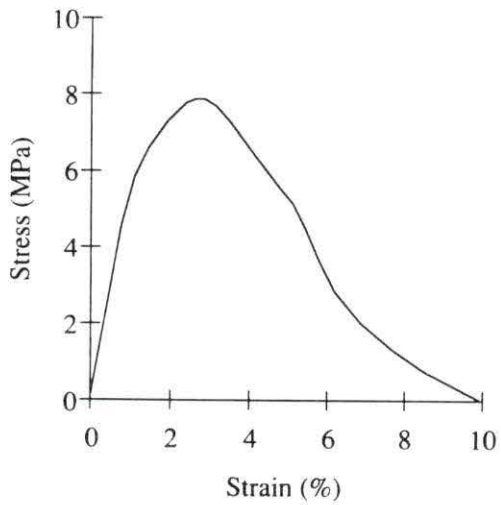

Figure 10. Tensile stress-strain behavior of trabecular bone (Gibson and Ashby, 1988)

Strength While most evidence suggests that uniaxial tensile and compressive strengths of trabecular bone are similar (Bensusan et al., 1983; Carter et al., 1980; Neil et al., 1983), there is some research that indicates that the tensile strength of cancellous bone may be less than its compressive strength (Kaplan et al., 1985; Stone et al., 1983). According to Goldstein (1987), the ultimate compressive strength of cancellous bone ranges from approximately 0.12 to 116 MPa. Since the post-yield load-carrying capacity of trabecular bone is very high in compression but negligible in tension, local failure in tension

is catastrophic (Keaveny and Hayes, 1993a). Melvin et al. (1970), Halawa et al. (1978), Saha and Gorman (1981) and Stone et al. (1983) found the shear strength of trabecular bone to range from approximately 1 to 21 MPa and to be, like compressive and tensile strength, dependent upon anatomic location and direction of testing.

There is not much data available regarding the multiaxial strength of trabecular bone (Keaveny and Hayes, 1993). Stone et al. (1983) found that the shear strength of cancellous bone is less when it experiences torsional loading in combination with tension loading versus torsional loading alone. Borchers (1991) reported that the strength of cancellous bone is affected by the magnitude of the mean stress or hydrostatic pressure component. This is consistent with Gibson and Ashby's (1988) classification of most trabecular bone as an open-celled material which also exhibits a sensitivity of multiaxial strength to mean stress.

Although there is not much data available regarding the fatigue properties of trabecular bone, Michel et al. (1991) suggest that the uniaxial compressive strength of trabecular bone can be reduced by an order of magnitude after exposure to 10^6 cycles. It appears that the resistance of trabecular bone to fatigue is greater than that of cortical bone (Keaveny and Hayes, 1993b). The mechanism of fatigue failure appears to be fracture followed by buckling of individual struts (Michel et al., 1991).

Viscoelasticity While there is no solid information regarding creep in cancellous bone, it has been determined that both the modulus of elasticity and strength show a weak dependence upon strain rate. An increase in strain rate from $.001 s^{-1}$ (slow walk) to $0.1\ s^{-1}$ (very strenuous walk) results in an increase in both the modulus of elasticity and strength of trabecular bone material of approximately 30% (Keaveny and Hayes, 1993). It has been demonstrated that at extremely high strain rates, such as $10\ s^{-1}$ (gunshot wound), bone marrow cannot flow through intertrabecular spaces. This results in the bone becoming stiffer, stronger, and better able to absorb energy (Keaveny and Hayes, 1993a). At normal physiologic strain rates, however, bone marrow does not contribute to the viscous behavior of the bone (Carter and Hayes,1976; Pugh et al., 1973b). Ochoa et al. (1991) studied the loading of femoral heads with and without marrow and found that, *in vivo*, marrow may have a stiffening effect on a bone's material properties.

Bone adaptation to mechanical loading

Bone is a dynamic tissue that is always changing due to osteoblast and osteoclast cell activities. Osteoblasts and osteoclasts are responsible, respectively, for the formation and

the dissolution or resorption of bone. The variable balance between these two cell activities allows bone to repair following injury, model and remodel during normal growth, and adapt to various environmental conditions, in particular, the mechanical demands placed locally on the bone. Many studies show that a reduction in normal physiological loading results in loss of bone mass, while additional loading results in increased bone mass (Smith et al., 1976; Goodship et al., 1979; Lanyon et al., 1982; Rubin and Lanyon, 1985; Meade, 1989; Jee and Xi, 1990). Extreme loading beyond the physiological range, such as that applied to cause orthodontic tooth movement, results in bone resorption, not formation (Imamura et al., 1990). The phenomenon of functional adaptation refers to the ability of bone to respond to some mechanical stimulus by altering its configuration and/or density to efficiently accommodate the mechanical demands placed upon it (Wolff, 1892). While the idea of functional adaptation is widely accepted (Rubin and McCleod, 1990), the structural goals of modeling and remodeling and the mechanical stimuli which control the process are still unclear. Bone adaptation occurs by two different processes termed modeling and remodeling.

Bone modeling is an uncoupled process in which cell activation (A) results directly in either bone formation (A-F) or resorption (A-R) on either the periosteal or endosteal surfaces of a given bone. The periosteum is the external lining that surrounds a bone and consists of an outer fibrous layer and an inner cellular layer. The endosteum is a cellular layer that lines the inner surfaces of cortical bone and Haversian canals and covers the outer surfaces of each trabecular bone strut. Modeling produces a net change in bone size or shape and occurs mainly during growth.

Bone remodeling occurs when previously formed bone undergoes an internal restructuring (Roberts et al., 1987) which effectively changes local material properties such as density, stiffness, and strength (Frost, 1973). Remodeling includes all localized changes in both osteons and trabeculae such as turnover, hypertrophy, atrophy or reorientation. Bone
remodeling is a coupled, tissue-level process in which cell activation (A) results in a sequence of resorption (R), quiescence or reversal (Q) and bone formation (Frost, 1964). The length of the entire remodeling cycle (A-R(Q)-F), termed sigma, is about 6 weeks in rabbits, 12 weeks in dogs and 17 weeks in man (Frost, 1964). Remodeling rates are greater during growth, but unlike modeling, remodeling rates can increase significantly in adult bone (Whedon and Heaney, 1993).

Mechanical stimulus of bone modeling and remodeling All loads and moments applied to bone cause the tissue to experience very small strains that are on the order of millionths of the original dimension (microstrain or μE). Rubin and Lanyon (1982) determined, from extensive *in vivo* strain gage animal studies, that in different areas of the same skeleton, as well as across different species, bone experiences a relatively constant pattern of strain when loaded. They found that strains experienced under peak loading ranged from 2500-3500 μE while routine loading produced strains in the 1000-1500 microstrain range. Irreversible bone deformation, or yield, occurs at approximately 7000 μE (Whedon and Heaney, 1993). Since the loads experienced by various bones can differ over several orders of magnitude, this constancy of strain suggests that the mass density of each bone may be a response to its typical loadings (Wheadon and Heaney, 1993).

In addition to the constancy of strain distribution described above, many *in vivo*, controlled loading experiments have demonstrated that the *type* of loading is an important variable in the phenomenon of bone adaptation. O'Connor et al. (1982), for example, determined that impact loading was more osteogenic than the same force applied slowly. The importance of dynamic versus static loading was demonstrated by Lanyon and Rubin (1985). They found that the application of a 2000 μE static load results in a 13% net bone loss, but a 2000μE trapezoid-shaped waveform loading applied at a frequency of 100 cycles per day showed a 24% increase in cross sectional area. Further studies by Rubin and Lanyon (1987) indicated that both remodeling and modeling are triggered at some cyclic threshold of applied loading above which there is no further increase in response. Brown et al. (1990) tried to correlate various mechanical parameter distributions in the bone, as determined by finite element analysis, to specific sites of remodeling activity observed in a controlled loading, *in vivo* model. They found that in the majority of cases (>95%) the mechanical parameters correlated poorly with the biological response. The best correlation ($r = 0.82$) occurred between new periosteal bone thickness and the distribution of the first or most tensile principal strain. Other reasonable correlations were found in the mechanical parameters of strain energy density ($r = 0.54$) and longitudinal shearing stress (0.66).

One way to describe how bone mass and form may be adapted is by using a feedback loop described by Turner (1991) and Beaupre et al. (1990) as shown in Figure 11. The strain under loading at any point in space and time is somehow monitored, possibly by osteocytes, and compared to some reference or setpoint. Any significant variation generates an error signal which controls the local resorption and deposition phases of modeling and remodeling. The change in bone mass makes the bone more or less stiff in response to the

same loading which returns the bone strain to the homeostatic range. This type of feedback system is very site specific (Whedon and Heaney, 1993).

Adaptation of trabecular bone to mechanical stimulus Hayes and Snyder (1981) propose that trabecular struts form along preferred orientations in such a way that bending of trabeculae is minimized. Their research indicated that trabeculae seemed to lie in the same direction as the principal stresses that were predicted by numerical analysis. Goldstein et al. (1990) proposed that the trabecular bone structure is adapted to minimize the strain energy density (SED). Huiskies et al. (1987) and Fyhrie and Carter (1986) also believe that SED is the controlling mechanical parameter. They have found positive correlations between results of adaptive finite element simulations based on this theory and the adaptive patterns observed in radiographs of the proximal femur. None of these theories, however, have been applied to the adaptation of bone around dental implants.

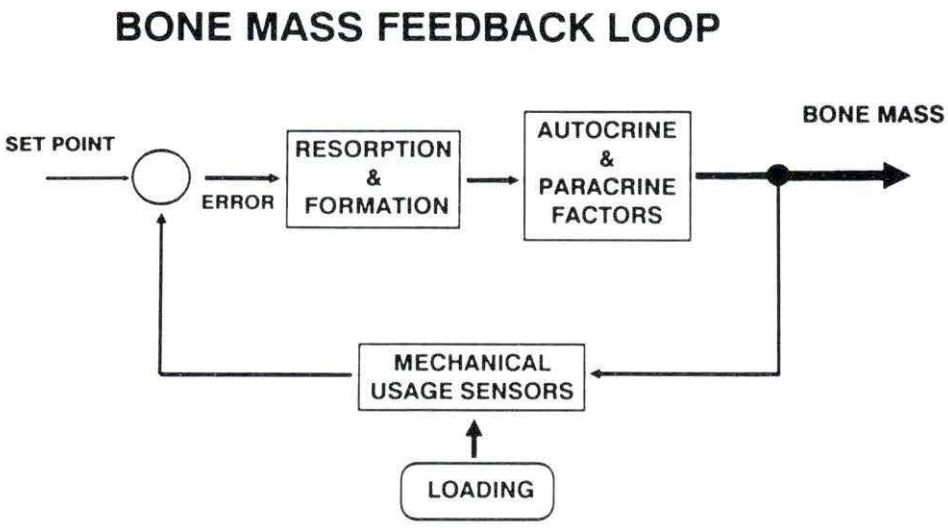

Figure 11. Suggested feedback loop controlling bone mass (Whedon and Heaney, 1993)

Bone adaptation to an implant Implantation of an artificial material into bone tissue will not only generate a repair healing process, but it will also influence the natural remodeling phenomenon of the host tissue (Davies et al., 1987). There is an interaction between the implant and the surrounding tissue that may begin at the nanometer level and extend to approximately a millimeter away (Brunski, 1992). The extent of this interface is dependent upon many factors including biomechanical, biomaterial, and surgical technique. Following implantation and formation of a hematoma, either regeneration or repair will occur. Regeneration involves replacement of the wounded region by bone, while repair leads to the formation of non-mineralized scar tissue (Spector, 1988). If regeneration occurs, then it is followed by bone modeling or remodeling which consolidates the bone at the site. According to Brunski (1992), the stability of an implant in its healing site, indicated by the amount of micromotion present, indicates whether repair or regeneration will occur. He believes that excessive micromotion destroys the hematoma and tissue scaffold that precedes regeneration and triggers the repair process instead. McLean and Marshall (1968) found that when a long bone is fractured, poor immobilization results in the formation of a cartilaginous scar, indicating that the repair process has dominated. Perren and Boitzy (1978) found that with good fixation little or no callus forms, and the site undergoes regeneration. Brunski (1992) found that at sham healing sites where surgery is performed, but no implant is placed, regeneration occurs.

Interface development The development of the interface between a dental implant and cortical bone was reported by Roberts (1988) for dental implants placed in rabbit femoral cortical bone. Following the surgical placement of a dental implant, approximately one mm of cortical bone adjacent to the implant undergoes necrosis. Initially, this dead bone serves as a structural support for the implant, and it is eventually revitalized through remodeling. A bridging callus of woven bone, which forms at both periosteal and endosteal surfaces, is the first step towards the adaptation of alveolar bone to the implant. This callus may originate as close as two or three mm from the implant. Roberts (1988) reported that this callus may reach the implant surface in two weeks (four weeks and 6 weeks for the dog and human, respectively). Gradually, over the next four weeks (eight weeks and twelve weeks for dogs and humans, respectively), the woven bone callus fills in with lamellar bone and becomes capable of resisting occlusal loads. At the same time that this lamellar compaction is taking place, callus reduction is occurring in conjunction with the remodeling

of the dead bone adjacent to the implant. During the next twelve weeks (36 weeks and 54 weeks for the dog and human, respectively), the bony interface matures via modeling and remodeling. Maintenance of this adapted, bony interface will hopefully proceed indefinitely via the continuous remodeling process of bone that is responsible for the lifetime maintenance of the skeleton.

Dental Implants

Dental implants are used to directly or indirectly replace the masticatory function of natural teeth. They provide retention for complete and partial overdentures or abutment support for single-tooth, partial and complete arch fixed restorations (Schnitman, 1993). This study focuses on single-tooth replacement with an endosseous, or within bone, implant. First the anatomy and biomechanics of natural teeth and their supporting tissues or periodontium are discussed. Second, an overview of the basic principles of dental implant design is presented. Finally, the types of dental implants currently used are discussed. This is followed by an evaluation of the success rates of endosseous dental implants and the factors that contribute positively and negatively toward a successful implant outcome.

Dental anatomy

A discussion of dental implants requires a preliminary review of the anatomy of natural teeth and their supporting tissues or periodontium. Figure 12 illustrates all the important anatomical landmarks discussed below. It is important to remember that the apex of the tooth is located at the base of the tooth root within the mandible or maxilla. Other reference directions and surfaces, pertinent to dental anatomy, are shown in Figure 13.

External tooth features Figure 14 shows the anatomy of a canine tooth in a dog. The external portion of the tooth can be divided into three major areas: the crown, the neck and the root. The crown is the portion of the tooth that extends above the gingiva. Enamel, which is approximately 96% crystalline hydroxyapatite, covers the surface of the crown. Enamel is the hardest tissue in the body. It is produced by ameloblasts. Enamel is subjected to wear and degradation by acids generated from bacterial activity. Unlike bone, enamel is incapable of regeneration when damaged. The modulus of elasticity of enamel is thought to range from approximately 40 to 80 GPa (Rees and Jacobsen, 1993).

The neck or cervical area is the portion of the tooth where the crown joins the root of the tooth at the cementoenamel junction. In most animals, this is located next to the gingival sulcus, which is the space between the gingiva and the tooth. In some animals, the cementum is not contiguous with the enamel, resulting in either exposed dentin or an overlapping of the enamel and the cementum.

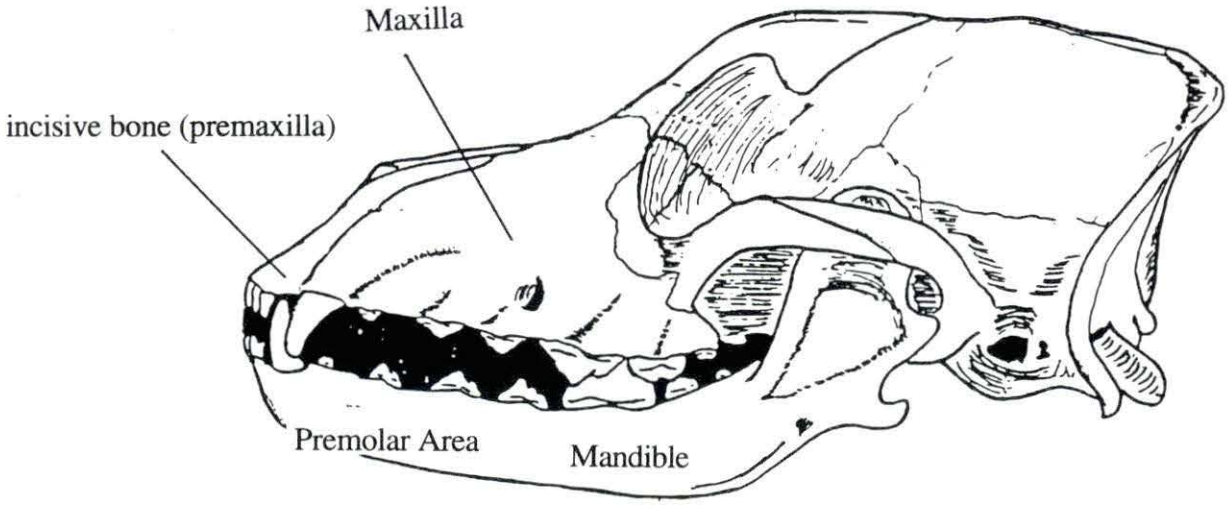

Figure 12. Canine skull (Wiggs, 1989)

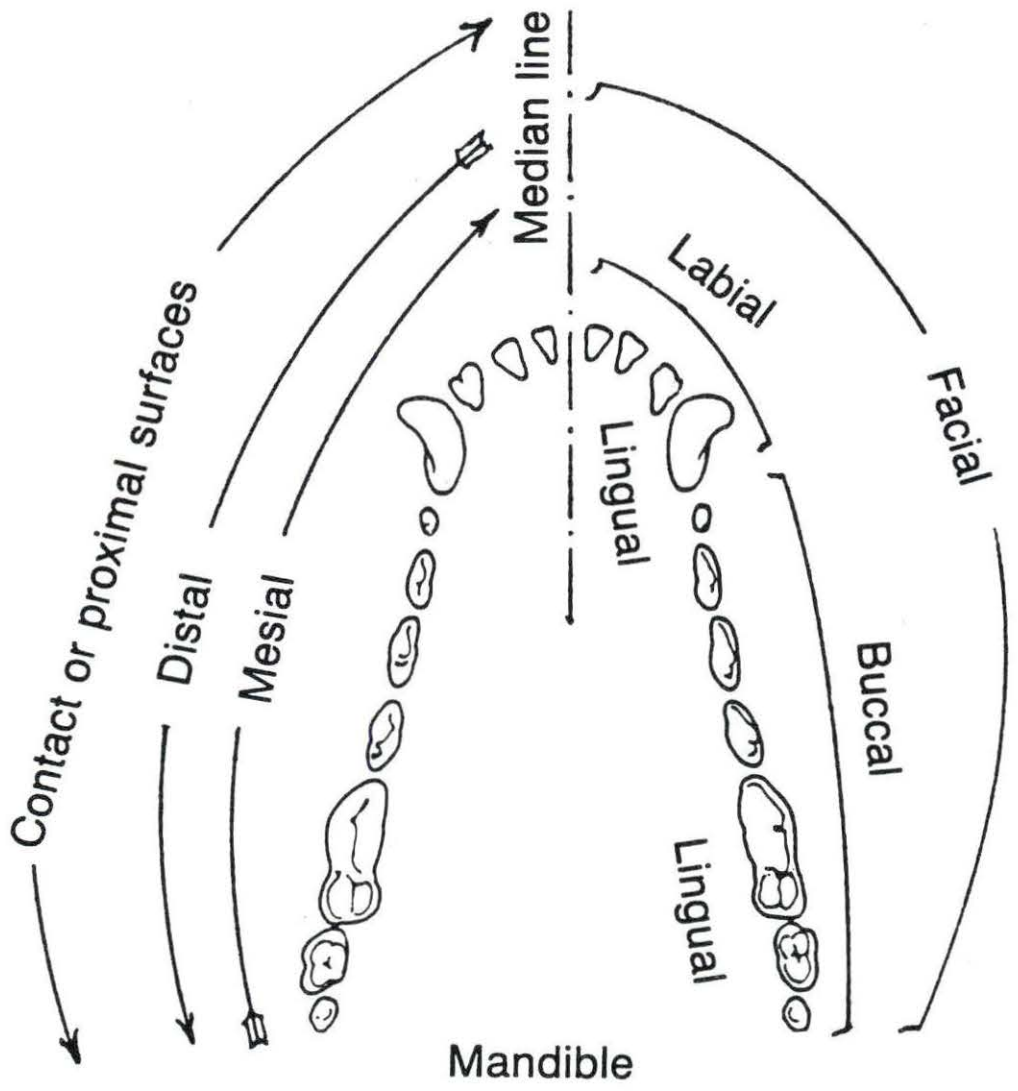

Figure 13. Tooth surfaces and nomenclature (Wiggs, 1989)

The root is the portion of the tooth that is apical to the neck and seated in the jaw. The number of roots present depends upon the type of tooth and its specific position in the jaw. The surface of the root consists of cementum, a thin layer of calcified tissue produced by cementoblasts. Cementum is composed of approximately 60% inorganic minerals and is therefore not as hard as enamel. Unlike enamel, cementum can regenerate.

Internal tooth features The internal components of a tooth are dentin and pulp. Dentin is produced by odontoblasts and contains approximately 70% inorganic mineral. This makes it softer than enamel but harder than either bone or cementum. Dentin comprises the major portion of the tooth in a mature animal, and it is usually surrounded by enamel in the crown, and cementum in the root. Dentin is produced throughout the life of the tooth and has a modulus of elasticity approximately equal to 15 GPa (Rees and Jacobsen, 1992).

The pulp is located within the interior portion or pulp cavity of the tooth. In the crown, the pulp cavity is called the pulp chamber but in the root, it is called the root canal. Pulp emerges from the apical or base portion of the tooth root and joins with the periodontum at either the apical foramen or delta (Figure 14). Pulp contains soft, nervous, vascular and connective tissue.

Periodontium The periodontium is the support mechanism of natural teeth, and consists of osseous tissue as well as the soft tissues of the periodontal ligament and the gingiva.

Osseous tissue Teeth are contained within the bones of the premaxillae, the maxillae, and the mandible (Figure 12). The portion of these bones that surround and support individual teeth is called the alveolar process (Figure 14). The outer wall of the alveolar process is a cortical plate. The inner wall is a thin layer of perforated cortical bone that lines the tooth socket. It is called the lamina dura. Trabecular bone is located between these inner and outer walls and acts as a support which transfers stresses from the lamina dura to the cortical plates. The occlusal portion of the alveolar process, which is located near the neck of the tooth, is called the alveolar crest.

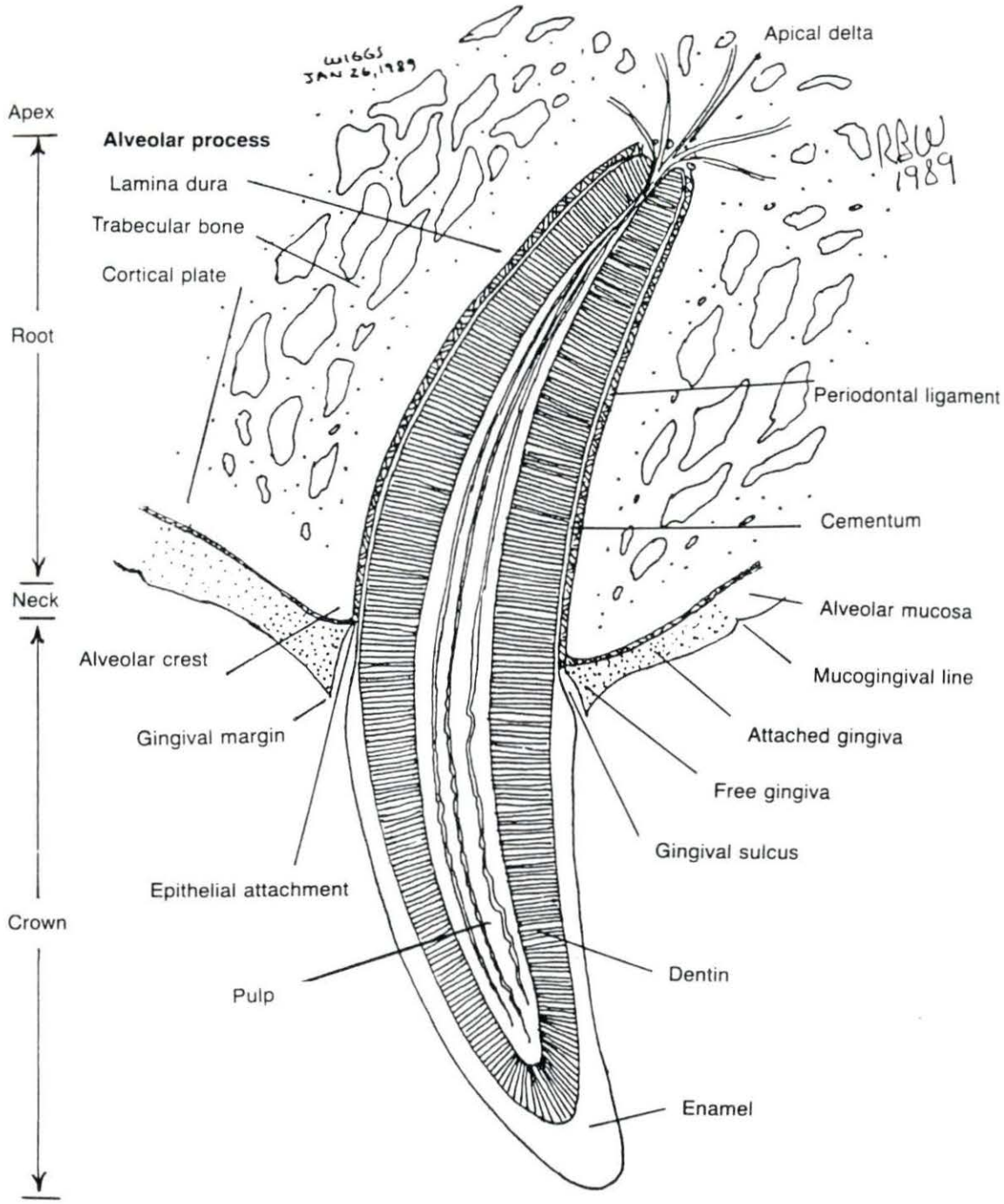

Fig 14. Canine tooth of a dog (Wiggs, 1989)

Gingiva Gingiva is a protective layer of keratinized, stratified, squamous epithelium that surrounds the tooth. Part of the gingiva is firmly attached to the alveolar bone beneath it. That portion of the gingiva that is directly adjacent to the tooth, however, is not attached to either bone or tooth, and is called the free gingiva. The resulting space between the tooth and the free gingiva is called the gingival sulcus. The bottom of the gingival sulcus is fused to the tooth by an epithelial attachment often called the junctional epithelium. This junctional epithelium acts as a seal to prevent the penetration of undesirable substances that are prevalent in the oral cavity to the underlying bone (Meffert, 1988).

Periodontal ligament The periodontal ligament (PDL) is a thin layer of connective tissue that contains collagen and elastic fibers which surrounds the root of the tooth. These fibers penetrate the lamina dura on one end and the cementum on the other during formation. This attachment holds or suspends the tooth in place in its socket. The fibers in the periodontal ligament are often called Sharpey's fibers, and, according to Tholen (1982), are oriented in many directions so as to best absorb the various multidirectional forces of mastication. It is also theorized by Kertesz (1993) that the combined system of blood vessels in the periodontal ligament and the alveolar bone acts like a hemodynamic damping system. Upon removal of a tooth, the PDL is destroyed and cannot regenerate; therefore, an endosseous implant does not have the mechanical benefits of shock absorption and stress distribution afforded the natural tooth by the periodontal ligament.

Biomechanics of natural teeth

Teeth are subjected to large, vertical, compressive forces which may be as great as 2440 N in humans (Brunski, 1988). Bite force magnitudes are location dependent within the mandible. Magnitudes are approximately four times greater in the molar area than those in the incisor area (Bidez, 1993). Teeth are also loaded in the transverse or horizontal direction with forces on the order of 30 N (Brunski, 1992). This force component is a result of the horizontal movement of the mandible and the inclination of the tooth cusps (Rangert et al., 1989). Additionally, it is likely that natural teeth are subjected to shear, bending, and torsional loads (Hylander, 1981). Masticatory forces applied to the teeth are transferred to the lamina dura of the alveolar process by the collagen fibers of the periodontal ligament. The stresses in the lamina dura are then transferred via the supporting trabecular struts to the cortical bone of the mandible and maxilla (van Mullem and Maltha, 1983). Based on data obtained regarding the maximum jaw closure speed and accelerations related to chewing, it is

believed that a static analysis of the system is probably sufficient, since dynamics and inertial loads don't seem to affect bite loads to any great extent (Osborn and Baragar, 1985; Throckmorten and Throckmorten, 1985). According to Graf (1969), forces are applied to the teeth and periodontal tissues of a human for approximately 17.5 minutes per day.

Resilience can be defined as the force, F, divided by the resultant elastic movement, s, and is used here to describe the mobility of a tooth in response to physiologic loading. The top graph in Figure 15 shows the two-stage mobility characteristic of a natural tooth. The first stage is characterized by extreme mobility which is mainly due to the presence of the periodontal ligament (Richter, 1989). The initiation of the more resilient second stage is dependent upon the load rate as well as the magnitude of the load, as shown in the middle graph of Figure 15 (Richter, 1989). The bottom graph in Figure 15 shows that the resilience of a dental implant fixed in bone is approximately 10 to 100 times higher than that of a natural tooth. This implies that it is much less mobile in response to physiologic stresses (Richter, 1989). This immobility is explained by the fact that there is no periodontal ligament between the implant and the bone. It represents a major difference in the biomechanical situation between a natural tooth and a dental implant.

Principles of dental implant design

The goals of all dental implant designs are to obtain a stable fixation of the implant within the surrounding alveolar bone and to maintain this fixation as the implant performs the chewing, cutting, grinding, and stress transfer functions of the missing tooth and periodontal membrane. The following principles must be considered when developing, evaluating or choosing an implant system:

- The implant material must be biocompatible, strong enough to withstand occlusal forces, and enduring in its strength.
- The implant must become fixed to the surrounding alveolar bone.
- The implant must transfer stresses to the surrounding bone in a manner that is conducive to the maintenance of the bone-implant interface.
- The implant tissue must form an adequate perimucosal seal to prevent infection.

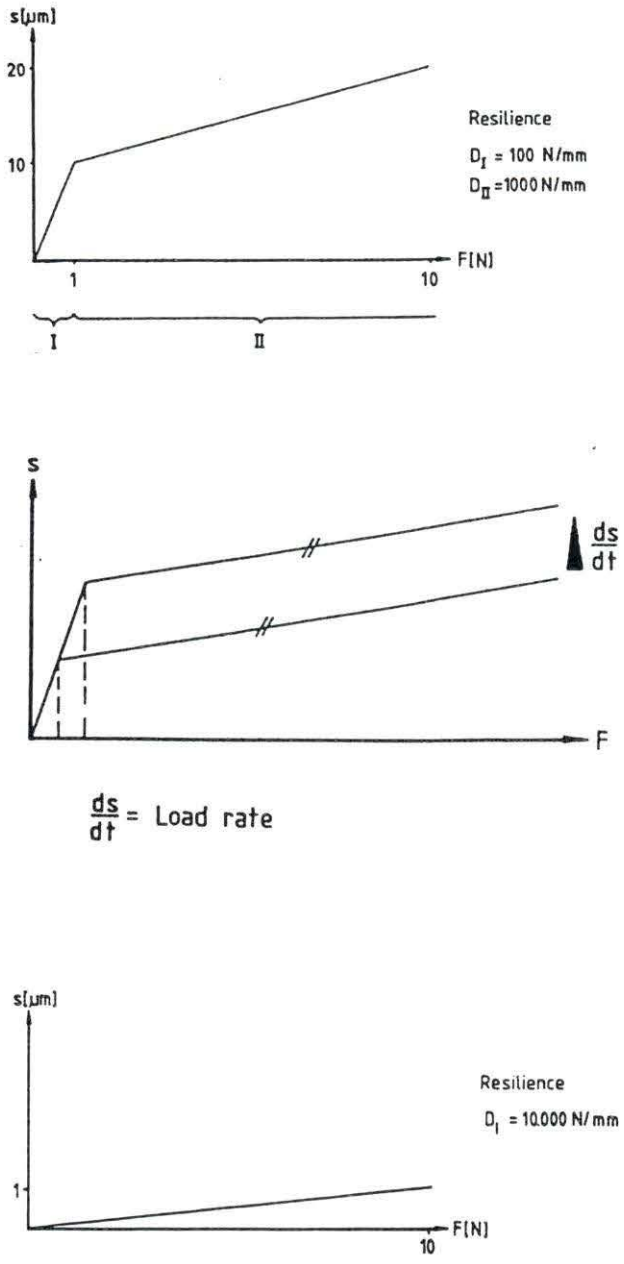

Figure 15. Top graph illustrates two-stage tooth mobility, where s = elastic movement and F = load. Middle graph indicates that the load rate (ds/dt) determines the level from which the secondary phase of movement starts. Bottom graph illustrates the force/movement ratio of osseointegrated implant (Richter, 1989)

Materials The first requirement of any proposed implant material is that of biocompatibility. The material and any of its reaction products must be well tolerated by the body. Dental implants are typically in contact with three different tissues: alveolar bone, supra alveolar connective tissue and oral epithelium (dePutter, 1984). Permanent implant materials must also maintain their mechanical integrity over time by remaining sufficiently unreactive to body fluids. Dental implants, for example, must maintain adequate strength *in vivo* to withstand the forces of mastication. ASTM standards have been developed for only twelve specific materials for use in orthopedics or dentistry (Bundy, 1989). Metals and ceramics are the most commonly utilized material classes in the manufacture of dental implants (Kohn, 1992).

Metals Titanium-based metals are the predominant materials used for dental implants because of their strength, relatively low modulus of elasticity, and perceived chemical inertness (Kohn, 1992; Schnitman, 1993). Titanium has replaced stainless steel as the material of choice for dental implants because of its superior resistance to corrosion. It has also replaced cobalt chromium alloys, except in cases when the implant must be cast, due to the poor mechanical properties and the potential for patient hypersensitivity to the elements of these alloys (dePutter, 1984). Titanium is used in its commercially pure form (c. p. Ti) or is alloyed with other metals to improve its mechanical properties. Titanium-aluminum-vanadium (Ti-6Al-4V) alloys, for example, are often used for dental implants.

The alleged chemical inertness of titanium is believed to elicit a minimal biological response due to the formation of a stable, passive oxide surface layer. It is important to realize, however, that any titanium-based material is not fully inert and that titanium ion release does occur from the chemical dissolution of the titanium oxide surface layer (Healy and Ducheyne, 1992). Another troublesome characteristic of titanium-based materials is that they have a relatively poor resistance to abrasion (McKellop et al., 1981). Williams (1981) questioned the biocompatibility of titanium-based materials due to reports of tissue discoloration surrounding titanium-based implants. He felt that this discoloration was caused by a slight diffusion of titanium through the passive oxide surface layer and/or abrasion to the outer surface of the implant. Bruneel and Helsen (1988) reported the presence of aluminum and vanadium elements in the tissues surrounding Ti-6Al-4V implants.

Because metals do not chemically bond to bone, the surface of a metal implant must be carefully designed to provide an opportunity for mechanical interlock to form between the implant and the healing bone. The stronger the resulting interface, the less the chance of

implant loosening and failure (Pilliar et al., 1975; Huiskies, 1984). Smooth-surfaced metal implants form the weakest possible interfacial attachment with bone. Textured, screw-threaded, plasma-sprayed, and porous-coated surfaces form progressively stronger interfaces (Kohn, 1992). An important consideration, however, is that these different surfaces require different time intervals before adequate interlock or osseointegration can occur. Additionally, it is important to remember that surface roughness and many other types of surface modifications will significantly reduce the fatigue strength of the metal (Kohn and Ducheyne, 1990).

Ceramics Ceramics are composed of metallic and non-metallic elements that are usually ionically or sometimes covalently bonded to one another. Ceramics are hard, brittle materials that are very sensitive to notching and microcracks. When a ceramic material is compressed, any existing cracks or pores are closed. While a ceramic is in tension, flaws act as stress concentrators. This explains why ceramics tend to be very strong in compression but very weak in tension.

The use of ceramic materials for dental implants is being investigated because of the lingering concern regarding the biocompatibility of metals. Ceramics are fully oxidized materials that are chemically more stable than metals which oxidize only at their surface. It is thought that ceramics will therefore elicit a less adverse biological response than metals. Additionally, the similarity of calcium-phosphate ceramics to the major constituents of bone mineral and their capacity to form a direct chemical bond with bone are very desirable features. Ceramics that are sufficiently biocompatible to be placed within the body are called bioceramics and can be classified as nearly inert or bioactive. These classifications, the use of ceramic coatings, and a description of the ceramic-ceramic composite used in this study will be discussed below.

Nearly inert ceramics Nearly inert ceramics do not interact with surrounding tissues to any measurable degree. This implies that, like metals, nearly inert ceramics must utilize some form of mechanical attachment to bone. Aluminum oxide (Al_2O_3), or alumina, is the strongest and most commonly used material of this type for dental implant applications. Aluminum oxide is formed by sintering which means that different porosities and densities may be incorporated. Aluminum oxide is usually used in its most dense form because of the improved mechanical properties and decreased tendency to spread infection (Klawitter et al., 1977). The compressive and tensile strengths of dense Al_2O_3 are approximately 4000 MPa and 400 MPa, respectively (Hench and Etheridge, 1982). Alumina has also shown excellent wear resistance *in vivo* (Hulbert et al., 1987). The weakness of all

bioceramics is their poor tensile strength and tendency towards catastrophic fatigue failures when used in a load-bearing capacity *in vivo.*

Bioactive ceramics de Groot (1983) defines a bioactive ceramic as a bioceramic material the surface of which consists of a layer of calcium phosphate following implantation. All bioactive ceramics have a lattice structure that is similar to calcium hydroxyapatite which is the predominant inorganic component of bone. According to Bauer (1990), these materials undergo chemical reactions with the physiological environment which result in the formation of a chemical bond between the osseous tissue and the surface of the implant. This phenomenon has been reported by many authors (Wood and McGee, 1974; Denissen and de Groot, 1979; Hench and Ethridge, 1982; de Putter, 1984; de Lange et al., 1986). The fixation achieved by such a chemical bond is more effective than any type of mechanical fixation. Bioactive materials induce quicker healing without the presence of soft tissue between the bone and the implant (de Lange et al., 1986). Some bioactive materials include glass, glass-ceramics, hydroxyapatite and tricalcium phosphate. Because these materials do not have sufficient strength to be used as dental implants, widespread research efforts are focused on the development of some type of composite that can utilize the biocompatibility of a bioactive ceramic while improving its mechanical integrity.

Bioactive ceramic coatings The most recent innovation in dental implant design has been the addition of a bioactive ceramic coating to a metal substrate. Typically, hydroxyapatite (HA) is plasma-sprayed on a metal implant. The coating is used as a barrier between the metal and the bone to prevent the migration of wear debris and metal ion release (Marquis, 1993). The HA coating is also believed to promote, and possibly increase, the rate of bone formation at the interface (Steflik et al., 1992; Yukna, 1991). Finally, the HA coating is hypothesized to yield a stronger interfacial attachment than a metal implant without a coating due to the formation of a chemical bond between the coating and the bone.

Albrektsson and Sennerby (1991) assert that the commercial use of coated implants is highly premature due to inadequate testing, evaluation and documentation. Listgarten et al. (1992) questions the long term stability of the HA coating as well as the strength of the HA-metal bond. They report that coated implants were outperformed by uncoated titanium-based implants. Kohn (1992) reports that all studies show that the coating does not increase long-term stabilization and fixation. Denissen et al. (1990) report the *in vivo* shear strengths of the following interfaces:

- Smooth surfaced titanium-based implant and bone: ~ 0.6 MPa

- Porous surfaced titanium-based implant and bone: ~20 MPa
- HA coating and titanium-based implant: ~22 MPa
- HA coating and bone: ~30 MPa

These results indicate that the ceramic/metal bond will tend to fail before the ceramic/tissue bond. This delamination has been observed *in vivo* (Parr et al., 1988; Luthy et al., 1987), and not only affects the mechanical integrity of the implant, but generates biomaterial particulate debris as well (Kohn, 1992). Particulate debris has the potential to cause local and systemic biological reactions, osteolysis, and abrasion of the metal substrate (Howie et al., 1988; Maloney et al., 1990). Some of the poor results associated with HA coatings may be attributable to the plasma-spraying process, and it is hoped that a new vacuum-spraying process may alleviate some problems.

Bioactive ceramic composite Tricalcium phosphate (TCP), $Ca_3(PO_4)_2$, is an extremely biocompatible bioactive ceramic material (Cutright et al., 1972; Ferraro, 1979). TCP undergoes extensive biodegradation *in vivo* where it is generally replaced by bone (Cutright et al., 1972; de Groot, 1981). This biodegradation quickly and significantly reduces the strength of TCP making it unsuitable for use as a dental implant (Jarcho et al., 1979). Janikowski and McGee (1969) suggested adding a magnesium aluminate spinal, $MgAl_2O_4$, to TCP to form a composite material that retains the biocompatibility of TCP while increasing its strength and endurance. This composite, termed osteoceramic (McGee and Wood, 1974), has a higher compressive strength and similar tensile strength as compared to cortical bone, and a modulus of elasticity similar to titanium (Graves, 1988). Tweden (1987) determined that the osteoceramic does not lose strength *in vivo*.

Perimucosal seal Endosseous dental implants differ from orthopedic implants because a portion of the implant extends beyond the domain of the body's hard and soft tissues and into the hostile environment of the oral cavity. Since bone is very sensitive to infection, it would be quite desirable for the gingiva to attach to the implant in a manner similar to the junctional epithelium found in natural teeth. This would prevent bacteria and chemicals from penetrating the mucous membrane and entering and adversely affecting the osseous tissue. There is ongoing research and debate regarding the need for and existence of

a perimucosal seal at the gingiva/implant interface of successful dental implants. The presence of a perimucosal seal has been reported for implants made from Ti-Al_6-V_4 (Karagianes et al., 1974), epoxy resin (Listgarten and Lai, 1975), cylindrically shaped dense HA (de Putter et al., 1983) and titanium (Schroeder et al., 1981). Other studies have reported an inadequate epithelial attachment for many implant types placed in different species (Natiella et al., 1974; Hammner et al., 1970; Piliero et al., 1973). More recently, McKinney et al. (1988) unequivocally state that gingiva will regenerate around a transmucosal post " forming a new free gingival margin complete with sulcus and free gingival groove." Ten Cate (1985) asserts that stability of the bone surrounding the implant is a necessary requirement to obtain an adequate epithelial tissue attachment at the perimucosal interface.

Interfacial stress transfer A dental implant must achieve and maintain fixation with the surrounding cortical and cancellous bone to be successful. If the bone tissue surrounding the implant is subjected to stresses or strains that are less than or greater than the normal physiological range, then atrophy or resorption will occur over time, and the implant will loosen and fail. The design of a dental implant would be a standard engineering problem if the typical loading experienced by a dental implant and the magnitude of the physiological range of stresses and/or strains conducive to bone maintenance were known. It is known that factors such as the implant shape, the modulus of elasticity of the implant material, the type of attachment between the implant and bone and the amount and type of bone present at the interface affect the interfacial transfer of stress. How these factors affect the transfer of stress to the bone is quite often controversial or unknown. The last section of the literature review discusses the use of finite element stress analysis to evaluate the stresses in a dental implant and the surrounding bone.

Types of dental implants

All dental implants fall into one of three categories based upon their position in the jaw. Subperiosteal implants are placed in either the maxilla or mandible just beneath the outer surface or periosteum of the occlusal portion of the jawbone. They form a framework over the bone and do not become integrated within the bone. They are used primarily in edentulous patients who cannot use dentures due to extensive resorption of the occlusal surface or alveolar ridge of the jawbone. Subperiosteal implants are used mainly in the mandible (Williams et al., 1990).

Transosseous implants consist of two or four posts that are placed through bone for simple overdenture application and removable denture or limited fixed-denture applications, respectively (English, 1990). These implants penetrate the bone of the mandible from the inferior border, and are used in edentulous mandibles that have experienced extensive bone loss due to trauma or bone tumors (Williams et al., 1990).

Endosseous implants, which are the subject of this study, are placed within bone. They are further classified according to their shapes which are quite variable and include: blades, cylinders/cones, screws, hollow baskets, pins/needles as well as combinations of these basic shapes (English, 1990). According to Schnitman (1993), the type of implant chosen for clinical use depends upon the amount and condition of the bone which is required to accommodate the implant. If the bone has adequate dimensions in both the horizontal and vertical planes, than an endosseous implant will most likely be chosen. 88% of all the dental implants placed in 1990 were endosseous implants (Stillman and Douglass, 1993). The most commonly used endosseous implant is cylindrically shaped and consists of three parts: the fixture, the transmucosal abutment and the prosthesis retainer (Worthington, 1988). The fixture is that portion of the implant located exclusively in bone. It may be threaded, grooved, perforated or textured to provide a surface that is capable of mechanically interlocking with the surrounding bone. The transmucosal abutment is connected to the fixture by screws, cement or swaging in place. The abutment is also often secured via an internal or external hex at the occlusal end of the fixture for anti-rotation purposes. The prosthesis is attached to the abutment with screws, cement, or precision attachments.

The success of endosseous implant systems

Dental implants are designed to be permanent. It is difficult to comment upon the actual lifetime of dental implants because of the variability of the guidelines that have been used to define the success of implant systems. There is an accumulating body of experimental data, however, indicating that, in general, a successful implant may function for ten years or more (NIH Consensus Development Conference Statement, 1988).

The following list contains five success criteria developed by Albrektsson et al. (1986) in an effort to standardize the evaluation of different implant systems:

1. Immobility of an individual, unattached implant when tested clinically.
2. No evidence of periimplant radiolucency.
3. Less than 0.2 mm vertical bone loss annually after the first year in service.

4. Absence of pain, infection, neuropathy, paresthesia, or violation of the mandibular canal.

5. Implant system must fulfill the above conditions at a minimum rate of 85% after five years, and 80% after ten years in service.

According to Albrektsson and Sennerby (1991), based on the guidelines stated above, only one implant system, the Branemark system (Figure 16) manufactured by Nobelpharma, has demonstrated an acceptable fifteen year success rate. Branemark implants are threaded implants made from commercially pure titanium. Five hundred and twenty-four Branemark maxillary fixtures demonstrated a fifteen year success rate of 78%, and 480 mandibular fixtures showed a success rate of 86% over fifteen years (Albrektsson and Lekholm, 1989). Some very popular designs, however, such as Core-Vent, IMZ and Calcitek hydroxyapatite-coated implants, have not shown acceptable success rates even over a limited, five year period (Albrektsson and Sennerby, 1991).

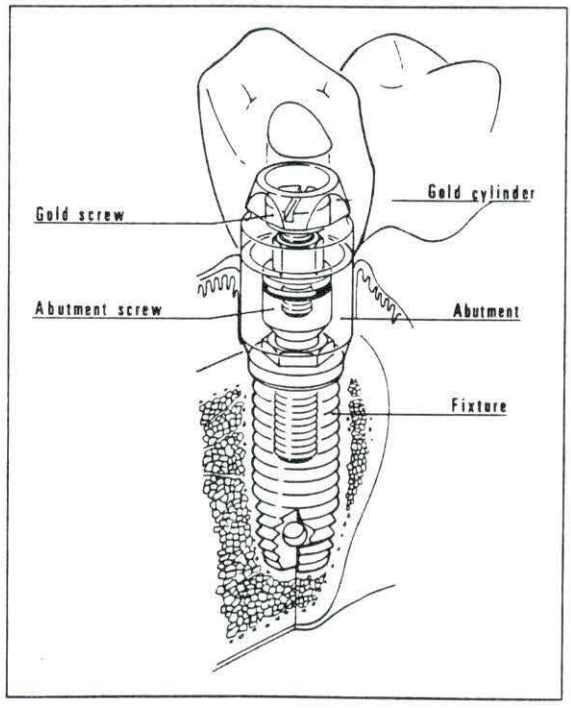

Figure 16. Components of a Branemark implant system (Rangert et al., 1989)

The American Dental Association (ADA) has developed similar guidelines, and compliance with their acceptance program is voluntary. Nobelpharma and IMZ, fully and partially edentulous arches with two or more units, and Oratronics, one-stage blade partially edentulous arches, have all been granted full acceptance by the ADA (Schnitman, 1993). Core-Vent, Integral, ITI and Steri-Oss implant systems as well as Nobelpharma single-tooth replacements have been granted provisional acceptance by the ADA (Schnitman, 1993).

Factors which affect the outcome of an implant procedure

There are many factors which influence the frequency of long-term success of endosseous dental implants. Linkow et al. (1990), after researching dental implants for more than thirty years, enumerated no less than twenty-four specific factors and the degree to which each one affects the outcome of implantation. These factors can be broadly categorized according to the quality of the surgical procedure, the physical health and mental attitude of the patient, the quality of the bone supporting the implant, and the design and manufacture of the implant. It may be interesting at this point to note that the Branemark implant system, which is considered the gold standard of dental implants, has stringent guildelines concerning patient acceptance and surgical procedure. It may be that the success of the Branemark implant system is equally or even more attributable to their stringent guidelines than to their implant design.

While most of the factors mentioned above act to either increase or decrease the probability of a successful outcome, there are some factors which, if present, negate any possibility of a successful outcome (Linkow et al., 1990):

- Septic operating conditions.
- Patients with uncontrolled diabetes mellitus, substance abuse, or blood dycrasias that compromise the healing of soft tissue and bone, chronic nutritional deficit, malabsorption syndrome or chronic digestive problems.
- Poor operator skill which results in bone necrosis or improper implant placement.
- Inadequate home maintenance and/or poor follow-up care.
- The use of a non-biocompatible implant material.
- Poor cleansing and passivation of implant before packaging.

One factor that is not readily controllable, but that has a significant and somewhat quantifiable role in determining the fate of a dental implant, is the location of implant placement. Implant survival is directly correlated to the bone density at the implant site which is quite variable throughout the jaw and maxilla. Bone density, and thus implant survival, is greatest in the anterior mandible and progressively decreases in the following locations (Schnitman, 1993):

1. The anterior maxilla which has less dense cancellous bone and a thinner cortex.
2. The posterior mandible which is of a hollow nature and contains the mandibular nerve.
3. The posterior maxilla which contains a hollow sinus and an eggshell-thin cortex.

In general, there is approximately a 10% difference in success rates between the maxilla and the mandible with long-term success greater than 95% in the anterior mandible, and approximately 72% in the posterior maxilla (Schnitman, 1993).

Finite Element Analysis

The finite element method is a computerized numerical technique of stress analysis which has been extensively implemented in traditional engineering fields (Zienkiewicz, 1988) and orthopedic biomechanics (Huiskies, 1983). The application of the finite element method in dental research began in the early 1970's (Farah et al., 1973) and has been used with two dimensional (2D), axisymmetric, and three dimensional (3D) finite element models to determine the stresses and strains in natural teeth, dental implants and their surrounding bone (Craig, 1986). This section will review finite element theory, describe the finite element process, and summarize current practices, assumptions and results associated with finite element analyses of dental implants.

Finite element analysis theory

Finite element analysis is based upon the displacement or stiffness method in which a mathematical expression describing the stiffness or resistance to deformation of the entire (global) structure is formulated. Displacements of various points in the structure described by this global stiffness formulation can then be calculated in response to various assigned

loads. These displacements are primary unknowns from which the secondary unknowns, stress and strain, are derived.

A mathematical model is developed by subdividing a representation of the structure of interest into a finite number of connected elements. The geometry of each element is completely defined by points or nodes that lie on its boundaries as well as an interpolation function (usually a polynomial) that describes the shape of its boundaries. The stiffness of each element is determined by its geometry and its assigned material properties. The global stiffness is then calculated by combining the individual element stiffnesses in a certain prescribed manner.

The displacement method assumes that the displacements of the nodes of an element are constrained to certain allowable displacements. The allowable displacement directions at each node are termed degrees of freedom (DOF). The polynomial which describes the displacements at the nodes is based upon the principle of minimum potential energy. This principle states that a loaded structure deforms in such a way that the energy stored within is minimal. When the allowable displacements are described by a function that is the same as the shape function that defines the element geometry, the elements are called isoparametric.

Finite element process

There are many commercial finite element processing codes available that may be used to perform a finite element analysis. To use one of these codes, a finite element model (FEM) must first be developed. Software, such as PATRAN Plus (PDA Engineering, California), is used as a preprocessor to create the FEM. The geometry of the implant-bone system is first input to the preprocessor. The operator then uses the preprocessor to create a mesh by subdividing the geometry into a large number of small elements. Each element is assigned the specific material properties associated with that portion of the actual implant-bone system which it represents. Boundary conditions are then assigned to the global structure and, if necessary, to the bone-implant interface. Once the model is created, loads are applied, and the model is submitted to the finite element processor for analysis.

An ideal FEM of an endosseous implant would be three dimensional in nature, and include the following:

- An accurate depiction of the gross geometry of the mandible.
- An accurate representation of the internal structure of the cancellous and cortical bone in the mandible and most particularly of the bone in contact with the implant.

- A fine mesh of elements (large number of small elements) with at least 30,000 degrees of freedom (Hart et al., 1992).
- Experimentally determined non-linear, viscoelastic, non-homogeneous bone properties of the cancellous and cortical bone of the mandible.
- Direct measurements of the actual loading that is applied to an *in vivo* dental implant in a mandible.

Unfortunately, most of the desired information listed above is unavailable. Furthermore, practicality suggests the use of the simplest model that will fulfill the purpose of the analysis. This implies that many assumptions must be made when creating a model of a biological system. Each assumption made detracts from the validity of the FEM. When finite element results are evaluated, these assumptions must be taken into account.

Finite element models

Three dimensional (3D) finite element models (FEMs) are becoming the state of the art in dental research. While many researchers have created 3D FEMs of the human mandible (Knoell, 1977; Elias and Brunski, 1991; Hart et al.. 1992), none have done any extensive implant design analysis using these models. An important characteristic of the finite element analysis is that as a mesh becomes more and more fine (more and more elements), the results approach or converge upon the actual mathematical solution for a particular model. Hart et al. (1992) determined that for a 3D FEM of a full mandible to be mathematically accurate, at least 30,000 DOF or 10,000 nodes were required. Most of the finite element models listed above use a much more coarse mesh. Even though a 3D model is more realistic than a 2D model, its results may be still be very inaccurate due to the coarseness of the mesh used.

It is generally held that a 2D model is sufficiently valid if it is used in a dental implant design parameter study and not to determine reference data (Huiskies 1983; Brunski, 1992). This is because the designer does not need to determine the actual magnitudes of stresses and strains, but rather, only needs to determine the stress and strain distributions of one design relative to another. According to Meijer et al. (1993), however, 2D FEM results did not yield results comparable to a 3D FEM in a design parameter study. This is corroborated by a similar study by Ismail et al. (1987). Interestingly, Meijer et al. (1993) also found that results from a 3D FEM of a portion of the mandible were comparable to those predicted with a 3D FEM of the entire mandible. Three dimensional models are not usually used in design

parameter analysis because they are difficult to construct, they use large amounts of computer time and resources, and their results are very difficult and time consuming to interpret. Furthermore, if you take into account that every time the implant geometry changes, the mesh needs to be recreated and material properties reassigned, it becomes apparent why there is a predominance of 2D FEM in dental implant design parameter analyses.

Many implant design parameter finite element analysis studies use a model which assumes that the implant is surrounded by a core of solid cortical or a combination of cortical and cancellous bone (Riegar et al., 1990; Clift et al., 1992; Siegale and Soltesz, 1989). While these studies are not very realistic, they do have the advantage that they allow for an easier comparison of implant design parameters since they remove the effect of interface variation from the results.

Types of 2D models Two dimensional finite element models use 2D elements that are plane stress, plane strain or axisymmetric formulations. Plane stress and plane strain formulations have been used extensively in dental implant analysis (Tesk and Widera, 1973; Atmaram, 1979; Kitoh et al., 1978; Lavernia et al., 1982; Paydar et al., 1991; Matsushita et al., 1990), but they are no longer as prevalent as axisymmetric formulations. A plane stress element is most often used to represent a "thin, membrane-like structure" (Hart, 1989). Plane stress constrains a structure from experiencing out-of-plane stresses but allows deformations outside of its plane of definition. Plane strain elements constrain structure deformation out-of-plane, but they permit stresses out-of-plane as long as there are no resultant strains. Plane strain elements are used to represent a structure that is constrained "to remain sandwiched between two rigid platens" (Hart, 1989). Plane strain elements seem to better represent a buccolingual slice taken from a mandible containing an implant than plane stress elements (Hart, 1989).

Axisymmetric elements are ring-like elements that are based upon a reformulation of plane strain or plane stress elements. They are associated with bodies of revolution about an axis of symmetry. Geometrically, they are 3D but mathematically are only 2D (Bickford, 1990). Unlike the other 2D elements, axisymmetric elements can account for hoop stresses. These elements are used most predominantly in 2D finite element models (Mihalko et al., 1992; Siegale and Soltesz, 1989; Riegar et al. 1990).

Interfacial boundary conditions Finite element stress analysis results are very sensitive to whether bonding is assumed to take place at the implant-tissue interface (Hipp et

al., 1985, Bidez et al., 1988; Brunski, 1988). If the implant is assumed to be bonded to the surrounding tissue, then the interface is capable of resisting compressive, tensile and shear forces. Interfacial bonding should be assumed only when the implant is composed of or coated with a bioactive material since it is believed that a chemical bond is formed between the two materials. Implants that are made from so-called bioinert materials such as titanium or titanium alloys should be modeled as having an interface of pure contact with the surrounding bone. Pure contact assumes that only compressive forces can be transmitted across the interface. Hipp et al. (1985) reported that finite element models of screw-shaped implants show areas of tensile displacement when no bonding (pure contact) takes place at the interface. A pure contact boundary condition should also be modeled at the interface if it is desired to model the implant surrounded by fibrous tissue (Skalak, 1988).

Material properties assigned to tissue surrounding an implant The tissues generally in contact with the root portion of an endosseous dental implant are cortical bone, cancellous bone and marrow, and/or fibrous tissue.

Bone The mechanical behavior of bone is not only very complex, but it is also highly dependent upon species, location, health and mechanical loading. Most FEMs assume bone to be a linear elastic material when it is actually anelastic. It is generally held, however, that this is a valid assumption since bone behaves similarly to a linear elastic material in the physiological range of stresses (Currey, 1984). According to Brunski (1992), all finite element analyses of dental implants have modeled bone as isotropic and homogeneous when it is actually anisotropic and nonhomogeneous. It is not difficult to model bone as anisotropic if the values of the elastic constants of a particular portion of bone are known. This type of data is very sparse, however, since it is very difficult to measure. Ashman and Van Buskirk (1987) used ultrasound techniques to determine the elastic constants of human mandibular cortical bone which was found to be orthotropic. Canine mandibular cortical bone was found to be isotropic with a modulus of elasticity of approximately 7.39 GPa (Ashman et al., 1985).

Cancellous bone is usually modeled in one of the following ways:

1. Young's modulus is assumed to have a value equal to 1/10th that assigned to cortical bone (Siegale and Soltesz,1989; Borchers and Reichart, 1983; Meijer et al., 1993).

2. Young's modulus is determined as some function of the apparent density

(material mass per specimen total volume) of the section of bone of interest (Knoell, 1977; Cook et al., 1982; Austriaccio et al., 1991).

3. Young's modulus is determined using Carter's empirically determined relationship between the compressive strength of any type of bone and its apparent density (d) :

$$\sigma_{cf} = 68r^{.06}d^{2} \text{ (MPa)} \qquad (5)$$

where r is the strain rate, and (σ_{cf}) is the compressive strength. The values of density are determined point by point from calibrated computed tomography scans. Values for all points within a given element are averaged (Bidez et al., 1992).

Whichever method is used, the cancellous bone is modeled as essentially a homogeneous material. This assumption does not take into account the mechanical contribution due to the inherent structural arrangement of the cancellous bone struts. Lavernia et al. (1981) investigated whether it mattered if the cancellous bone around an implant was modeled as homogeneous and or as individual struts. They found that both models yielded similar stress distributions but significantly different magnitudes.

The effect of the properties assigned to bone around the implant has also been investigated using finite element stress analysis. Borchers and Reichart (1983) found increased stress concentrations when the implant was modeled as if it were surrounded with cancellous bone (E=1.37 GPa) rather than cortical bone (13.7 GPa). Lavernia et al. (1981) reported that the state of stress predicted in a dental implant system is most dependent upon the elastic modulus assigned to the interfacial bone. Going one step further, Clift et al. (1992), using an axisymmetric finite element model of a hydroxyapatite coated Branemark implant in a bone plug, found that " the stress distribution in the bone surrounding the implant was highly dependent upon the density and Young's modulus of the bone and any component of lateral loading".

Fibrous tissue Some researchers postulate that a fibrous tissue layer would act as a pseudo-periodontal ligament and transfer stresses to bone in a similar fashion. This hypothesis has never been verified either experimentally or clinically. It has been found clinically that the presence of a fibrous layer is usually associated with implant failure due to loosening. The fibrous tissue is thought to predominate due to micromotion between the implant and the bone. Skalak (1988) asserts that the fibrous layer will result in a sliding or shearing response that may adversely affect the adjacent bone. Finite element studies have

been conducted to investigate the effect of a fibrous tissue at the interface (Buch et al., 1974; Privitzer et al., 1975). These studies indicate that this type of interface tends to dampen or eliminate stress concentrations that would occur if the implant were in direct contact with bone. Lavernia et al. (1982), in a similar study, found that a soft tissue interface "negates the effect of implant elastic modulus". This finding is supported by Borchers and Reichart (1983) using a 3D finite element model of an anchor-type Al_2O_3 dental implant. Brunski (1992) pointed out, however, that these results may be questionable since there is little experimental evidence available to indicate what boundary conditions most appropriately mimic the implant bone interface.

Implant design

The finite element method has been used in a number of studies to determine stresses and strains in dental implants and their surrounding bone. A major problem associated with any stress analysis of a bone prosthesis is that the biological significance of the stresses and strains predicted by the finite element analysis is unknown with any degree of certainty (Brunski, 1992). Results, therefore, must be interpreted in terms of trends found in various mechanical parameters and how they vary in response to changes in implant design, implant loading and tissue properties.

Crestal bone resorption Most implant failures are believed to be caused by implant loosening which results from bone resorption at the crest of the alveolar bone adjacent to the implant. This is commonly referred to as saucering (Parr et al., 1988; Steflik et al., 1992). This saucering phenomenon has been observed in many different implant systems (Soltesz et al., 1982; d'Hoedt et al., 1985; Nentwig, 1985; Clift et al, 1992). While factors such as material incompatibility, surgical technique, poor bone healing and infection are all possible causes of this resorption, the stress transferred to the bone at this sight appears to be the major cause of crestal bone resorption (Pilliar et al., 1991; Clift et al., 1992). Soltesz et al. (1982) and Huiskies and Nunamaker (1984) compared numerical calculations and experimental results and found a correlation between high stress and bone resorption. According to Soltesz and Siegale (1982), this overstressing may occur when there is direct bonding between the implant and the surrounding cortical bone. Riegar et al. (1990), using an axisymmetric FEM of commercial implants surrounded by a cortical bone core, predicted that three commercial designs could cause saucerization of crestal bone due to high stress transfer in this area. Due to the perception that a major cause of implant failure is

overstressed crestal bone, the goal of many finite element analyses is to minimize stress concentrations along the implant-bone interface, in particular, at the crestal interface (Pilliar, 1991; Clift et al., 1992; Atmaram, 1979; Siegale and Soltesz, 1989).

Implant shape Siegale and Soltesz (1989) used an axisymmetric finite element model (FEM) of different shaped implants placed in "blocks" of bone. It was found that implant shape significantly affected the stresses at the bone-implant interface. Implants with a cylindrical shape that were bonded to bone exhibited stress concentrations at the alveolar crest, but they showed stress concentrations near the implant base when they were merely in contact with the surrounding bone. Screw implants were found to have stress concentrations near each thread tip whether they were in contact with or bonded to the bone. Mihalko et al. (1992), using a 2D axisymmetric FEM of a titanium implant, found that the addition of two circumferential grooves provided a better stress transfer from the implant to the bone by reducing the shear stresses that would occur at the interface of an ungrooved, similar implant.

In a recent paper, Brunski (1992) uses the Siegale and Soltesz study (1989) to illustrate a problem that is prevalent in many typical finite element studies of dental implants. This study reports that a fixed-bond interface, in which compressive stresses range from 1.5 to 5 MPa, is preferable since it provides a more uniform stress distribution at the interface than a contact only interface in which compressive stresses range from 6 to 25.4 MPa. Brunski asserts that, first of all, there is no proof that a uniform stress distribution is beneficial. Secondly, he thinks that if these predicted stresses (1-25.4 MPa) are compared to the uniaxial strength of bone, which is approximately 100 MPa, or its uniaxial fracture stress of 150-200 MPa, then all implants in this study will provide a safe transfer of stress to the surrounding bone. Brunski concludes that neither this study (Siegale and Soltesz, 1989) nor any other similar study has succeeded in determining an optimal shape for a dental implant as regards stress transfer to bone.

Implant elastic modulus The effect of implant modulus on interfacial stresses has also been investigated with finite element analysis. Privitzer et al. (1975) reported that for a fixed implant shape, a change in implant elastic modulus caused little change in the bone stress distribution. Cook et al. (1981) compared LTI carbon (E~14 GPa) to Al_2O_3 blade-type dental implants (E~350 GPa) and found that LTI implants produced stresses approximately 3 times larger in the crestal bone area than Al_2O_3 implants. No studies have

indicated an optimal implant modulus (Brunski, 1992). Riegar et al. (1990) reported that if E (implant)/ E(bone) increases, stresses at the crest decrease, and the stresses increase at the base of the implant.

Implant diameter Matsushita (1990), using a 2D finite element method of a hydroxyapatite implant bonded to surrounding bone, found that the stress concentrations in cortical bone decreased inversely to increasing implant diameters.

MATERIALS AND METHODS

This study involves a two-dimensional finite element stress analysis of a dental implant placed in a canine mandible. The overall finite element process is summarized in Figure 17 and involves the creation of a finite element model with a pre-processing program, the submission of the completed model to a finite element analysis package, and the post-processing and interpretation of the analysis results.

Finite Element Model (FEM) Generation

A finite element model is developed by inputting the geometry and behavior of the real system to a pre-processing program which is used to subdivide or mesh the global geometry into a large number of small elements. The materials and methods used to formulate the geometry and mesh of the various finite element models employed in this study are described below. The assignment of material properties to specific elements and boundary conditions to the global structure is then reviewed. The pre-processing program used in this study to create the FEM was PATRAN Plus (PDA Engineering, Costa Mesa, CA).

Geometry

Biological specimen In a previous study (Niederauer, 1990) ceramic composite dental implants were placed in the premolar region of 10 dogs. The ceramic composite, called osteoceramic, was developed by Dr. Thomas McGee at Iowa State University and consists of equimolar quantities of magnesium alumina spinel and α –calcium phosphate tribasic. Following euthanasia, the dogs' mandibles were sectioned into blocks, each containing a single implant, and fixed in 70% ethanol (Niederauer, 1990). These specimens were then dehydrated and embedded in Spurrs' standard medium A (Niederauer, 1990). One of these specimens was used to develop the finite element models used in this study. This particular specimen contained an implant that had been placed for 20 days in the left, front premolar region of dog #8736 (Niederauer, 1990). The specimen was sectioned using a Buehler Isomet Low Speed saw, model 11-1180 (Buehler, Evanston, IL), with a 5 inch high-concentration wafering blade. The sections were cut at a speed of 5.5 using a cutting fluid, CO-102 (Mager Scientific Inc., Dexter, MI), as a lubricant. The center section (#8) of this specimen, which was 472 μm thick, was then microradiographed with a Faxitron X-ray

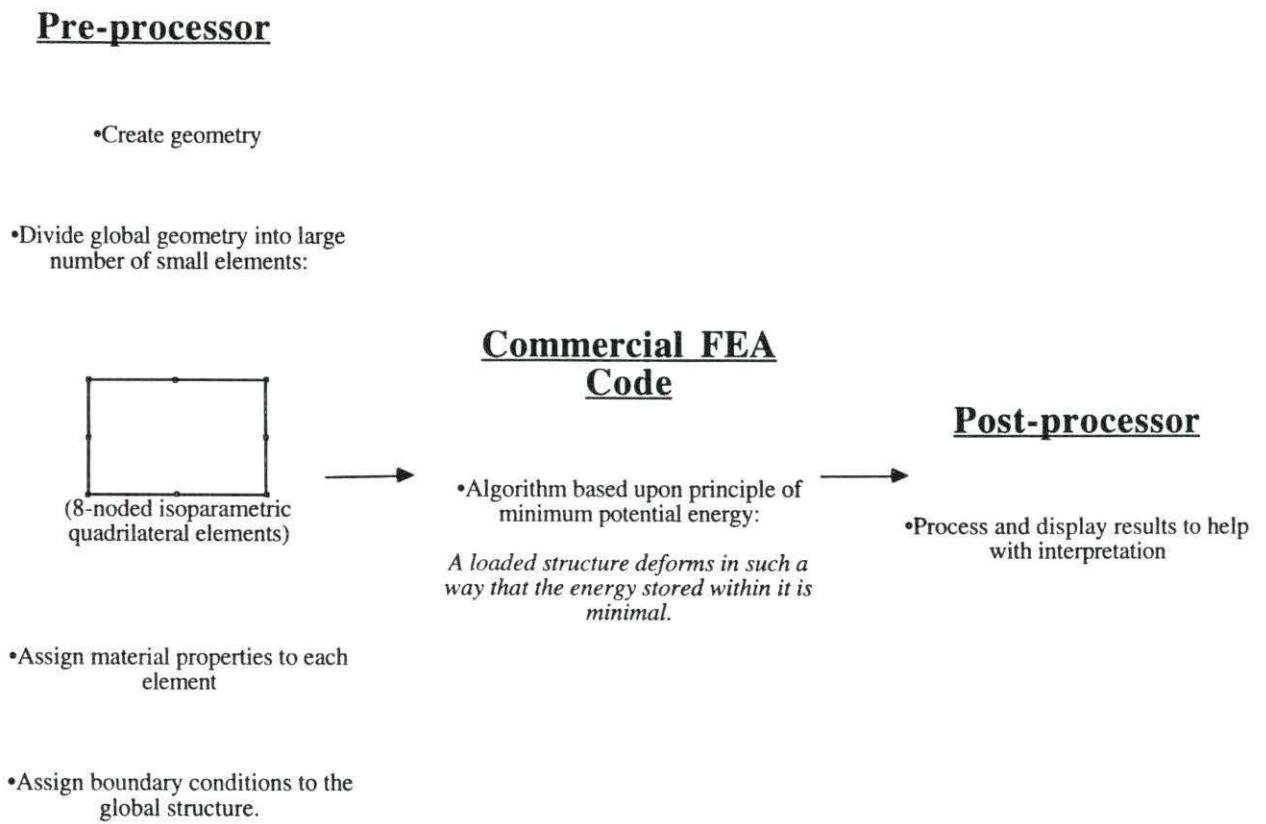

Figure 17. Overview of the finite element process

Inspection System (Field Emission Corp., McMinnville, OR), operated at 20 mA and 68 kV for 20 seconds. Kodak electron microscope film was used and developed on a DENTX 9000 developing machine.

Image analysis and processing The microradiograph of the center section of the bone/implant system was transilluminated using a ChromaPro 45 lightbox and viewed with a Sony DCX-3000A color video camera. The resulting image was captured and processed using a Zeiss SEM-IPS image analysis system (Zeiss-Kontron, IBAS version 2.0). The capabilities of this system allowed the removal of the implant from the image by tracing its edges using a digitizing tablet. This was done because the specimen section was slightly oblique and didn't properly represent the true center section of the implant. This action also dramatically reduced the amount of data generated. Every pixel that represented every strut of cancellous bone and cortical bone was extracted from the image and transferred to a software program called PV-WAVE (Visual Numerics, Boulder, CO). This program was used to assign x-y coordinates to each of these pixels. The PV-WAVE output was converted, using a short C program, to a neutral file format that was required for input to PATRAN . Appendix A contains a short listing of the PV-WAVE file format. Appendix B contains a printout of the format conversion program. Appendix C contains a sample of the neutral file format required for input into PATRAN. Figure 18 is a video print of the microradiograph used as the source of the FEM. Compare Figure 18 to the image shown in Figure 19 which is the digital image input to PATRAN. The generation of the geometry of the implant/bone system was completed by drawing an appropriately dimensioned, center cross-section of the dental implant and properly positioning it within the digital image.

Mesh

Patches The image originally input to PATRAN was essentially a series of points or grids in space. This is not a structure suitable for a finite element analysis. These grids were used as guidelines to create a two-dimensional surface representative of the histological section. Patches are geometric entities used in the pre-processing software, PATRAN, that are continuous surface regions which are represented as bicubic parametric surfaces (PATRAN Plus User Manual, 1990). These patches were usually created by designating 4 grids as corners of a quadrilateral or by creating curved lines from grids located at rounded portions of the image and creating a patch between two of these lines.

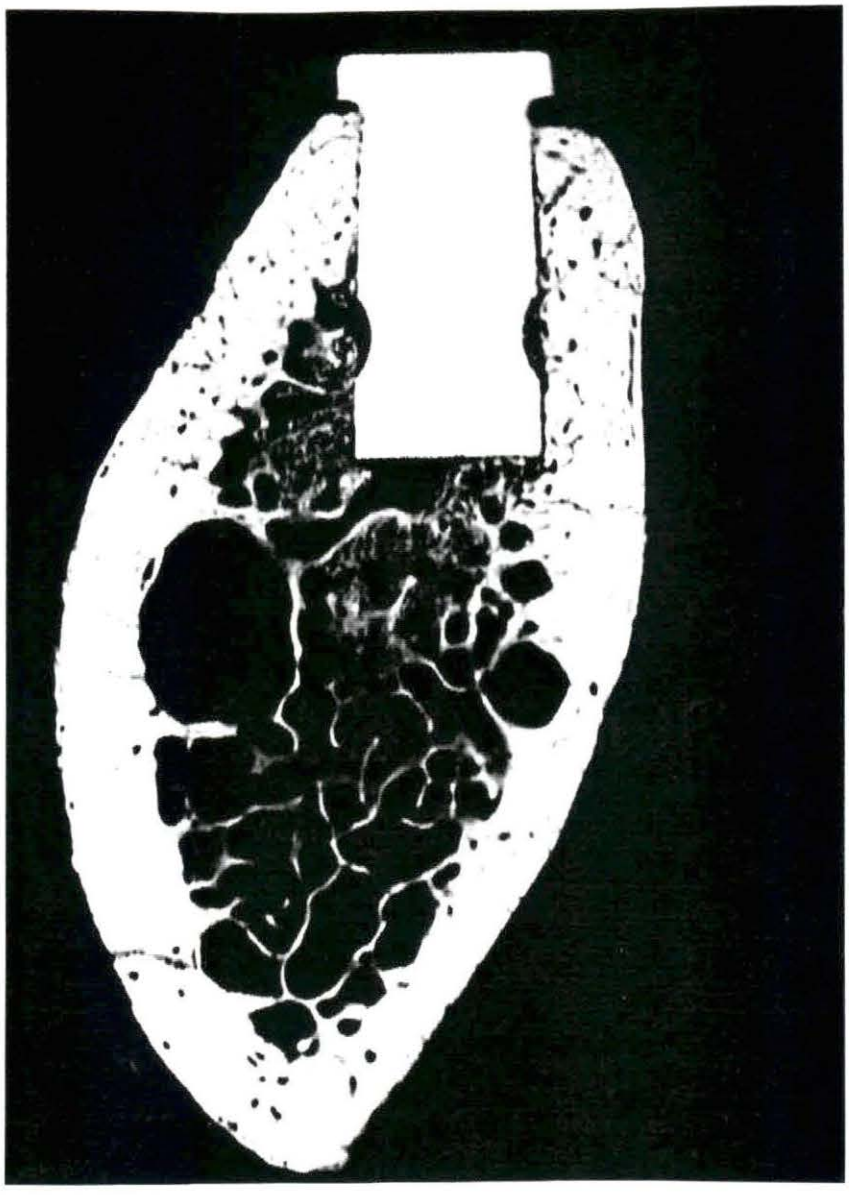

Figure 18. Video print of a microradiograph of the center section of an osteoceramic dental implant placed in the left, front premolar area of a canine mandible of dog #8736 (Niederauer, 1990)

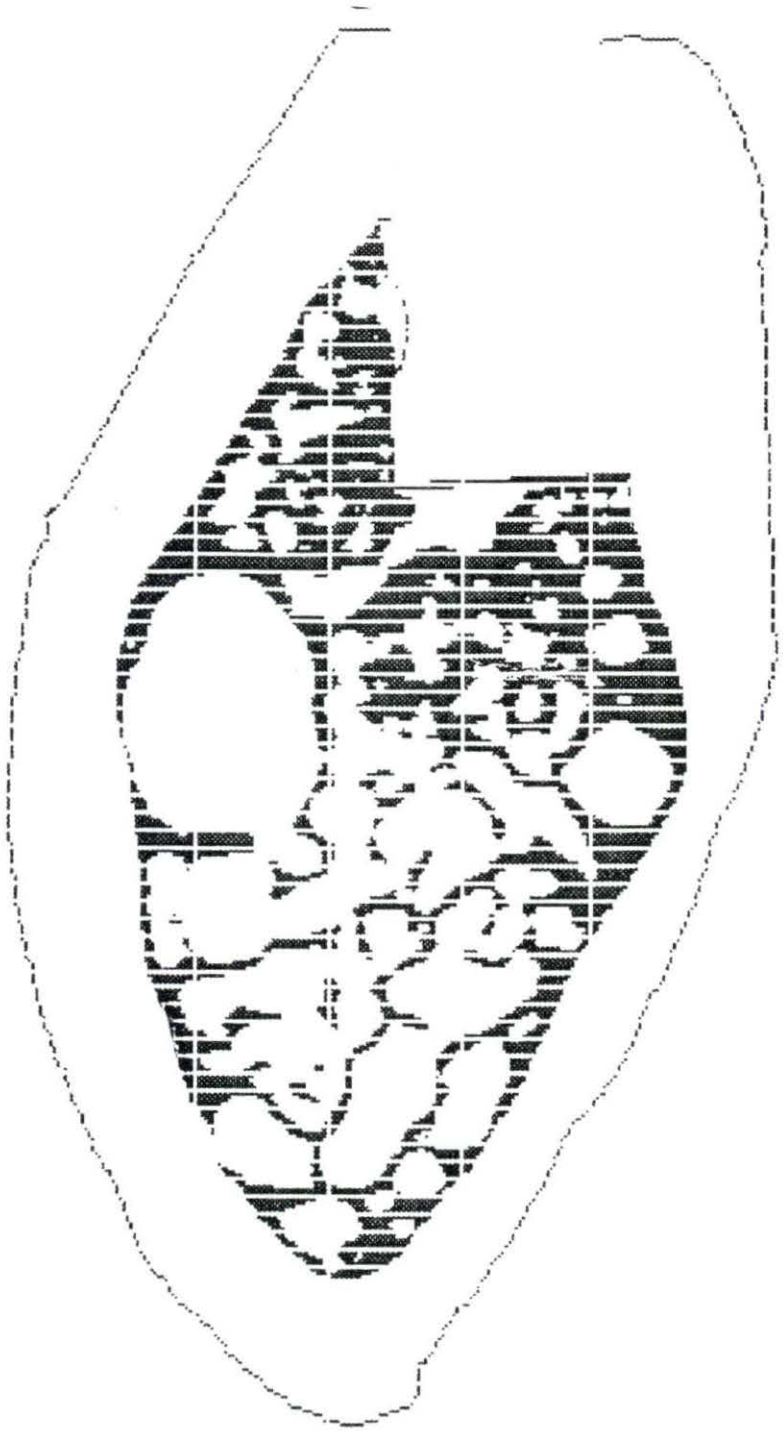

Figure 19. Digital image of the microradiograph shown in Figure 18 as input to the finite element preprocessor program PATRAN (PDA Engineering, Costa Mesa, CA)

All patch edges were constrained to be contiguous to no more than one other patch edge, and patches could not overlap areas that had different material properties. For example, one patch could not cover an area of cancellous bone and an area of cortical bone. Every effort was made to create patches that were not unduly warped or deformed since this simplified the meshing operation. Figure 20 shows the final two-dimensional representation of the original image.

Generating elements A mathematical model is typically developed by subdividing a given geometric structure into a finite number of connected elements. The geometry of each element is then completely defined by points or nodes that lie on its boundaries and an interpolation function (usually a polynomial) that describes the shape of its boundaries. Two types of elements were used in this study: an 8-noded, isoparametric, plain strain, quadrilateral element and a six-noded, isoparametric, plain strain, triangular element.

Each quadrilateral element was assigned eight nodes, which allowed a node to be placed in the middle of each edge of the element. This permitted each edge to become curved, if necessary, to more accurately model the curved geometry so often present in biological entities. Interpolation along each edge of the 8-noded quadrilateral is quadratic instead of linear as in 4-noded quadrilaterals elements. This significantly improves the accuracy of the analysis (Bickford, 1990). This element is recommended for use in a 2-D FEM by Hart (1989) because it is complex enough to accurately approximate displacements but not too complex to allow a sufficiently fine mesh to be developed for the analysis. Six-noded triangular elements were automatically assigned in areas where the geometry was too irregular to accommodate the quadrilateral elements. Six nodes were assigned to these elements to allow the edges of the triangle to also curve, if necessary. Figure 21 shows a typical representation of an 8-noded quadrilateral element and a 6-noded triangular element.

All of the elements of the model were isoparametric elements. Isoparametric elements have allowable nodal displacements that are described by a function that is the same as the shape function that defines the element geometry. This type of element is usually considered to be the most desirable (PATRAN Plus User's Manual, 1990). A useful characteristic of isoparametric elements is that they will always approach the exact mathematical solution from below. This means that any result will either be mathematically accurate or will slightly underestimate the exact mathematical solution. This is referred to as *h*-convergence.

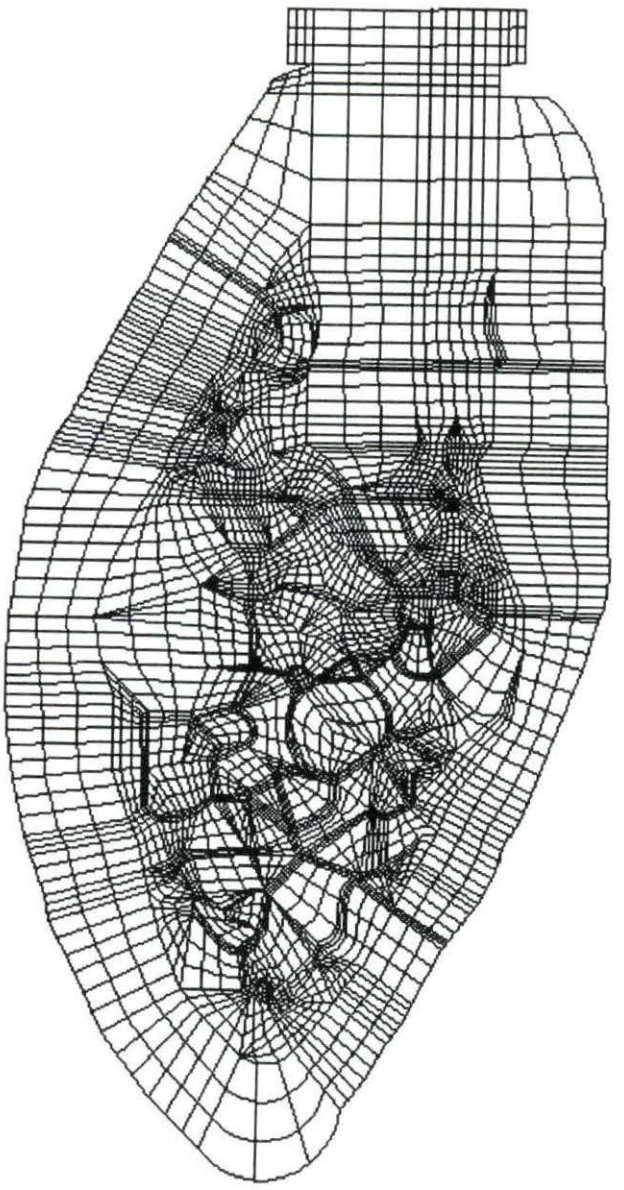

Figure 20. Two-dimensional surface created from the digital image of Figure 19 using patches

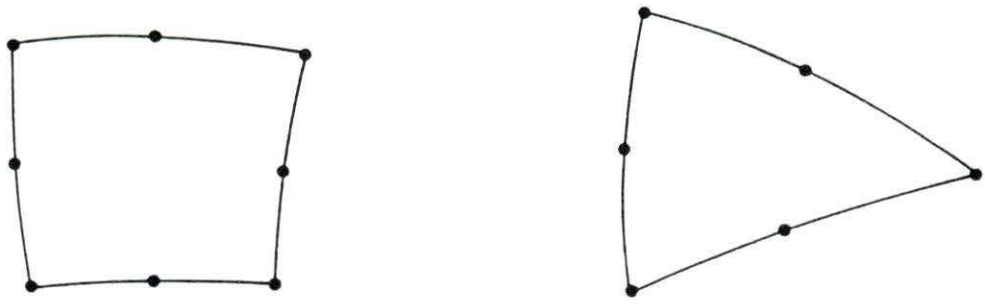

Figure 21. Typical 8-noded quadrilateral and 6-noded triangular elements that were used in this study to subdivide the global geometry

Each element was assigned plane strain properties. Plane strain elements constrain structure deformation out-of-plane but permit stresses out-of-plane as long as there are no resultant strains. Plane strain elements are used to represent a structure that is constrained "to remain sandwiched between two rigid platens" (Hart, 1989), or to model a thick structure with a constant cross sectional shape (PATRAN Plus User's Manual, 1990). Plane strain elements seem to better represent a buccolingual slice taken from a mandible containing an implant than do plane stress elements (Hart, 1989). Figure 22 shows a canine mandible and the approximate position from which the bone/implant section was taken. This figure illustrates how the 2-D biological section fits the plane strain assumption used throughout this study. Plane strain elements require all loads to be applied in the plane of the section. Out-of-plane (Z) strain is assumed to equal zero, and the normal stress in the Z direction is generally not zero. The section is assumed to have a unit thickness which in all finite element models was equivalent to 1 mm. Plane strain elements assume that ε_{xx}, ε_{yy}, and ε_{xy} are nonzero and that σ_{xx}, σ_{yy}, σ_{zz} and σ_{xy} are non zero as well.

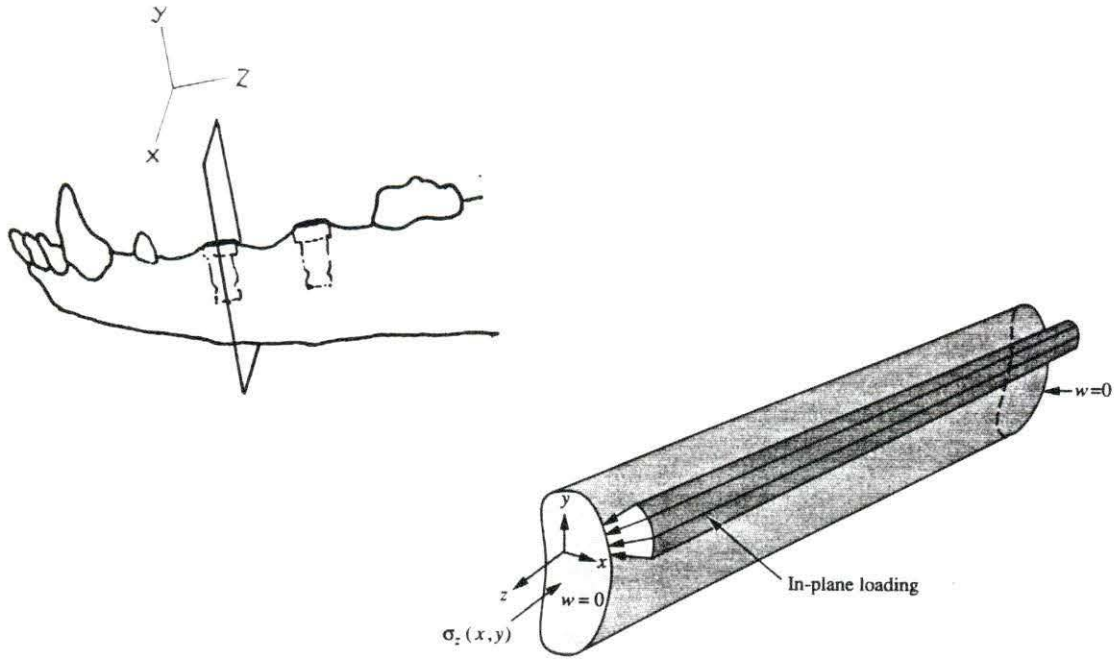

Figure 22. Comparison of a mandibular section to a typical plane strain configuration

Each patch was subdivided or meshed separately. Patches that shared common edges were required to each have the same number of elements. Care was taken to use a large enough number of elements in each patch so that the quadrilateral elements would remain as square as possible. According to Bickford (1990), the ratio of the longest to the shortest end of the quadrilateral, known as the aspect ratio, should be less than approximately 2.50 to 3.00. Only 28 of the 2,915 quadrilateral elements used to create the finite element mesh had an aspect ratio greater than 3.00, and only 12 of these had aspect ratios greater than 3.50. The largest aspect ratio measured 4.58. Figure 23 shows the mesh that was developed. Note that in certain areas, where large stress and/or strain gradients might be expected, every effort was made to decrease the size of the elements to more accurately represent these gradients.

Convergence A convergence test was run to determine if the mesh was fine enough to ensure the mathematical accuracy of the analysis results. As the number of elements or

nodes used to discretize the geometric structure increases, the accuracy of the analysis increases (Hart, 1989). A point is reached, however, when further increasing the number of elements no longer significantly improves the solution accuracy. This point is referred to as the point of convergence, and it determines the degree of mesh refinement required for a particular analysis.

Specifically, the implant/bone geometric model was first meshed with a very coarse mesh. A finite element analysis was run, and displacements at 4 nodes were determined. These nodes were chosen because they were located in areas of material property discontinuity, where large stress/strain gradients were anticipated, which would require the greatest number of elements to ensure mathematical accuracy. Then the mesh was further refined by increasing the number of elements, and displacement results were again determined for the same 4 nodes. This procedure was repeated to the limit of our computational resources. Figure 24 is a graph of the displacements at each of the four nodes versus the number of nodes in a given FEM. This graph clearly shows that convergence occurs near 3000-4000 nodes. Since either approximately 5000 or 9200 nodes were used in every FEM developed in this study, it is safe to say that the mesh was sufficiently fine to ensure the accuracy of the mathematical analysis.

Material properties

All elements were assumed to be linear elastic, homogeneous and isotropic. Since the behavior of any isotropic material can be adequately characterized by specifying the values of two technical constants, each element was assigned a value for the modulus of elasticity (E) and Poisson's ratio (ν). Three different types of finite element models were developed; each of these modeled the cancellous bone of the buccolingual section in a different way. The development of each model is described below.

Homogeneous model Figure 18 illustrates the actual buccolingual section of the dental implant/mandibular bone system which was modeled. Note that the outer shell of dense bone is cortical bone and that the composite structure of bone struts and intertrabecular spaces contained within this shell is referred to as bulk cancellous bone. Based upon a study by Ashman et al. (1985), in which ultrasound techniques were used to determine that canine mandibular cortical bone was isotropic, every element that represented cortical bone was assigned an $E = 7.39$ GPa and a $\nu = 0.403$.

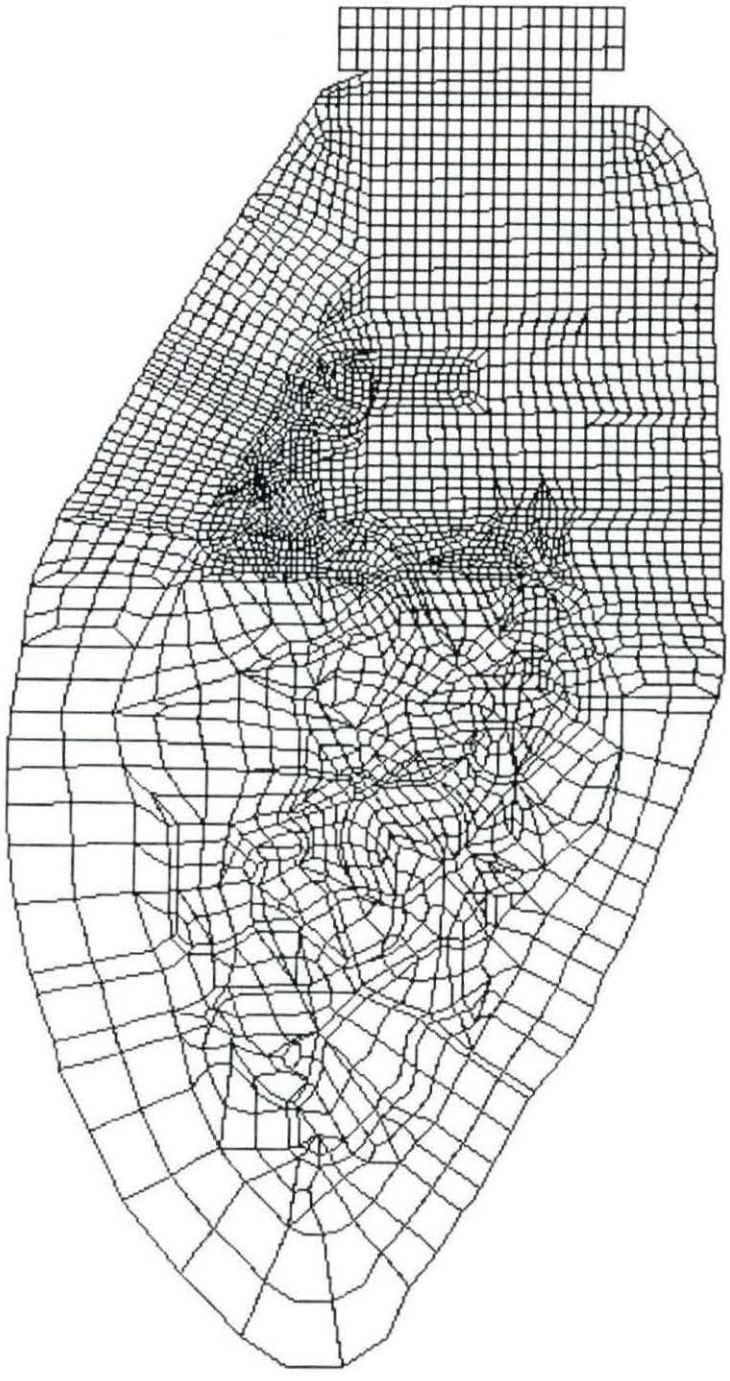

Figure 23. Finite element mesh used for all finite element models

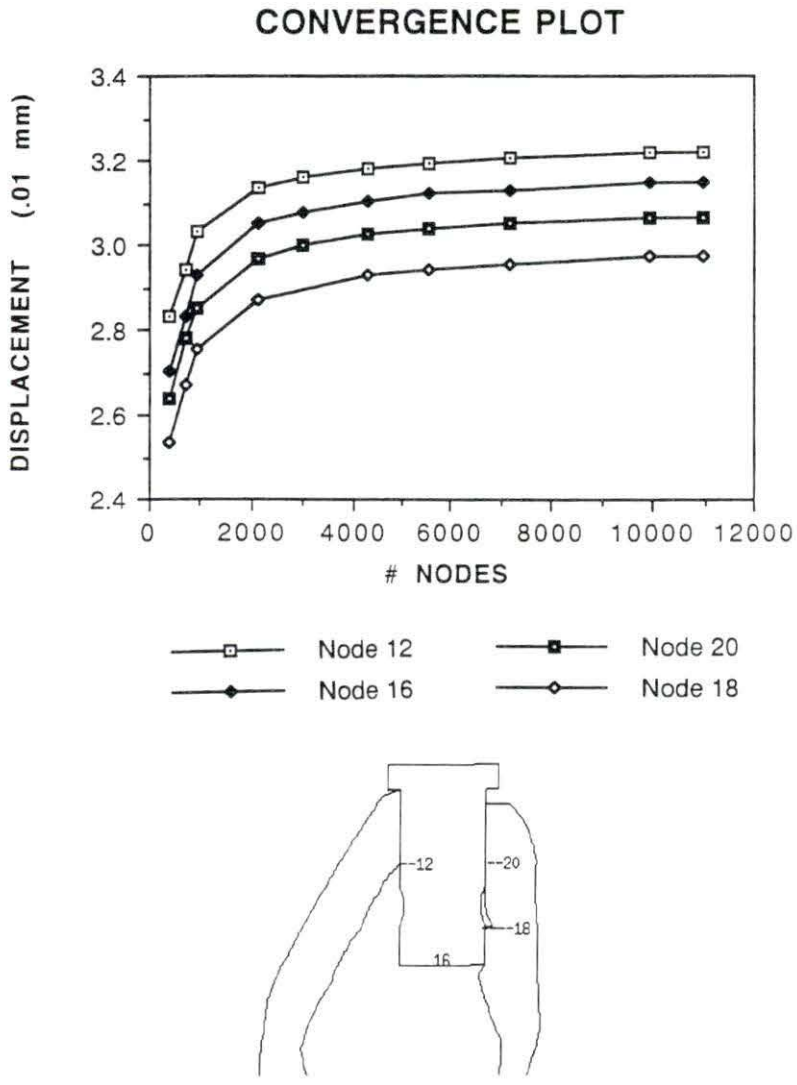

Figure 24. Finite element displacement convergence test results indicating that convergence occurs with 3000-4000 nodes. Note that the nodes chosen are located in areas likely to experience large stress/strain gradients

The implant was assigned an E = 114 GPa (Graves, 1988) and a $\nu = 0.25$. The bulk trabecular bone was assumed to be a single homogeneous material, and each element was assigned $\nu = 0.30$ (Keaveny and Hayes, 1993). The determination of a single approximate value of E for this entire area is described in the following section.

Modulus of elasticity The E of this homogeneous or bulk representation of cancellous bone was determined based upon the apparent density of the bone in this area. There have been many empirical determinations of E as a function of apparent density for bulk trabecular bone test specimens from a variety of locations, species and loading directions (Goldstein et al., 1983; Stone et al., 1983; Mente and Lewis, 1987). The following power law relationship was determined experimentally by Kuhn et al. (1989) from 130 specimens of canine femoral cancellous bone that were orthogonally tested in uniaxial compression at a strain rate of .01 s^{-1}:

$$E = 572 \, x^{1.39} \quad (r = 0.89) \qquad (7)$$

where E is the mean modulus of elasticity (MPa) of cancellous bone and x is the apparent density (g/cm^3). According to Austriaco et al. (1991):

$$x = V_f \rho_m \qquad (8)$$

where V_f is the volume fraction of the bone material within the entire cancellous bone area (volume occupied by bone material/volume occupied by bone and intertrabecular spaces) and ρ_m is the real density of the trabecular bone material (bone mass/volume occupied by bone material). Gong et al. (1964) determined that the real density of canine vertebral trabecular bone is 1.911 g/cm^3. Since the volume fraction of bone can be estimated by a measurement of the area fraction (A_f) of bone according to the Delesse principle (Weibel, 1979), the following equations, derived from equation (7), are valid:

$$E = 572 \, (V_f \rho_m)^{1.39} \qquad (9)$$

$$E = 572 \, \{ (A_f) (1.911) \}^{1.39} \qquad (10)$$

where A_f is the area of trabecular bone material divided by the total area occupied by the bone plus the intertrabecular spaces. Equation (10) is the final form of the equation used in this study to determine the E of the bulk cancellous bone structure contained within the cortical shell of the buccolingual section in Figure 18.

To determine the area fraction measurement of the bulk cancellous bone, a digital image of the microradiograph of the center section of the bone/implant system was again acquired by the ISU Image Analysis Facility using a Zeiss SEM-IPS image analysis system (Zeiss-Kontron; IBAS version 2.0). This image was digitized to a 512 x 480 pixel spatial resolution and 256 gray levels. Using a digitizer, a contour line was drawn between the cancellous bone/cortical bone interface and the cancellous bone/implant interface. The image within the contoured perimeter was extracted from the whole image, effectively isolating the entire cancellous bone area. Any pixel that had a gray level greater than or equal to 127, was designated as bone by the IBAS software (version 2.0). This gray value level of 127 was determined subjectively from direct observation of the image. Standard IBAS software (version 2.0) then calculated that the area fraction of the bulk cancellous bone was 0.375. Putting this value into equation (10) yielded a modulus of elasticity equal to 360 MPa which was assigned to every element that represented either cancellous bone struts or intertrabecular spaces. This method was also used to obtain the modulus of elasticity of selected portions within the bulk cancellous bone area in the two models described in the next sections. Figure 25 illustrates the material distribution for the homogeneous model and the mechanical properties assigned to these materials.

Partially inhomogeneous model This model is similar to the homogeneous model described above. The material properties assigned to every element representing cortical bone and the dental implant were the same. The cancellous bone, however, was modeled slightly differently. Instead of determining one value for the modulus of elasticity which represents the entire area of the section that is occupied by the bulk cancellous bone structure, several values were determined that represented small portions of the cancellous bone area. According to a finite element study of the human patella performed by Hayes et al. (1982), it is more important to take into account the variation in the density and thus the E of the bulk trabecular bone than to model the bulk trabecular bone as anisotropic. This model tried to account for the variation in the density, and thus area fraction, of the bone.

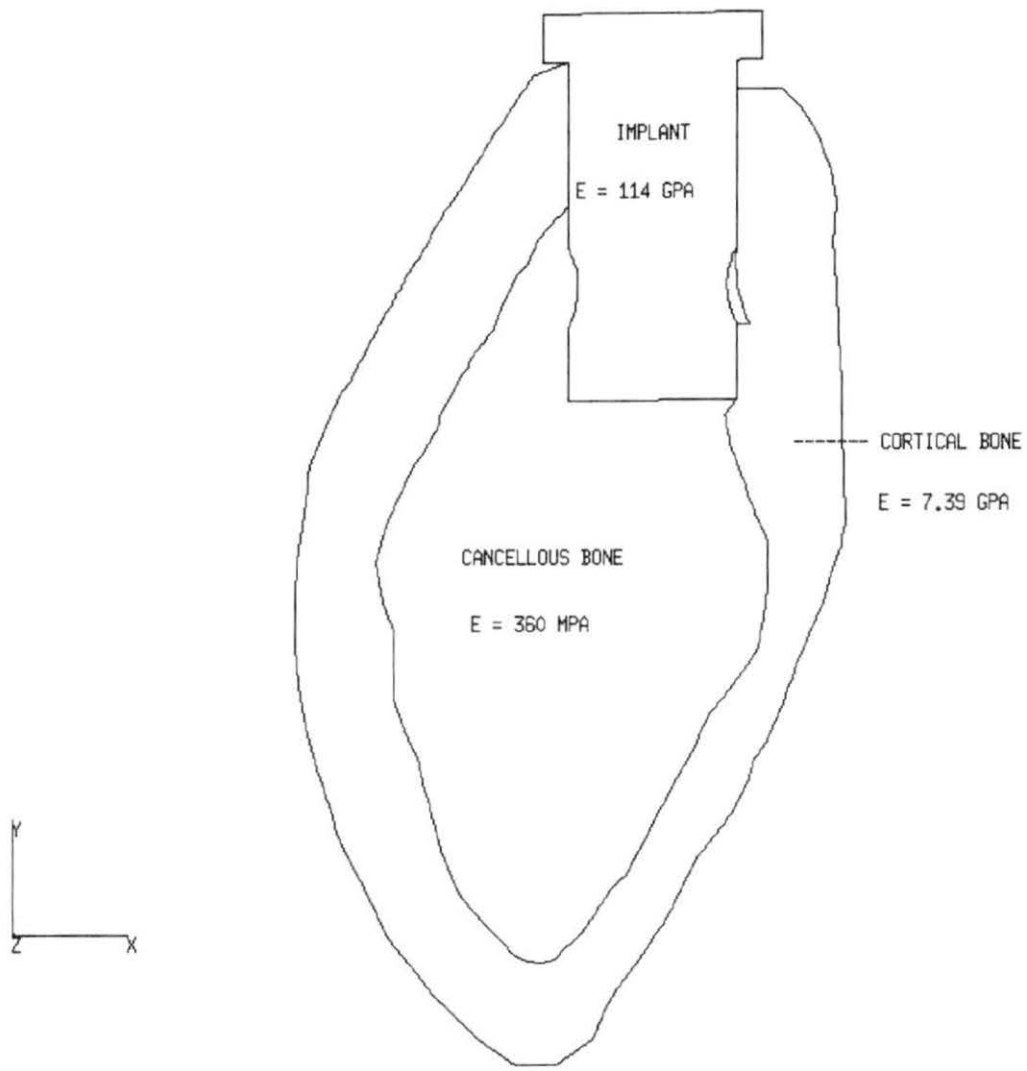

Figure 25. Material property distribution for the homogeneous finite element model

The surface of the section occupied by the bulk cancellous bone was divided arbitrarily into 14 subsections. The coordinates of each of these subsections were used to select the corresponding area on the image previously extracted using the Zeiss SEM-IPS image analysis system, in order to determine the area fraction of the entire cancellous bone structure. The area fraction of each of these 14 separate regions was determined using standard IBAS software. Figure 26 lists the area fraction and resultant modulus of elasticity as determined from equation (10) for each of the 14 regions. Poisson's ratio for each element was assigned a literature value of 0.30 (Keaveny and Hayes, 1993). Figure 26 shows the material distribution for the partially inhomogeneous model and the mechanical properties assigned to each of these materials

Strut model The cortical bone and the implant were represented the same way in this model as in the previous models. In the strut model, however, an attempt was made to model each spicule of cancellous bone as a separate entity relative to the intertrabecular spaces located in-between. Some struts of bone, not visible in Figure 18, were added to the model. This was done because, in normal circumstances, trabecular bone struts constitute a 3-D continuous structure that efficiently transfers stress. A 2-D representation, such as that shown in Figure 18, will indicate a lack of continuity in this structure that is not realistic. The struts added to the model were approximated very subjectively from the histological sections that were adjacent to the center section. These adjacent sections showed the orientations of the bone spicules that were not in the plane of the section modeled but that were required to adequately represent the continuity of the trabecular structure.

There are several areas near the implant that clearly indicate the presence of bone but not individual struts (Figure 18). These areas are most likely areas of woven bone since this implant was only *in vivo* for 20 days. Each of these areas was assigned a modulus of elasticity based upon the density of bone in that area. Using the Zeiss SEM-IPS image analysis system (Zeiss-Kontron, IBAS version 2.0) as described previously, a contour was drawn around each of these ambiguous areas to separate it from the rest of the digital image. The area fraction of each of these individual subsections was calculated by standard IBAS software and put into equation (9) to obtain the modulus of elasticity of each area. The individual struts were assigned the same modulus of elasticity as the cortical bone (7.39 GPa) and a Poisson's ratio of 0.30. Figure 27 shows the material distribution for the strut model and the mechanical properties assigned to each of these materials.

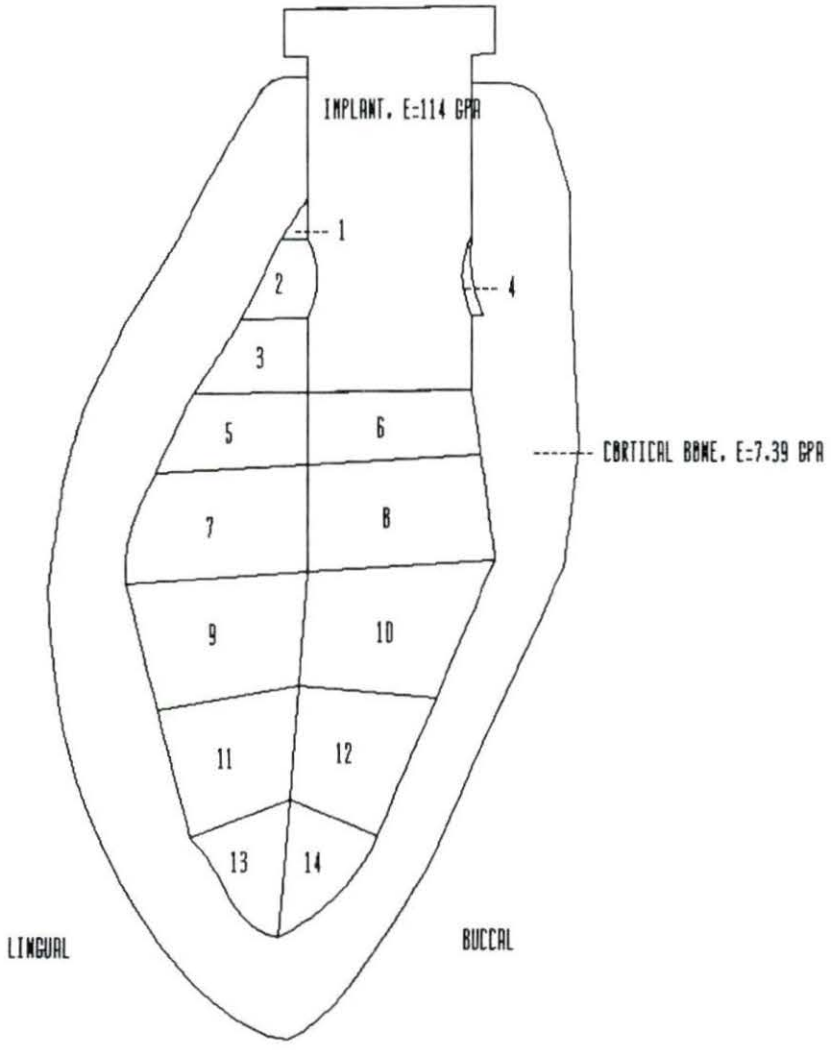

Section	Area Fraction (%)	E (MPa)
1	100.00	1402
2	21.77	169
3	69.34	846
4	23.88	192
5	73.58	919
6	49.21	525
7	26.53	222
8	72.30	897
9	17.10	121
10	31.48	282
11	18.11	131
12	22.35	175
13	21.58	167
14	16.43	114

Figure 26. Material property distribution for the partially inhomogeneous finite element model

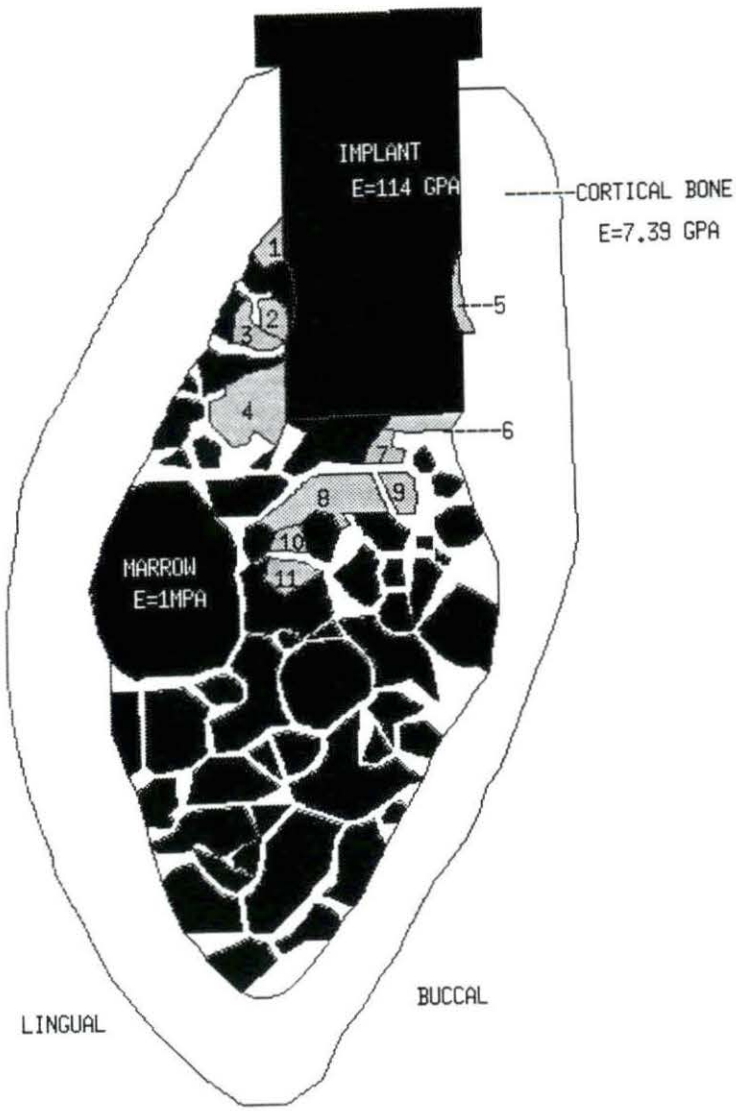

Section	Area Fraction (%)	E (MPa)
1	100.00	1402
2	86.11	1139
3	63.23	742
4	85.50	1128
5	65.85	784
6	70.71	866
7	66.98	803
8	82.86	1080
9	71.87	886
10	51.72	561
11	23.88	192

Figure 27. Material property distribution for the strut cancellous bone model

Boundary conditions

Displacement constraints Figure 28 shows the boundary constraints used in each finite element model to limit the rigid body motion of the global structure. Each circled node was constrained from moving in the x and y directions. This type of constraint is typical of previous 2-D finite element studies (Lavernia et al., 1981; Kitoh et al., 1978; Matsushita et al., 1990). The bone/implant interface was assumed to be fully bonded due to the bioactive nature of the osteoceramic. Nodes common to the implant and the bone, therefore, experienced the same deformation to a given loading.

Loading There is not much data available regarding the physiological loading on a submerged dental implant in humans, let alone in canines. Brunski and Hipp (1984) reported limited strain gage data describing the axial forces applied to dental implants placed in the premolar region of a canine mandible. They found that most of the bite forces, in all dogs, were less than 30 N. One dog registered a bite force as great as 150 N. According to Brunski (1993), forces as great as 500 N have been observed in other studies. Most of the analyses in this study subjected the implant to a 30 N compressive load applied at an angle 15 degrees from the vertical, as shown in Figure 28. This introduces a relatively small horizontal force of 7.76 N, applied from the lingual to the buccal surface, that more accurately represents physiological loading. The portion of the study which determined the maximum tensile stresses experienced by the implant also investigated some of the larger stress magnitudes observed, which were applied at various angles.

Analysis

P/FEA is a module in the PATRAN Plus system that is a general purpose finite element code capable of solving a wide variety of structural problems. P/FEA uses the finite element displacement method. The completed finite element models were submitted to P/FEA as static equilibrium problems. They took approximately 2.5 hours to process.

Three separate investigations were conducted; each of which involved the submission of one or more finite element models to P/FEA:

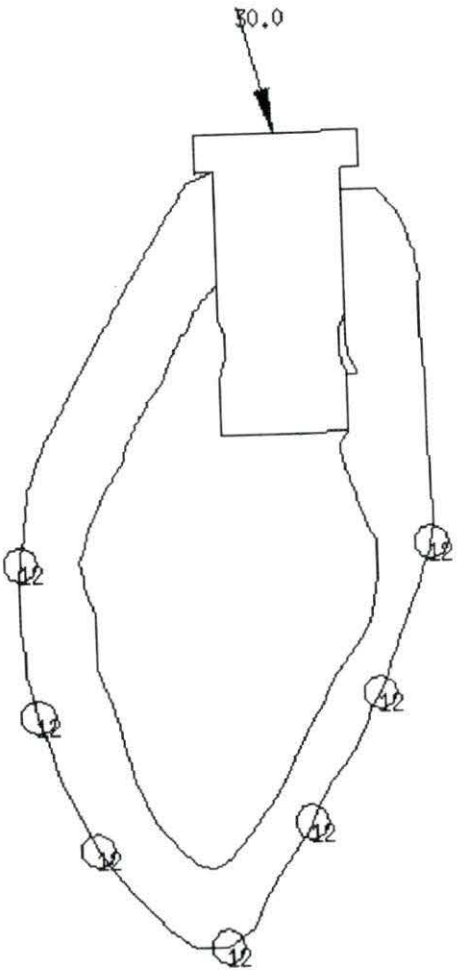

Figure 28. Boundary conditions applied to all finite element models

1. The first study used the homogeneous model to predict the location and approximate magnitude of the maximum tensile stresses experienced by the implant due to physiological loading. Since the osteoceramic material used for the dental implant is weak in tension, it is important to obtain a reasonable estimate of the tensile stresses it is likely to encounter *in vivo*. Forces of 30 N, 150 N and 500 N were applied to the implant at each of the following angles relative to the positive x-axis: 90°, 105°, 135° and 165°. Figure 29 illustrates the directions of these applied forces.

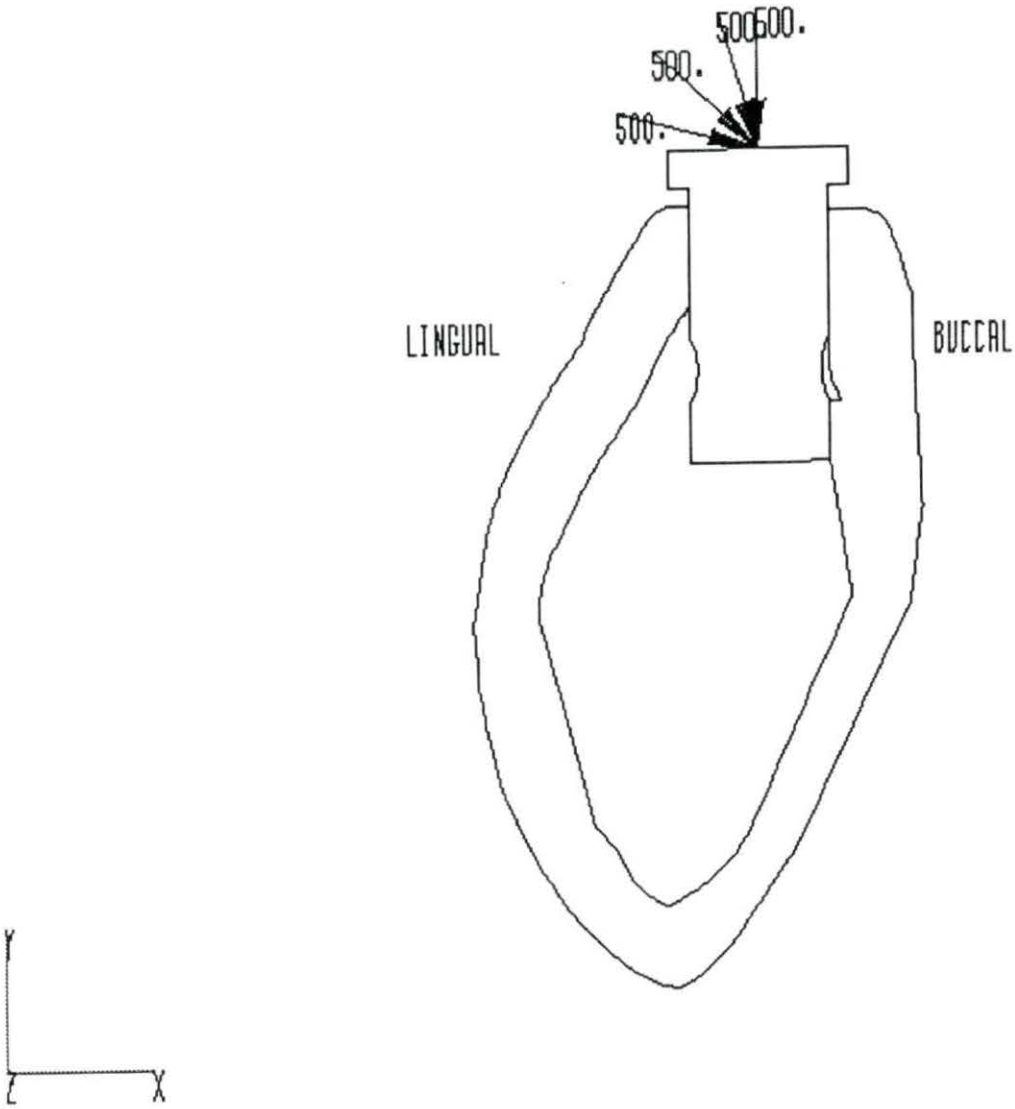

Figure 29. Directions of forces applied to the implant for FEAs run in investigation #1

2. The second study investigated the effect of three design modifications on the stress and strain distribution in the implant and the surrounding bone. First the implant was pivoted slightly (Figure 30b), then it was lengthened by 4 mm (Figure 30c). The final modification removed the grooves from the implant (Figure 30d). The models created for each of the design modifications were adapted from the previously described homogeneous, partially inhomogeneous and strut models.

3. The final study investigated whether the method of modeling the cancellous bone affected the magnitudes and distributions of the resultant stresses and strains in the implant and bone. Specifically, a finite element analysis of the lengthened implant was run with the cancellous bone modeled as homogeneous, partially inhomogeneous and as represented in the strut model. The finite element models developed from the histological section of the original implant placed in a canine mandible (Figures 25, 26 and 27) were used to develop the homogeneous long implant FEM (Figure 31), the partially inhomogeneous long implant FEM (Figure 32) and the strut long implant FEM (Figure 33).

Post-processing

P/FEA analysis results were processed and displayed using PATRAN Plus as a post-processor. The mechanical parameters used to interpret the extensive amounts of data produced from each analysis were primarily the maximum and minimum principal stresses and strains. It was possible to obtain results at any of the nodes located throughout the model or at the centroid of any element.

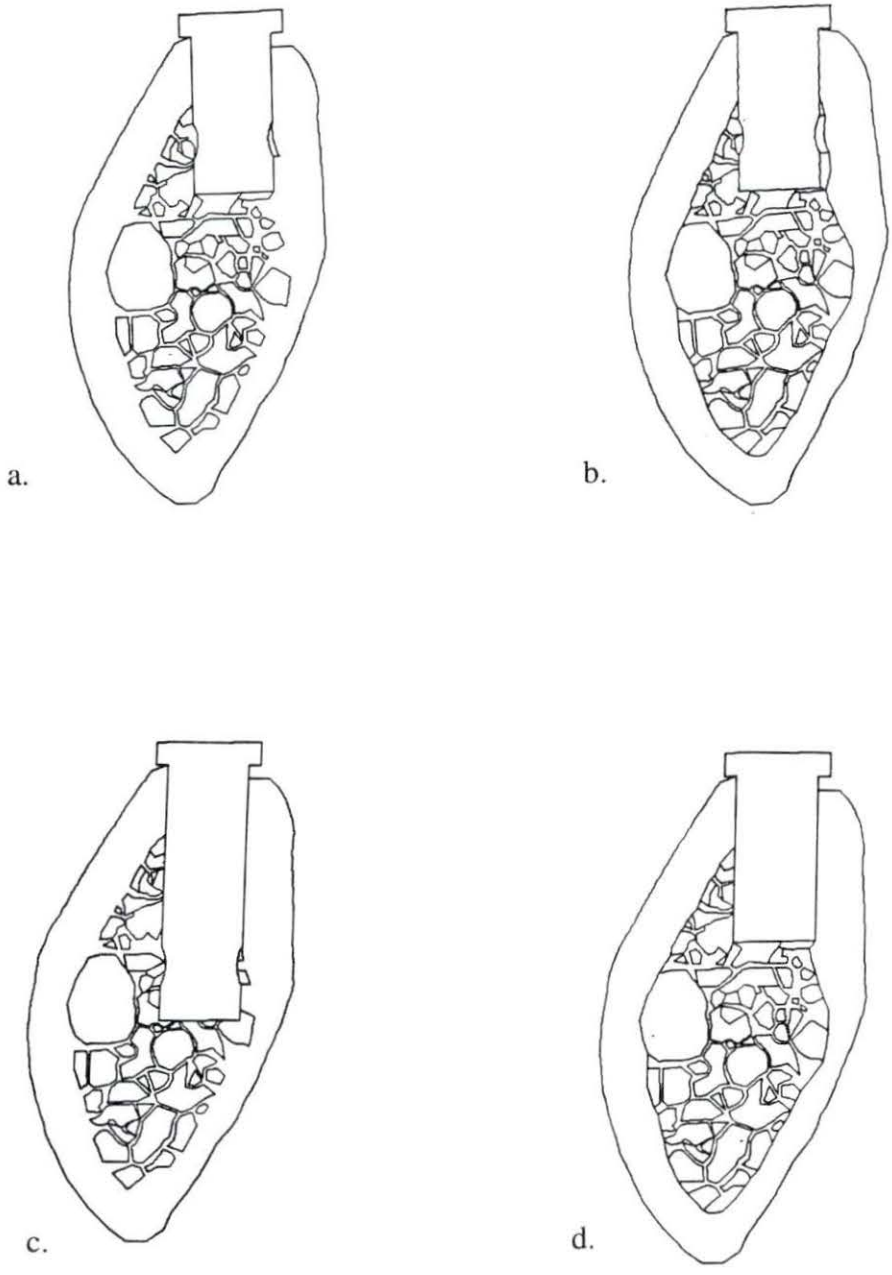

Figure 30. (a-d) Illustration of original implant design, pivoted implant design, lengthened implant design and grooveless implant design, respectively

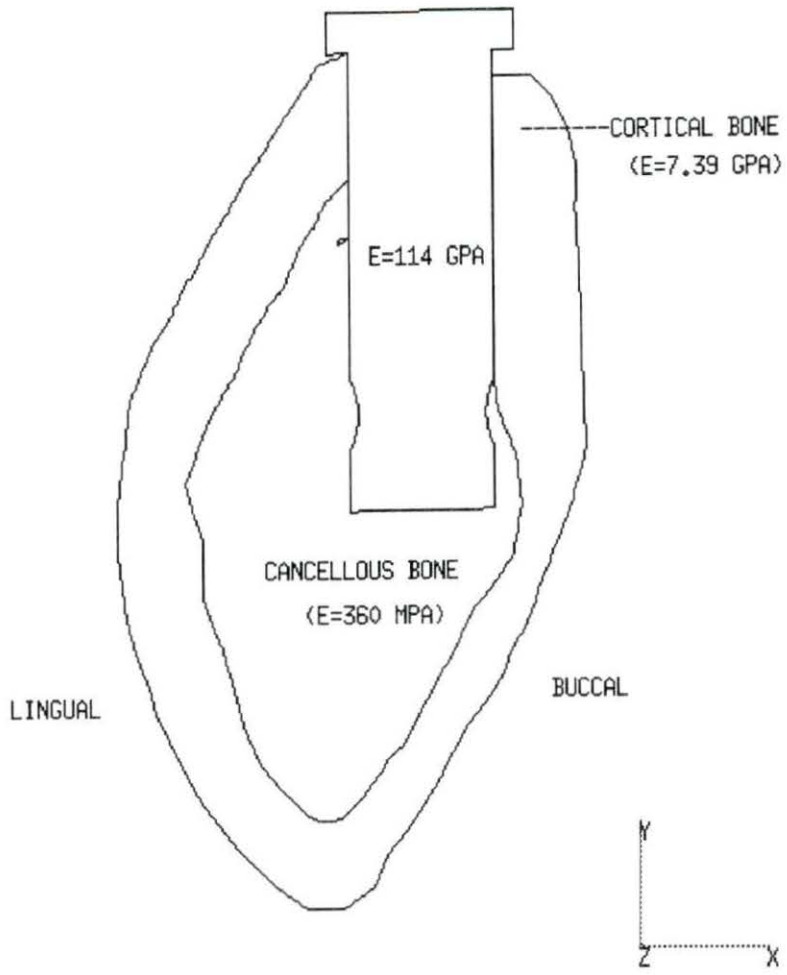

Figure 31. Homogeneous FEM of the long implant

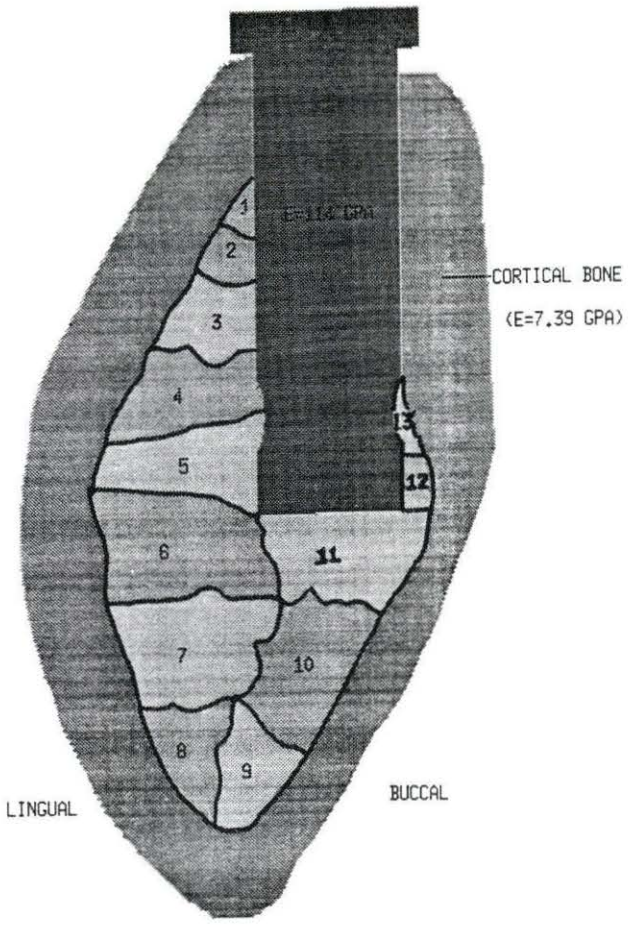

Section	Area Fraction (%)	E (MPa)
1	100.00	1402
2	21.77	169
3	69.34	846
4	73.58	919
5	26.53	222
6	17.10	121
7	18.11	131
8	21.58	167
9	16.43	114
10	22.35	175
11	31.48	282
12	100.00	1402
13	23.88	192

Figure 32. Partially inhomogeneous FEM of the long implant

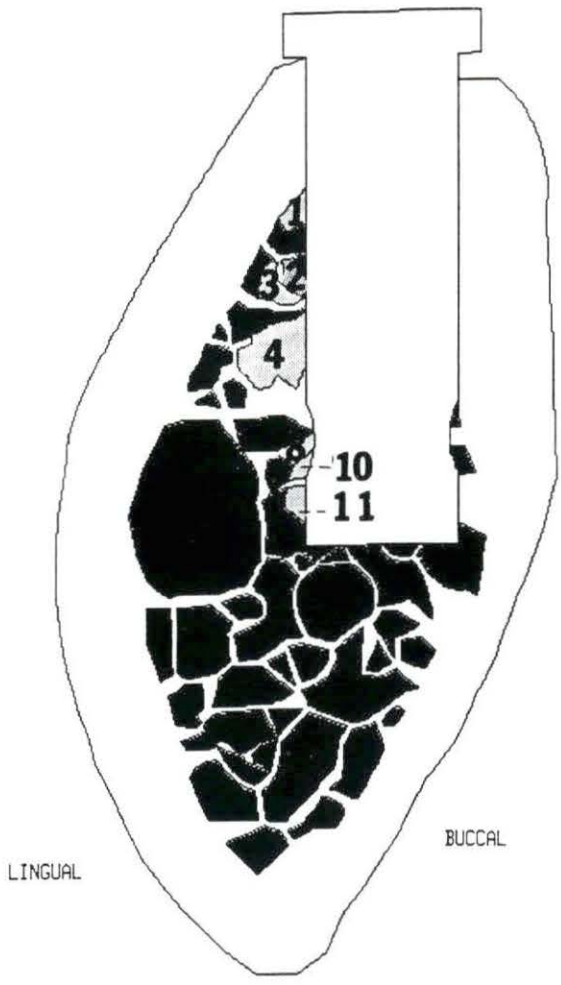

Section	Area Fraction (%)	E (MPa)
Implant	----	114,000
Cortical bone/ struts	----	7,390
1	100.00	1402
2	86.11	1139
3	63.23	742
4	85.50	1128
8	82.86	1080
9	71.87	886
10	51.72	561
11	23.88	192

Figure 33. Strut model of the long implant

RESULTS AND DISCUSSION

Investigation #1

The objective of investigation #1 was to estimate the magnitudes and locations of any tensile stresses experienced by the implant in response to the variety of loads that might occur *in vivo*. Maximum principal stresses were determined via finite element analysis of models which were subjected to loads of 30 N, 150 N and 500 N applied at 90°, 105°, 135° and 165° relative to the positive x-axis (Brunski, 1992).

Results

Figures 34-37 illustrate the orientations and relative magnitudes of the maximum principal stresses for elements of the homogeneous FEM when a load of 30 N was applied at each of the 4 angles described above. Results are presented only for those elements that had a maximum principal stress ≥ 2.5 MPa. This was done to reduce the clutter in Figures 34-37 while preserving the pertinent results. Each set of arrows indicates the orientation of the plane of the maximum principal stress for each element. The lengths of the arrows are scaled to display the relative magnitudes of the stresses throughout the implant.

Figure 34 shows the results from the axially loaded FEM. Figures 35, 36 and 37 show the results obtained as the 30 N load was applied at angles which introduced a horizontal force component which progressively increased in magnitude. Figure 34 indicates that, for a purely axial load, the implant experiences a maximum tensile stress of approximately 10 MPa near the buccal corner of the implant base (point F). Another tensile stress concentration (3-5 MPa) is located both along the lingual implant edge, between points B and C and the upper half of the lingual groove.

Figure 35 (Fx= 8 N, Fy= -27 N) illustrates a stress distribution similar to that of Figure 34 (axial loading), except that the tensile stress concentration just above the lingual groove (between points B and C) is alleviated, but a new region of tensile stress concentration occurs near the center of the unsubmerged portion of the implant. The overall stress magnitudes for the loading represented in Figure 35 are slightly larger than those predicted for purely axial loading with the largest maximum principal stress also located near point F (12 MPa).

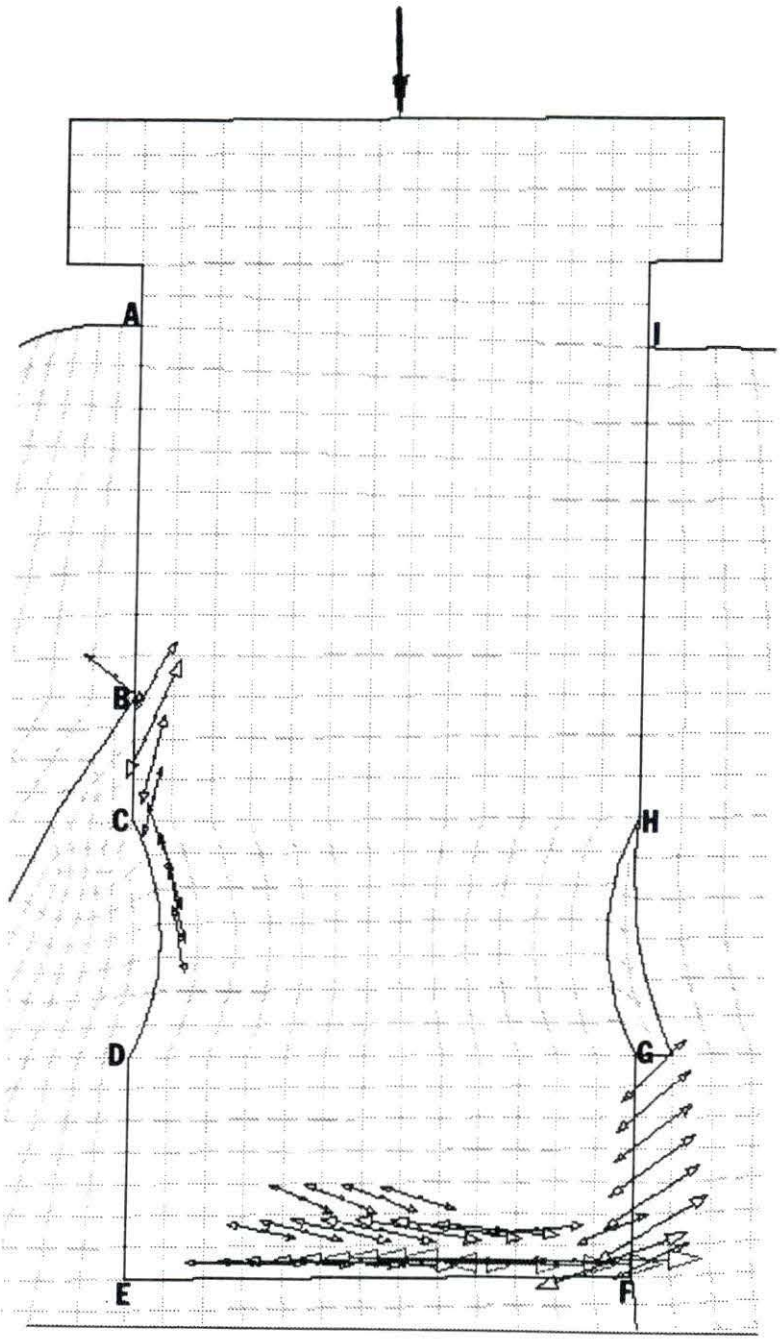

Figure 34. Tensor plot of the maximum principal stresses predicted by FEA of the homogeneous original implant for an applied load of Fx = 0 N, Fy = -30 N

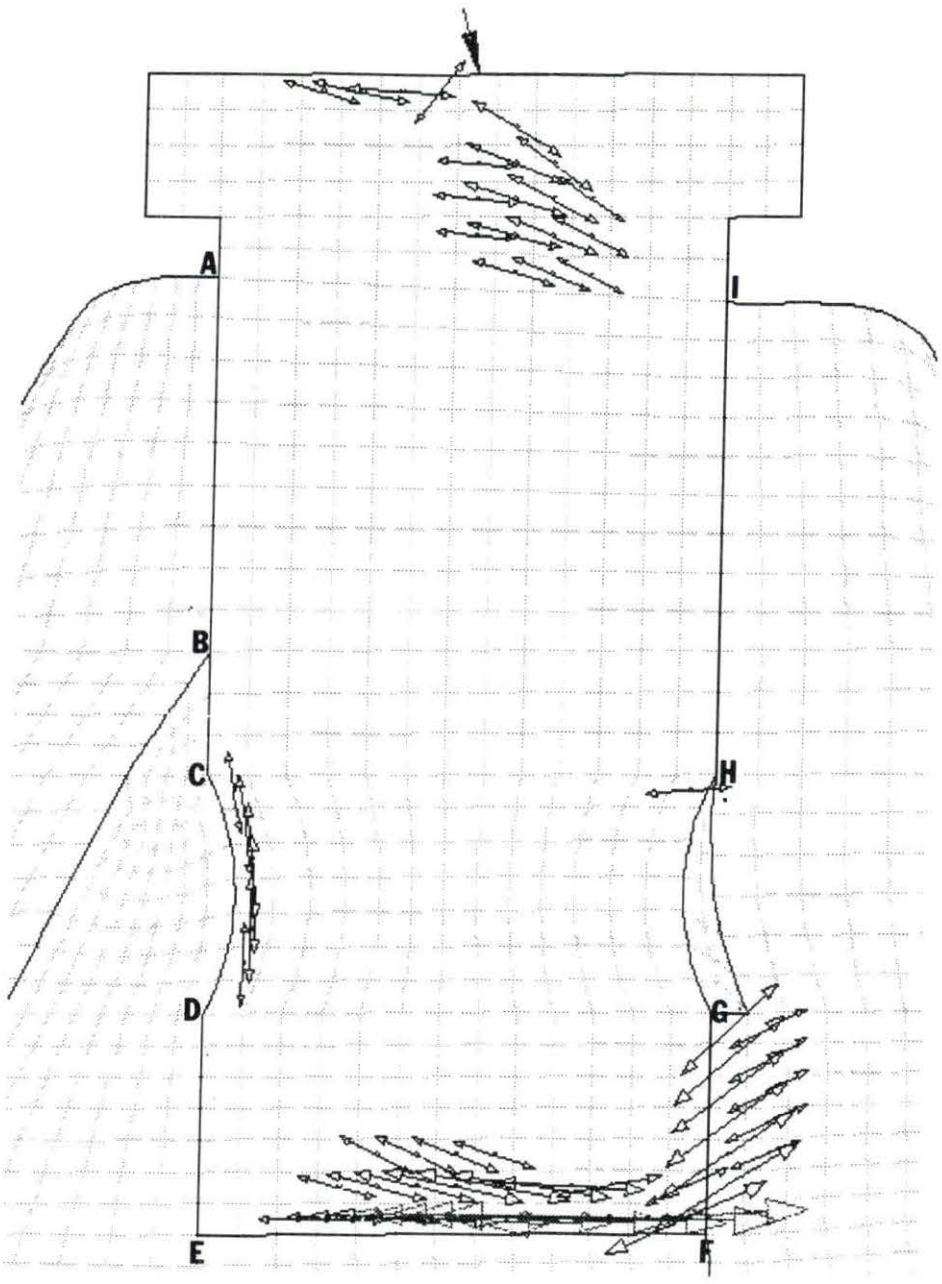

Figure 35. Tensor plot of the maximum principal stresses predicted by FEA of the homogeneous original implant for an applied load of Fx = 8 N, Fy = -29 N

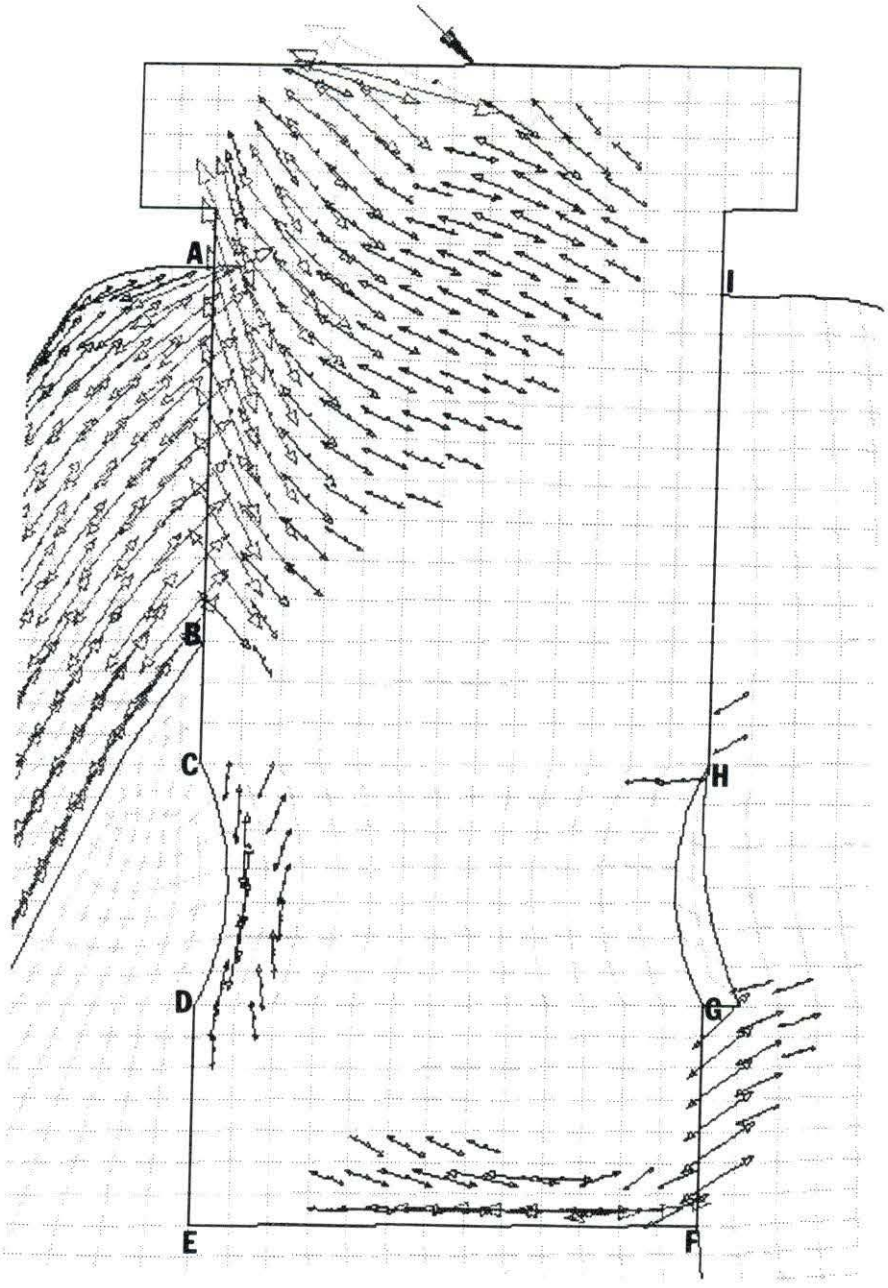

Figure 36. Tensor plot of the maximum principal stresses predicted by FEA of the homogeneous original implant for an applied load of Fx = 21 N, Fy = -21 N

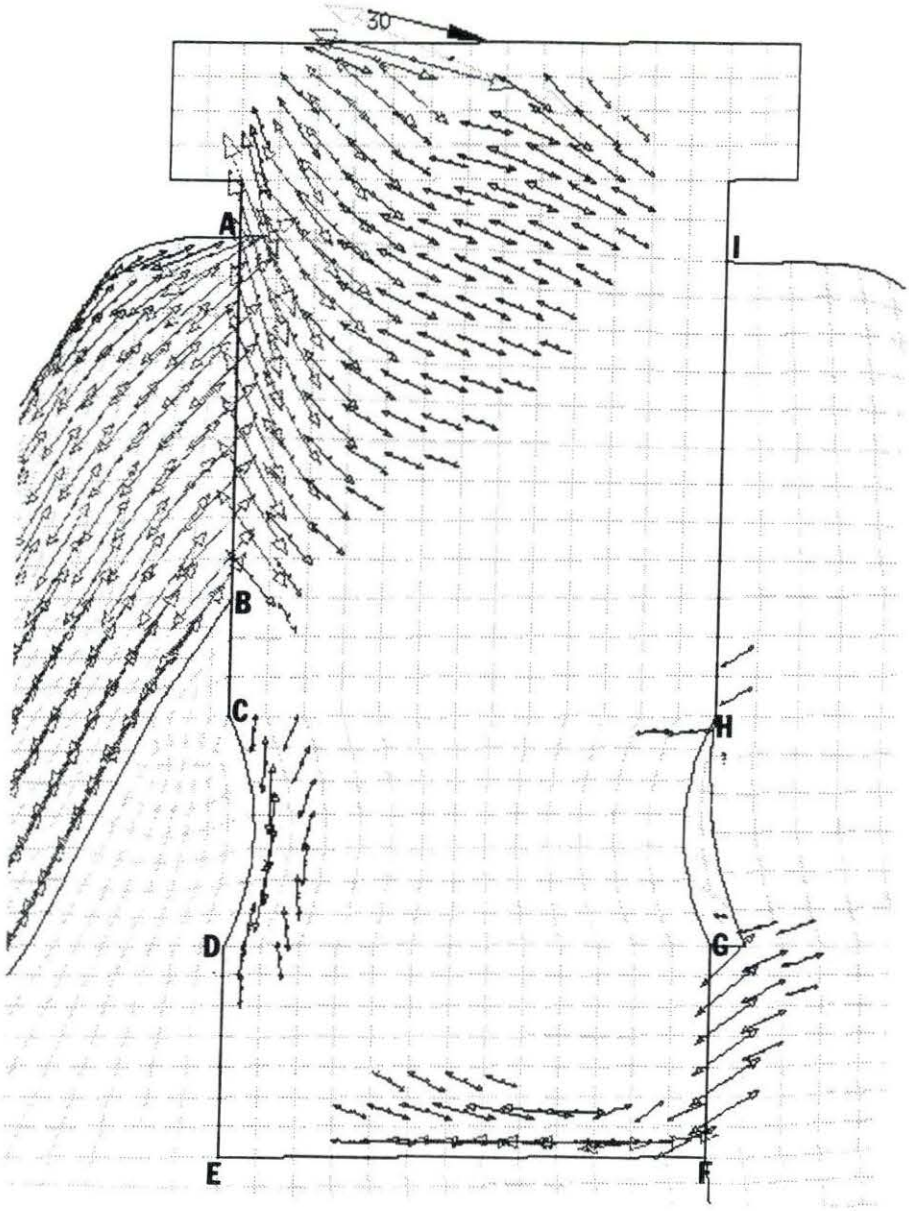

Figure 37. Tensor plot of the maximum principal stresses predicted by FEA of the homogeneous original implant for an applied load of Fx = 29 N, Fy = -8 N

Figure 36 (Fx= 21 N , Fy= -21 N) shows the same general stress distributions that are present in Figures 34 and 35, but it also shows an additional area of tensile stress concentration located between points A and B, that is dominant with stresses as large as 17 MPa. This area is located on the lingual portion of the implant, where it first encounters the lingual crestal bone (point A). Figure 36 also indicates a large distribution of significant tensile stresses (7-13 MPa) throughout the lingual cortical bone. These stresses were nonexistent for the previous loadings.

Figure 37 (Fx= 29 N, Fy= -8 N) shows a maximum principal stress distribution similar to that of Figure 36 (Fx= 21 N, Fy= -21 N) except that the magnitudes of the stresses in the lingual crest area (point A) are much larger with a maximum value of 28 MPa .

Figure 38 is a graph of the magnitudes of the maximum principal stresses at the centroid of the edge elements, located along a path around the implant, for each of the applied 30 N loadings. This path begins just beneath the lingual shoulder of the implant (A) and travels in a counterclockwise direction, ending just beneath the buccal shoulder of the implant (I). This graph summarizes the results that are illustrated in Figures 34 through 37. Figure 39 is a graph similar to that in Figure 38, except that the magnitude of the four load cases is 150 N, and 500 N is the magnitude assigned to each of the four load cases in Figure 40. The maximum principal stress experienced by the implant in response to the 150 N load was 132 MPa, which occurred at the lingual crest cortical bone/implant juncture (A). The maximum principal stress experienced by the implant in response to the 500 N load was approximately 300 MPa at point A.

Figure 41 shows an exaggerated representation of the predicted deformations of the implant subjected to the 30 N load applied at each of the four angles described previously. The deformed geometry is exaggerated so that the maximum deflection of the model will appear to be equal to 1/10 of the maximum dimension of the model. These plots, coupled with the maximum principal stress tensor plots in Figures 34 - 37, indicate the bending mechanism which causes the tensile stresses to form in response to horizontal loading. Figure 42 shows an even more exaggerated deformation plot of the implant subjected to horizontal loading in which the actual bending of the implant can be seen. The lingual side of the implant experiences tensile bending stresses, but the buccal side, in general, experiences compressive bending stresses.

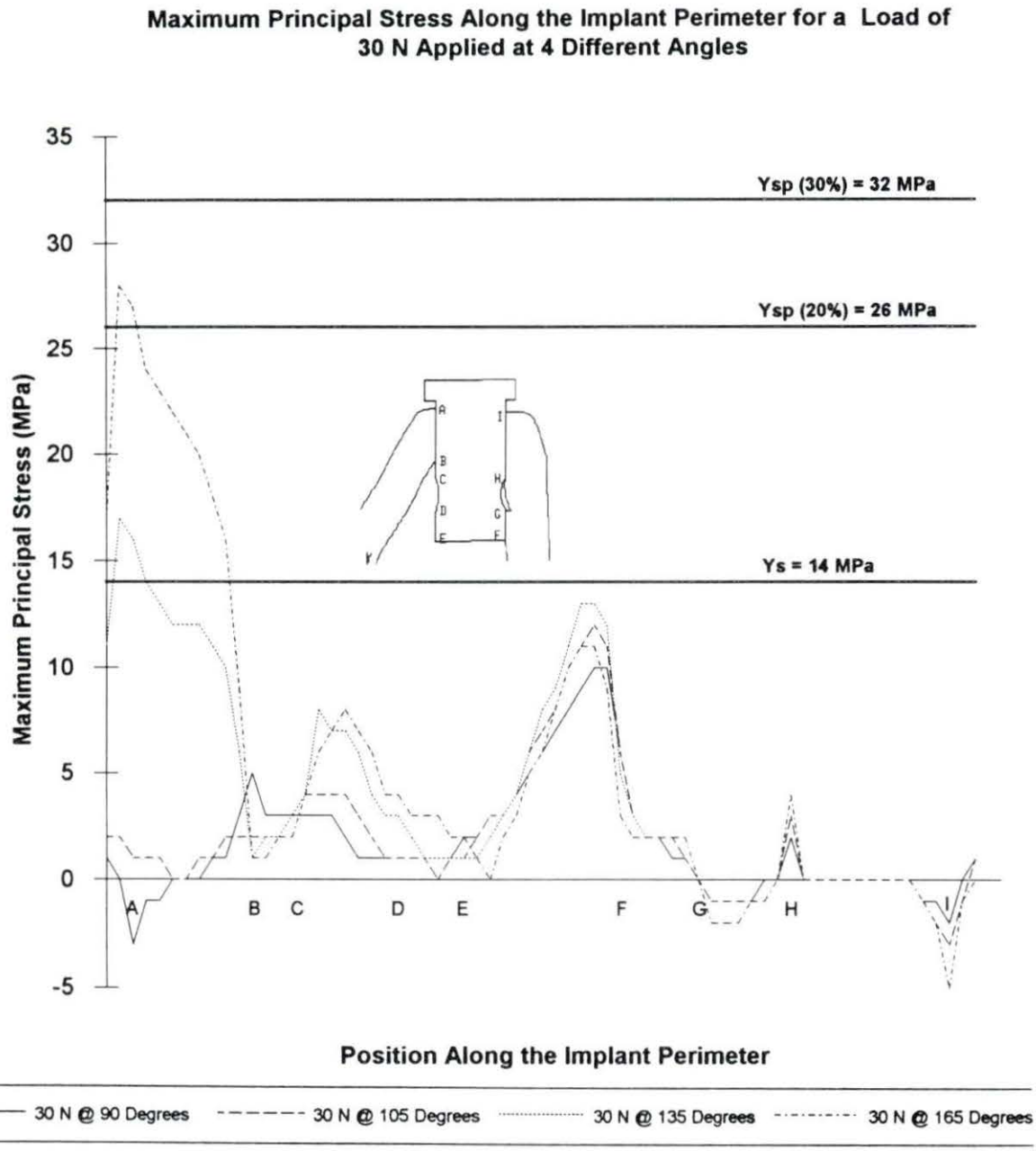

Figure 38. Graph indicating the magnitude of the maximum principal stresses at the centroid of the edge elements, located along a path around the implant, for each of the applied 30 N loadings. Y_S, Y_{SP} (20%) and Y_{SP} (30%) refer, respectively, to the maximum allowable tensile stress of the osteoceramic when not prestressed and when prestressed to 20% and 30% of its compressive strength

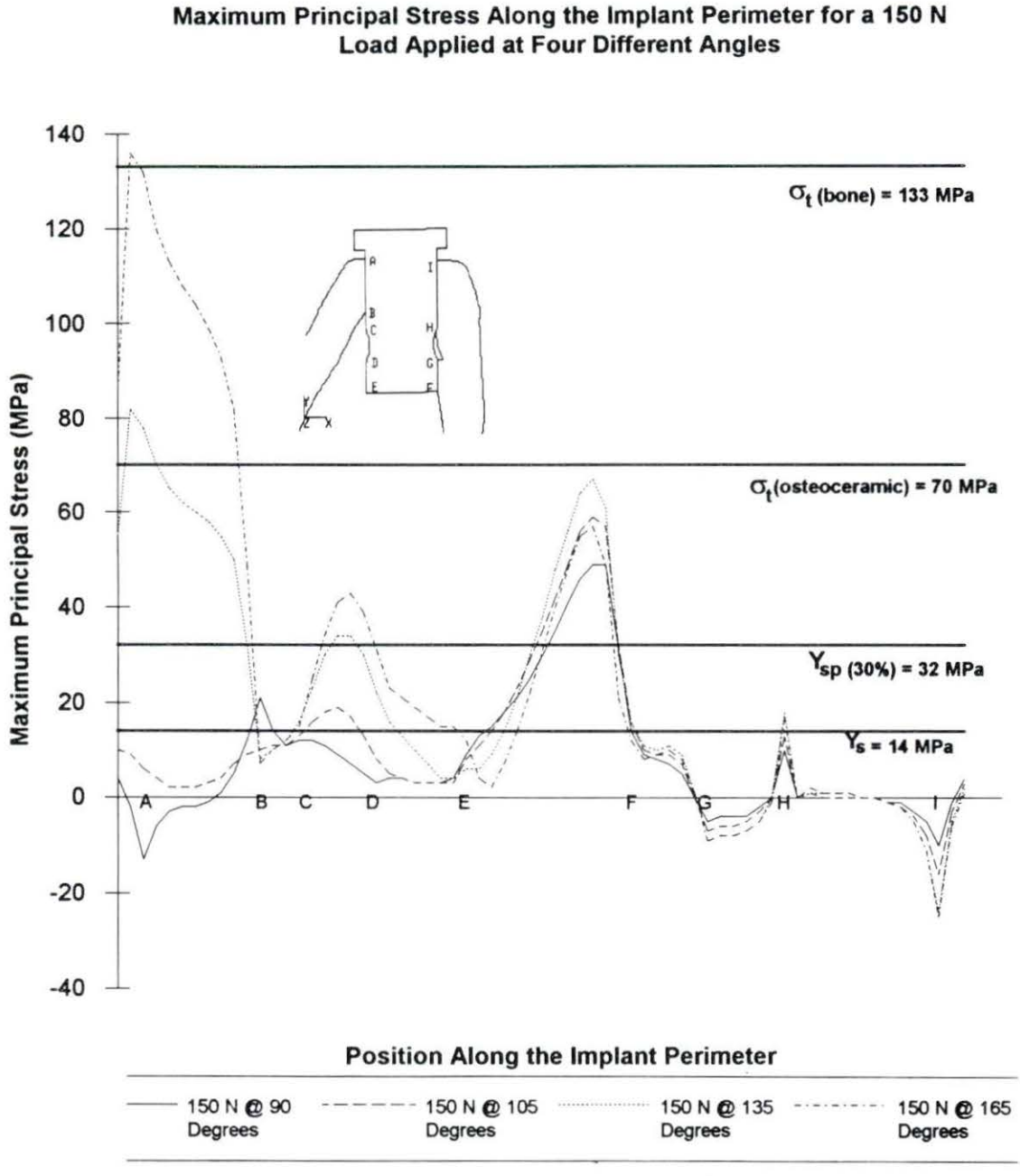

Figure 39. Graph indicating the magnitude of the maximum principal stresses at the centroid of the edge elements, located along a path around the implant, for each of the applied 150 N loadings. Y_S and Y_{SP} (30%) refer, respectively, to the maximum allowable tensile stress of the osteoceramic when not prestressed and when prestressed to 30% of its compressive strength

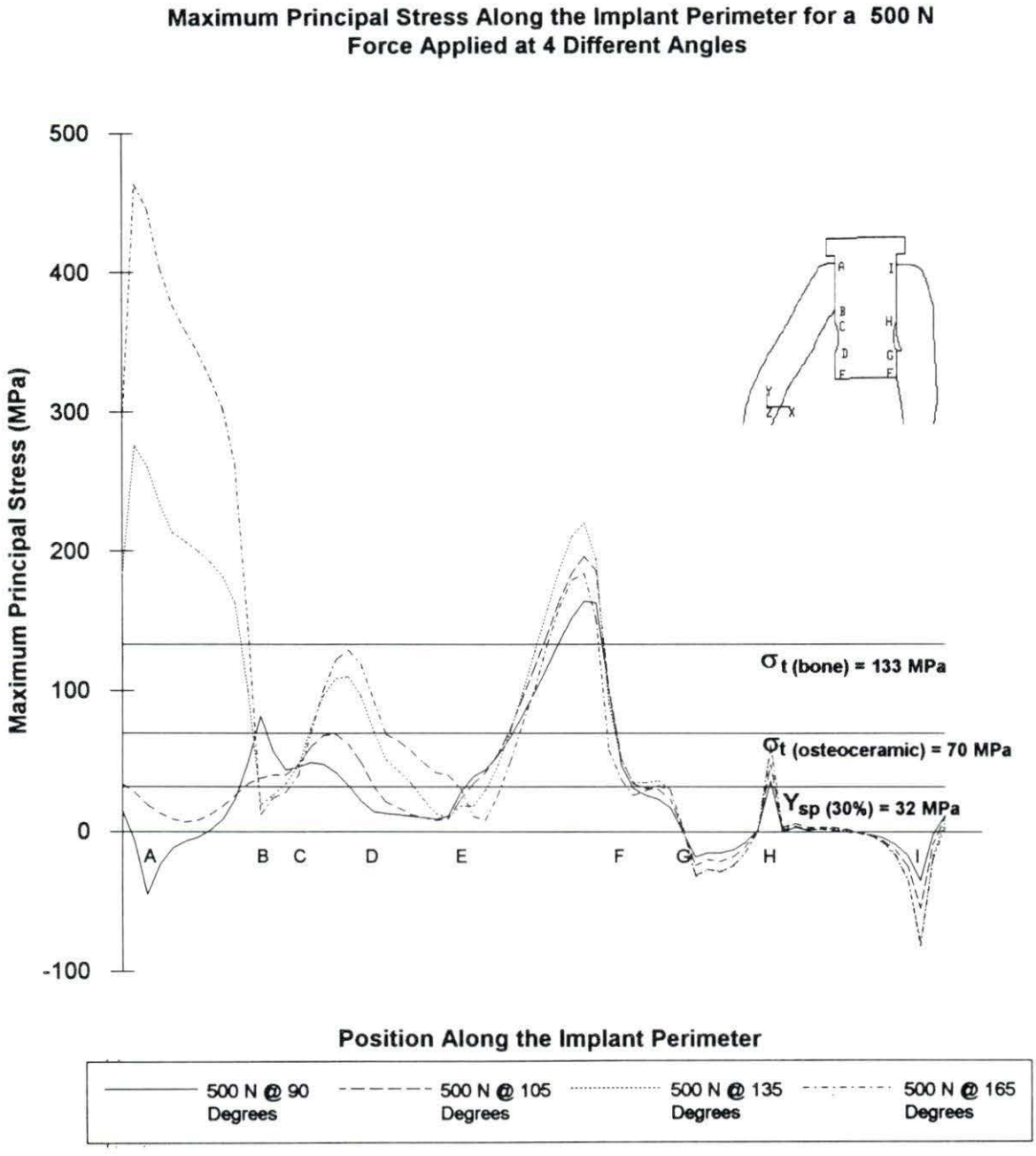

Figure 40. Graph indicating the magnitude of the maximum principal stresses at the centroid of the edge elements, located along a path around the implant, for each of the applied 500 N loadings. Y_S, Y_{sp} (20%) and Y_{sp} (30%) refer to the maximum allowable tensile stress of the osteoceramic when not prestressed and when prestressed to 20% and 30% of its compressive strength, respectively

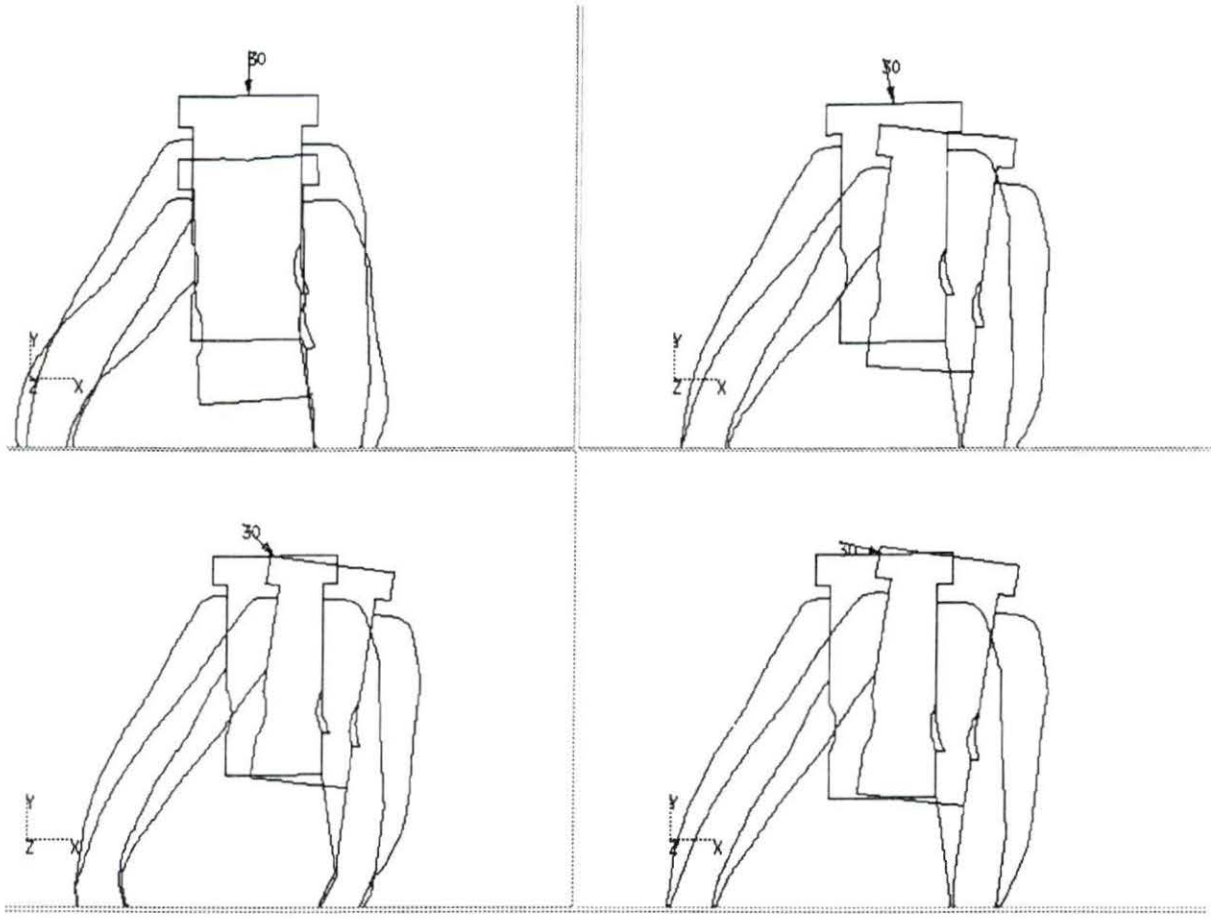

Figure 41. Exaggerated representation of the predicted deformations of the implant when subjected to the 30 N load applied at each of the four angles described previously

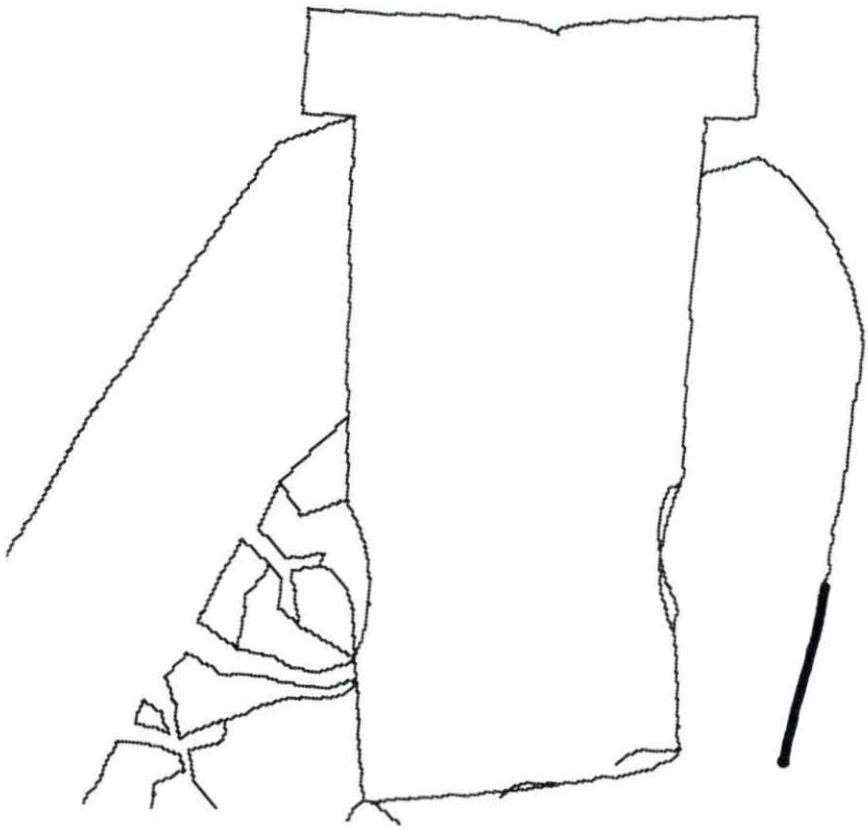

Figure 42. Highly exaggerated representation of the predicted deformation of the implant in which the actual bending can be seen

Discussion

Ceramic materials usually fail by brittle fracture (Aksaci, 1981), particularly when tensile stresses act in a direction perpendicular to the plane of a crack within the material. Microcracks are inherent flaws that are present in any polycrystalline ceramic material, such as the osteoceramic used in this study (Kingery, 1976). These flaws occur due to the high temperatures and subsequent cooling to which the material is subjected during processing (Heimke, 1990). At its tip, each crack has a large stress concentration that is a function of its length and the radius of curvature of its tip. These stress concentrations severely limit the tensile strength of many ceramic materials. Ceramics are also highly susceptible to static fatigue fracture. This means that their tensile strength is dependent upon the total length of time that they are subjected to tensile loading (Kingery, 1976). Although a ceramic material might be able to withstand a given stress over a short period of time, lower stresses can lead to fracture if applied for a sufficient time.

The tensile strength of the osteoceramic (σ_t), as measured by Graves (1988) using a modulus of rupture test, was found to be 70.3 +/- 8 MPa for 18 samples. The tensile strength of the titanium-based metals commonly used for dental implants is much greater: 400-620 MPa for titanium and 896-1020 MPa for annealed Ti-6Al-4V (Heimke, 1990). A factor of safety, n, is used in this study to take account of the uncertainties in the determination of the strength of the implant material, as well as the uncertainties related to the stresses predicted to occur in the implant due to physiological loading. It is rather a subjective matter to determine the factor of safety for a particular design. The safety factor typically assigned to metal screws that are to be used with bone plates is 3 (Park, 1979). According to Fitzgerald (1982), however, brittle materials such as the osteoceramic should have a higher factor of safety applied to them than that used for ductile materials such as the metal bone screws. Also, if one or even two bone screws in a plate fail, the effect is not as damaging as if a dental implant fractures. Bidez et al.(1992) recommend that the use of a safety factor ≥ 5 (common in most conventional engineering structures) is indicated for dental implants, due to the broad range of possible bite forces to which they may be subjected. This study used a safety factor of 5. The following equation was used to determine the maximum allowable tensile stress (Y_S) that the implant may safely tolerate:

$$Y_S = \sigma_t / n \qquad (11)$$

$$Y_S = 70 \text{ MPa} / 5 \qquad (12)$$

$$Y_S = 14 \text{ MPa} \qquad (13)$$

The finite element analysis results summarized in Table 5 indicate that the tensile stresses in the implant would exceed Y_S (14 MPa) for all orientations of the 150 N and 500 N loads. The osteoceramic experiences tensile stresses less than Y_S for 30 N loads applied vertically and 15° from the vertical. If the 30 N load is applied at an angle ≥ 45° to the implants vertical axis, however, σ_{tmax} exceeds Y_S. Note that when |Fx| ≥ |Fy| (for the 16 applied loads examined), the location of the maximum principal tensile stress in the implant is at point A (lingual crest). When |Fx| << |Fy|, however, the maximum principal stress is at point G along the buccal base of the implant.

Table 5 also summarizes the maximum compressive stress (σ_{Cmax}) experienced by the implant in response to each loading investigated. The compressive strength of the osteoceramic, σ_C, is 299 MPa (Graves, 1988). All of the 30 N and 150 N loadings would impart compressive stresses far below the compressive strength of the osteoceramic. Any orientation of the 500 N load, however, would cause the implant to experience compressive stresses which would easily exceed σ_C.

Prestressing One way to increase the osteoceramic's resistance to tensile stresses would be to prestress the material. This is accomplished by applying a compressive stress to the material that is larger than any anticipated tensile stress that the implant is likely to encounter. Prestressing of cylinders of dense hydroxyapatite dental implants was performed by de Putter (1984). After two years *in vivo*, all of the unprestressed implants had fractured, but only one prestressed implant had fractured. de Putter (1984) suggests that the ceramic be prestressed to approximately 20% of its compressive strength. Since the σ_C of the osteoceramic is 299 MPa, a first approximation would be to prestress the implant by 60 MPa. This would effectively increase σ_t from 70 MPa to 130 MPa. This would effectively increase the maximum allowable tensile stress from 14 MPa (Y_S) to approximately 26 MPa (Y_{SP}).

Figure 38 shows that, for an applied load of 30 N, a prestressed implant would increase the implant's resistance to large, horizontal loading, but would not totally eliminate all tensile stresses. If the osteoceramic was prestressed by 30% of the σ_C, then Y_{SP} would increase to 32 MPa. This would remove all tensile stresses from the osteoceramic for any orientation of

a 30 N load (Figure 38). The largest σ_{Cmax} experienced by the unprestressed implant in response to a 30 N load is 43 MPa (Table 5). Therefore, the largest σ_{Cmax} of a prestressed osteoceramic subjected to a load of 30 N would be approximately 133 MPa. This implies that the osteoceramic could also tolerate the compressive stresses experienced by the implant in response to a force of 30 N.

Figures 39 and 40 illustrate that prestressing the implant does not prevent the implant from experiencing tensile stresses in response to loads of 150 N and 500 N. Since the majority of bite forces applied to dental implants placed in the premolar area of dogs were found to be $\leq$ 30 N (Brunski, 1987), it is recommended that prestressing of the osteoceramic dental implant be pursued with *in vivo* testing.

Correlation with *in vivo* results Twenty one of the forty implants placed in canine mandibles by Niederauer (1990) were found to have one or more cracks in them upon retrieval; four implants fractured completely. Nine of these cracks (two of which were complete fractures) were associated with the grooves and were horizontal in orientation. The finite element analysis results for each loading condition, as shown in Figures 34 through 37, predict a tensile stress distribution at the lingual groove in which the maximum principal stress orientation is normal to the horizontal crack direction detected in the implants. Since this distribution was present in response to all the loading conditions, it is assumed that the lingual groove experienced these tensile stresses for a significant portion of the total loading time. These cracks were most likely static fatigue fractures. Five of the cracks in the retrieved implants were located at the base of the implants, as might be predicted by the tensile stress concentrations along the implant bases illustrated in Figures 34 through 37. This stress distribution was also predicted for each of the applied loads, implying that these cracks might also have resulted from static fatigue. Two of the implants fractured completely, just below the lingual shoulder. This might be explained by the large tensile stresses predicted by FEA for this portion of the implant (Figure 36 and Figure 37) when it is subjected to significant horizontal loading. Overall, there was a fairly good correlation between the stresses predicted by the finite element analyses and the occurrence of cracks in the retrieved implants.

Table 5. Greatest principal stress magnitudes in the implant for each applied loading

Applied Force (N)	Greatest Implant Tensile Stress(MPa) σ_{tmax}	Location of Greatest Tensile Stress	Greatest Implant Compressive Stress (MPa) σ_{cmax}	Location of Greatest Compressive Stresses
F = 500 N				
Fx = 0 Fy = -500	164	G	-336	H
Fx = 129 Fy = -483	196	G	-503	H
Fx = 354 Fy = -354	276	A	-725	H
Fx = 483 Fy = -129	463	A	-753	H
F = 150 N				
Fx = 0 Fy = -150	49	G	-98	H
Fx = 39 Fy = -145	59	G	-146	H
Fx = 106 Fy = -106	82	A	-210	H
Fx = 145 Fy = -39	36	A	-217	H
F = 30 N				
Fx = 0 Fy = -30	10	G	-20	H
Fx = 8 Fy = -29	12	G	-30	H
Fx = 21 Fy = -21	17	A	-43	H
Fx = 29 Fy = -8	28	A	-45	H

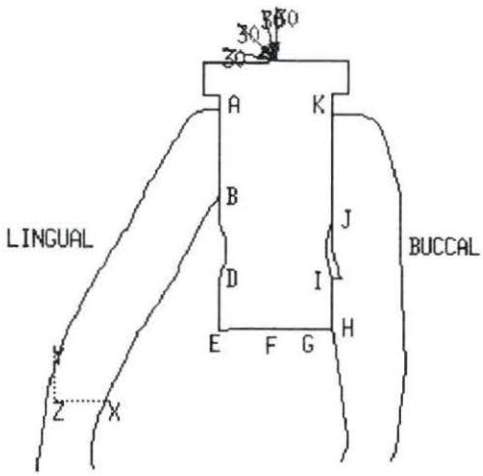

Horizontal loading Table 5 shows that, if a load of a given magnitude is applied at an angle which introduces a horizontal component, σ_{max} may be 20-280% larger than those stresses experienced by the implant under a purely axial load of the same magnitude. This implies that the osteoceramic implant that was placed in canine mandibles by Niederauer (1990) would likely fracture at loads that were even less than 30 N in magnitude, if they were applied at an angle away from the vertical axis of the implant. Other finite element studies have also demonstrated the importance of including lateral loads in finite element analyses of dental implants (Clift et al., 1992; Richter, 1989). de Putter et al. (1983) demonstrated the importance of considering the effects of lateral loads in the design of dental implants. They reported that 80% of dense hydroxylapatite dental implants placed in canine mandibles fractured in response to large horizontal forces.

Horizontal loads have been found by finite element analysis to also cause high stresses in cortical crestal bone (Richter, 1989; Soltesz and Siegale, 1984; Borchers and Reichart, 1983). These large stresses are believed to cause the craterlike crestal bone destruction that is so often correlated with dental implant failure (Clift et al., 1992; Huiskies and Nunamaker, 1984). Finite element results in the present study also demonstrated that widespread and significant tensile stresses (greater than the ultimate strength of cortical bone) are experienced by the lingual crestal bone in response to loadings with significant horizontal components (Figure 36 and Figure 37).

Horizontal loading of dental implants does occur *in vivo* and is caused by the horizontal movement of the mandible and the inclined occlusal surfaces of the various suprastructures attached to them (Rangert et al., 1989). In addition to this normal type of loading, bruxism (grinding of teeth) produces a continuous, predominantly horizontal load for minutes at a time several times during a night's sleep (Graf, 1969). It is very possible that horizontal loads play a significant role in crestal bone destruction adjacent to an implant because of the resulting large, tensile stresses that occur in the crestal cortical bone, the strength of which is much less in tension (133 MPa) than in compression (193 MPa).

Investigation #2

The objective of investigation #2 was to determine the effects that some simple implant design modifications would have upon the stresses and strains experienced by the implants and surrounding bone. Each design modification was evaluated in comparison to the original implant design. Specifically, the maximum principal stresses in the implants and the

principal strains in the bone adjacent to the implants were evaluated. Two different loading conditions (Fx = 8 N, Fy = -29 N; Fx = 21 N, Fy = -21 N) were assigned to each FEM when evaluating the tensile stresses in a given implant. This was done to evaluate implant stresses in response to what is believed to be a typical physiological load (Fx = 8 N, Fy = -29 N), and a more extreme, less frequent physiological load (Fx = 21 N, Fy = -21 N). The finite element model created for each modification was adapted from the homogeneous FEM.

Pivoted implant

The first modification involved changing the angle of implantation, by pivoting the implant slightly, as shown in Figure 30.

Maximum principal stress Figure 43 illustrates the maximum principal stress distribution experienced by the pivoted implant in response to a stress of 30 N applied 15 ° from the vertical axis of the implant. Figure 44 represents the maximum principal stress distribution for the original implant subjected to the same loading. The magnitude of the principal stresses at the centroids of the elements along the implant perimeter are presented in Figure 45 for both the original and the pivoted implant.

A comparison of Figure 43 and Figure 44 indicates that pivoting the implant removes the large tensile stress distribution at the base of the implant and the tensile stress concentration at the lingual groove. These stress concentrations are alleviated because the lower buccal edge of the pivoted implant (between points F and G in Figure 43) is adjacent to a much more compliant cancellous bone (E=360 MPa) as opposed to cortical bone (E=7.39 GPa) in the original implant design (Figure 44). Pivoting the implant also introduces a new area of significant tensile stress concentration, just above point H on the implant (Figure 43), where the implant/cortical bone interface becomes an implant/cancellous bone interface. A comparison of the graphs in Figure 45 shows that, while pivoting the implant is effective in reducing both the magnitude and distribution of tensile stresses in the osteoceramic implant along its lingual edge (A-E) and base (E-F), it also introduces a tensile stress of ~11 MPa between points H and I. Although the stress peak introduced by pivoting is less than the maximum allowable tensile stress (Y_S = 11.6 MPa) of the osteoceramic that was derived in investigation #1, this area could still be an area of potential failure. If stresses greater than 30 N are applied to the implant, or if this FEM tends to underestimate implant stress magnitudes, then this area of the implant might eventually fracture.

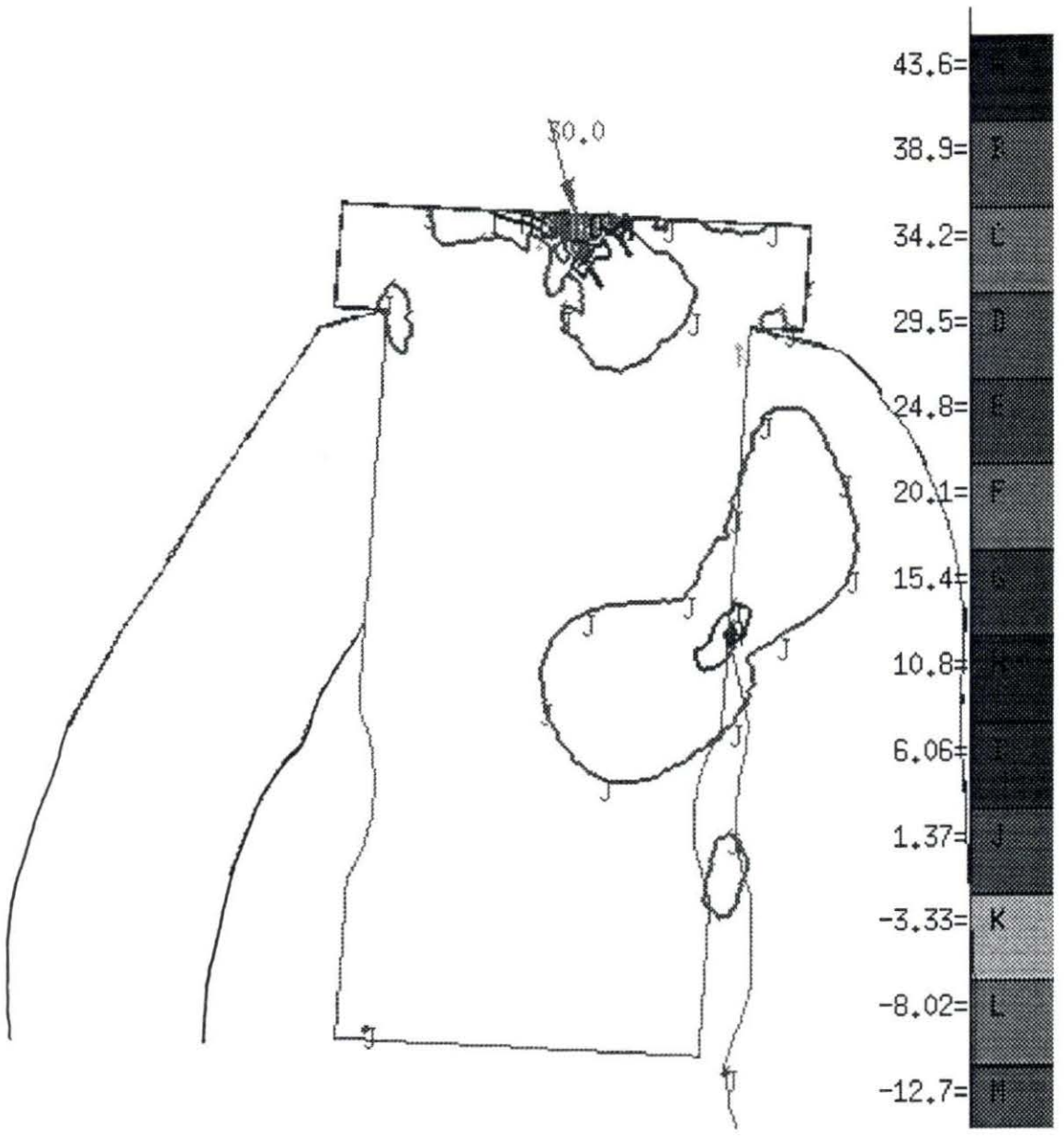

Figure 43. Contour plot illustrating the distribution of maximum principal stresses in the pivoted implant for an applied load of Fx = 8 N, Fy = -29 N

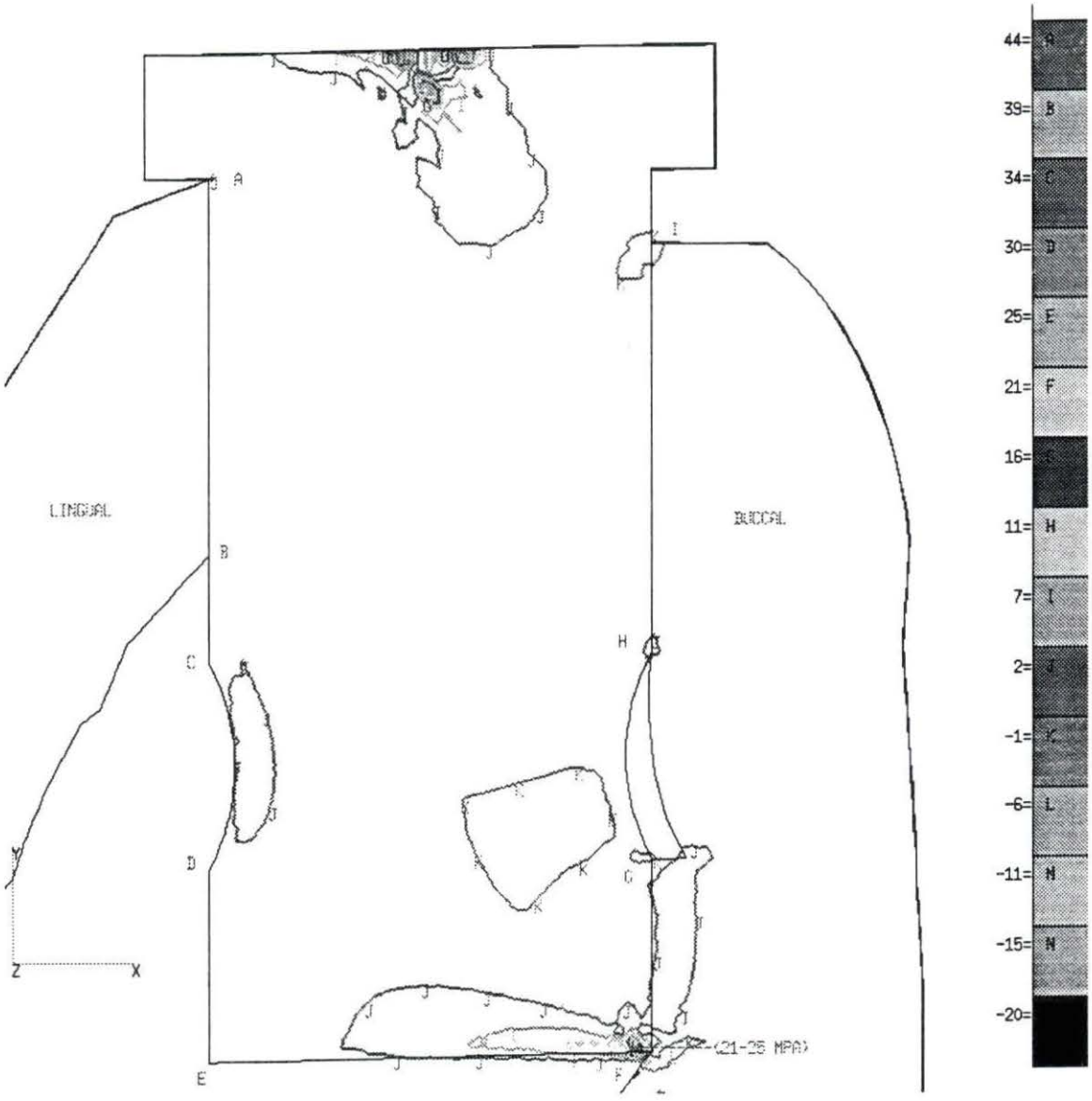

Figure 44. Contour plot illustrating the distribution of maximum principal stresses in the original implant for an applied load of Fx = 8 N, Fy = -29 N

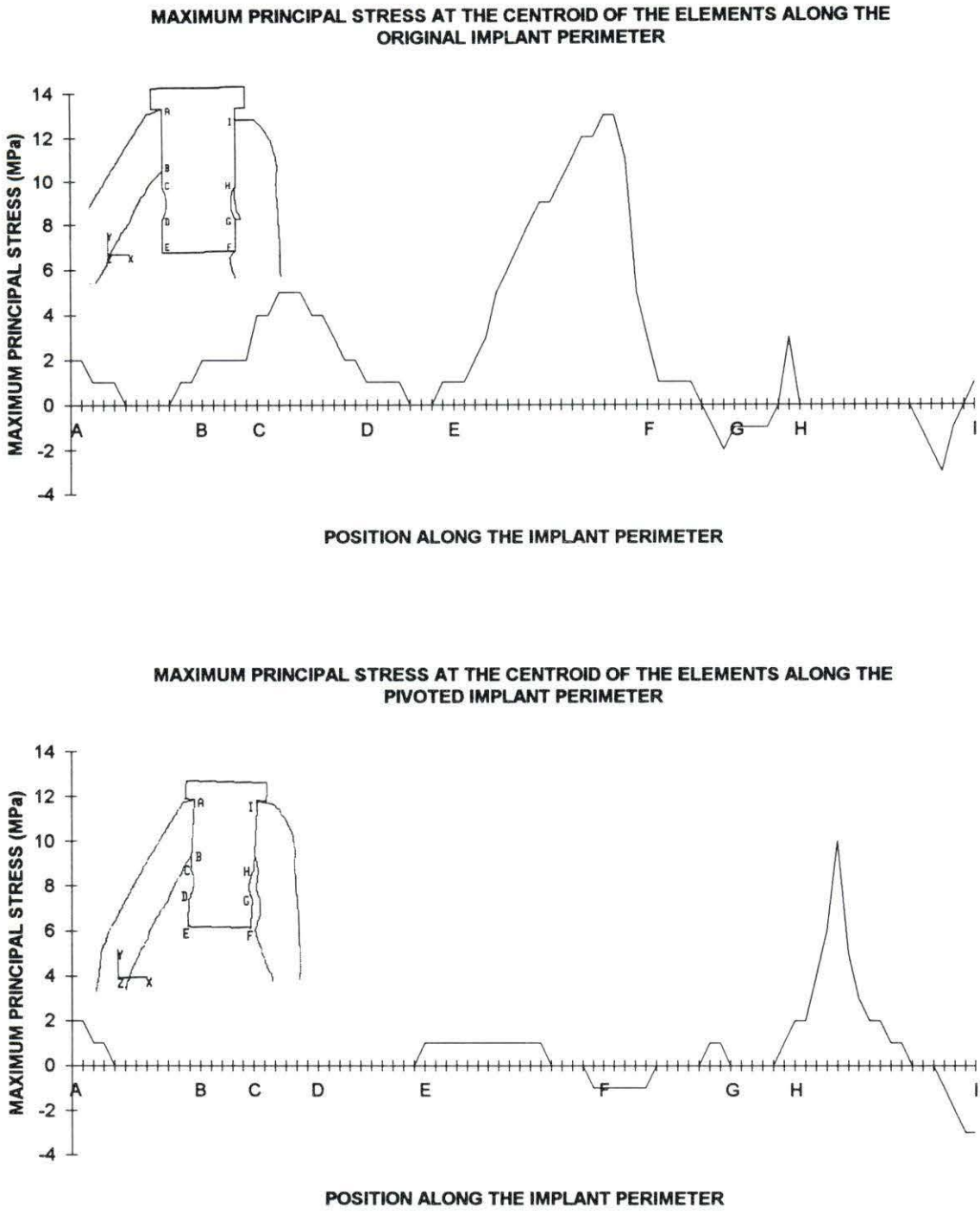

Figure 45. Two graphs illustrating the magnitude of the maximum principal stress at the centroid of the elements along the perimeters of the original implant (top) and the pivoted implant (bottom)

Figure 46 contains two graphs which illustrate the magnitudes of the maximum principal stresses at the centroid of the edge elements, located along a path around the perimeter of the pivoted and original implants, for a load of 30 N applied at an angle 135° to the positive x-axis (Fx = 21 N, Fy = -21 N). This loading was shown in investigation #1 to cause very large stress concentrations in the original implant adjacent to the lingual crest. A comparison of the graphs in Figure 46 indicates that pivoting the implant reduces the magnitude of the large tensile stresses in the lingual crest area (A) of the implant from approximately 16 MPa to approximately 11 MPa. Pivoting the implant also significantly reduces the large tensile stresses in the lingual groove and along the implant base. The stress concentration that is introduced to the implant from pivoting (~11 MPa, as shown in Figure 43, for Fx = 8 N, Fy = -29 N) increases in magnitude to ~14 MPa when the magnitude of the horizontal component is increased to Fx = 21 N. It would be reasonable to expect that, should the implant experience even greater horizontal loads, pivoting would dampen the increase in tensile stresses observed at the lingual crest of the original implant in investigation #1 but would also increase (at a slower rate) the stress peak just above the buccal groove (just superior to point H).

Pivoting the implant decreases the probability of implant failure by reducing both the amount of osteoceramic subjected to tensile stresses as well as the magnitude of any tensile stresses that it does experience. These results demonstrate that the angle of implantation of a ceramic dental implant is very critical in determining the tensile stresses that the implant will experience *in vivo*. It is recommended that the implant be placed as symmetrically as possible in the mandible so that one of the edges does not abut the cortex.

Significance of principal strains Critical to the clinical success of a dental implant is the minimization of bone resorption around the implant (Clift et al., 1992). Bone remodeling is known to be related to changes in mechanical environment (Smith et al., 1976; Goodship et al., 1979; Lanyon et al., 1982; Rubin and Lanyon, 1985; Jee et al., 1990; Meade, 1989). It is hypothesized that significant variations from the typical physiological strains experienced by a particular bone site are somehow detected by the bone cells (Frost, 1988, 1990, Currey, 1984; Hart and Davy, 1989). These cells adjust their rates of activity such that bone mass will increase or decrease resulting in a change in stiffness which will in

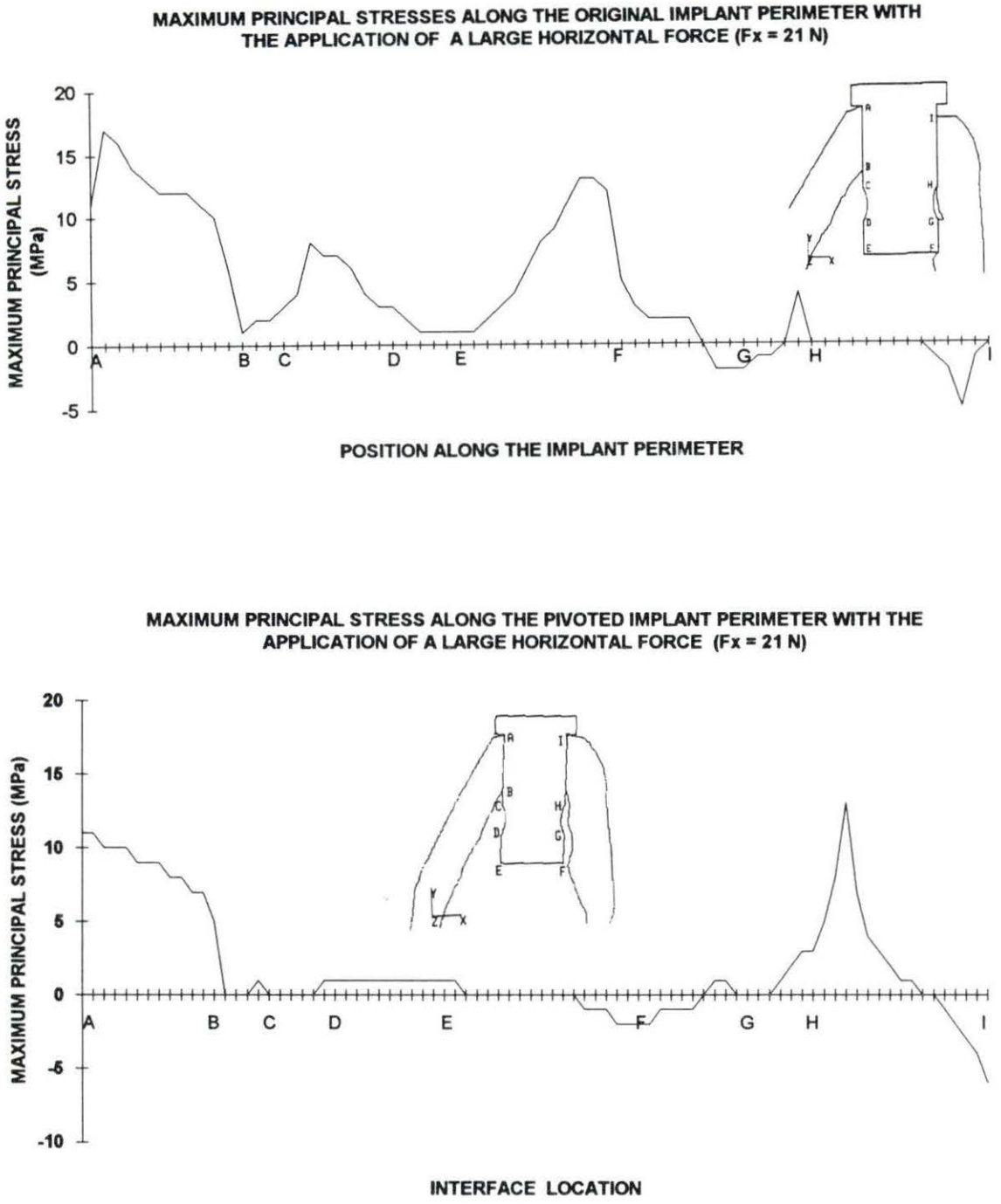

Figure 46. The top and bottom graphs illustrate the maximum principal stresses in the centroid of each of the perimeter elements of the original and pivoted implants, respectively, as predicted by FEA for large horizontal loading (Fx = 21 N, Fy = -21 N)

facilitate a return to the "normal" straenvironment. Rubin and Lanyon (1982) determined, from extensive *in vivo* strain gage animal studies, that in different areas of the same skeleton as well as across different species, bone experiences a relatively constant pattern of strain when loaded. They found that strains experienced under peak loading ranged from 2500-3500 μE, but routine loading produced strains in the 1000-1500 microstrain range. This range of normal physiological strains (~1000 μE to ~3500 μE) was used as a physiological window in this study to describe those strains that would maintain existing bone around the dental implant. Strains in the bone that were far below 1000 μE would indicate that there was a possibility that resorption might occur at that particular site. Areas of bone that were predicted by finite element analysis to experience strains greater than ~3500 μE were identified as areas likely to exhibit bone growth (Clift et al., 1992). Strains that approach the yield strains of cortical bone, ~7000 μE (Whedon and Heaney, 1993), or of cancellous bone, ~7400 μE (Turner, 1989) were assumed undesirable.

It is important to remember that the stresses and strains determined in the finite element analyses throughout this study are only gross approximations of the actual magnitudes that might be experienced *in vivo*. When presenting the bone strains predicted by FEA, some possibilities regarding resultant bone activity are also presented. Many FEA studies have presented strain results in a similar fashion (Clift et al., 1992, Riegar et al., 1990). It is important to remember that these strain magnitudes do not take into account the strains experienced by the mandible due to its actual 3-D structure (versus 2-D FEM) and the various muscles that insert upon it. Therefore, these strain magnitudes are really only useful in comparison of one design to another. These magnitudes would also be quite useful in a highly controlled experiment in which bone adaptation to controlled loading was analyzed and correlated to the strains predicted by FEA.

Principal strain results Figure 47 contains two graphs which show the magnitude of the principal strains located at the nodes along the bone/implant interface for the original and the pivoted implants. A comparison of the two graphs shows that the magnitudes of the strains at the interface are similar along the lingual side and base of both implants. The very small interfacial strain magnitudes present from points A to B for both implants suggest that bone resorption might occur over a long period of time. This would be similar to that reported for hip prostheses (Huiskies, 1986). Strains along the base of both implants (E-F) range from about 1000 μE to 2000 μE. This would most likely be adequate to maintain the bone in this area. The buccal base corner (point F) of both implants experiences the greatest

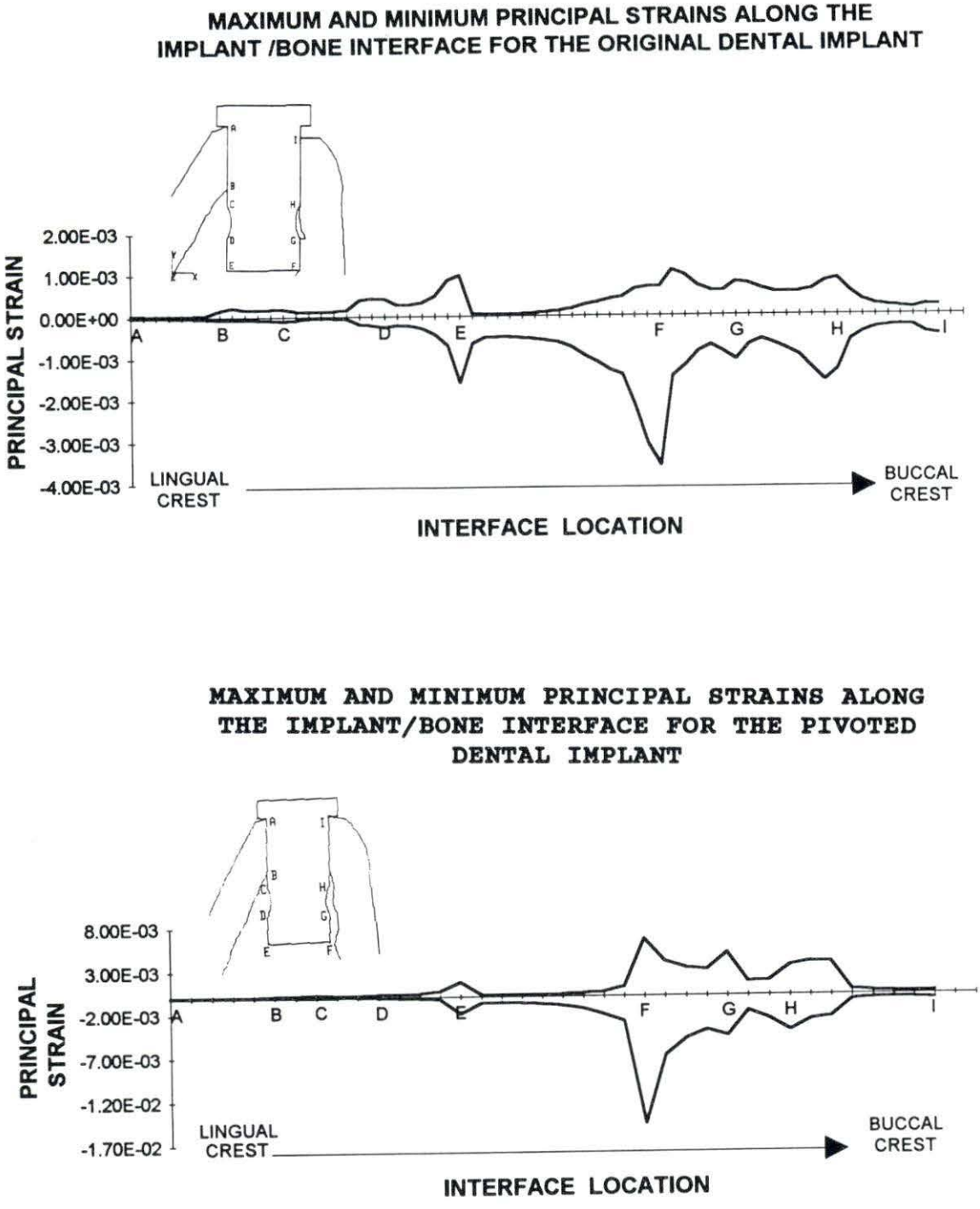

Figure 47. Two graphs which show the magnitude of the principal strains located at the nodes along the bone/implant interface for the original and the pivoted implant, respectively

strain magnitudes. This peak strain in the original implant is ~3500 μE. This would indicate bone maintenance or possibly bone deposition. The same area (point F) on the pivoted implant experiences a strain of ~14,000 μE. This would seem to indicate irreversible deformation and possibly pathological bone resorption. If resorption did occur in this area, then strains in adjacent areas would increase, possibly causing further resorption. The strain magnitudes along the implant/cancellous bone buccal interface (point F through point H and just beyond) are much greater for the pivoted implant versus the original implant. The magnitudes for both implants, however, seem adequate to maintain the bone density in this area. Finally, buccal crestal bone (point I) resorption due to low strain magnitudes is possible for both implants. Overall, the pivoted implant provides an interfacial strain distribution that is fairly similar to that of the original design.

Grooveless implant

The second design modification involved removing the grooves that were present in the original implant design to provide an area for bone ingrowth to improve implant stability.

Maximum principal stress Figure 48 illustrates the maximum principal stress distribution experienced by the grooveless implant in response to a stress of 30 N applied 15 ° from the vertical axis of the implant. The tensile stress distribution shown in Figure 48 is similar to that of the original implant subjected to the same loading (Figure 44). The magnitude of the principal stresses located at the centroid of the elements along the implant perimeter are presented in Figure 49 for both the original and the grooveless implant. These graphs indicate that the grooveless implant reduces the magnitude of the tensile stresses along most of the implant perimeter, except for a small area just below point B which shows a very small and localized increase in stress magnitude. Removing the grooves also completely eliminates the tensile stress concentration located just below point H of the original implant.

Figure 50 contains two graphs which illustrate the magnitudes of the maximum principal stresses at the centroid of the edge elements, located along a path around the grooveless and original implants, for a load of 30 N applied at an angle 135° to the positive x-axis (Fx= 21N, Fy = -21N). A comparison of these graphs indicates that removing the grooves from the implant also slightly reduces the magnitudes of the large tensile stress distributions introduced by the large, horizontal component of the applied load.

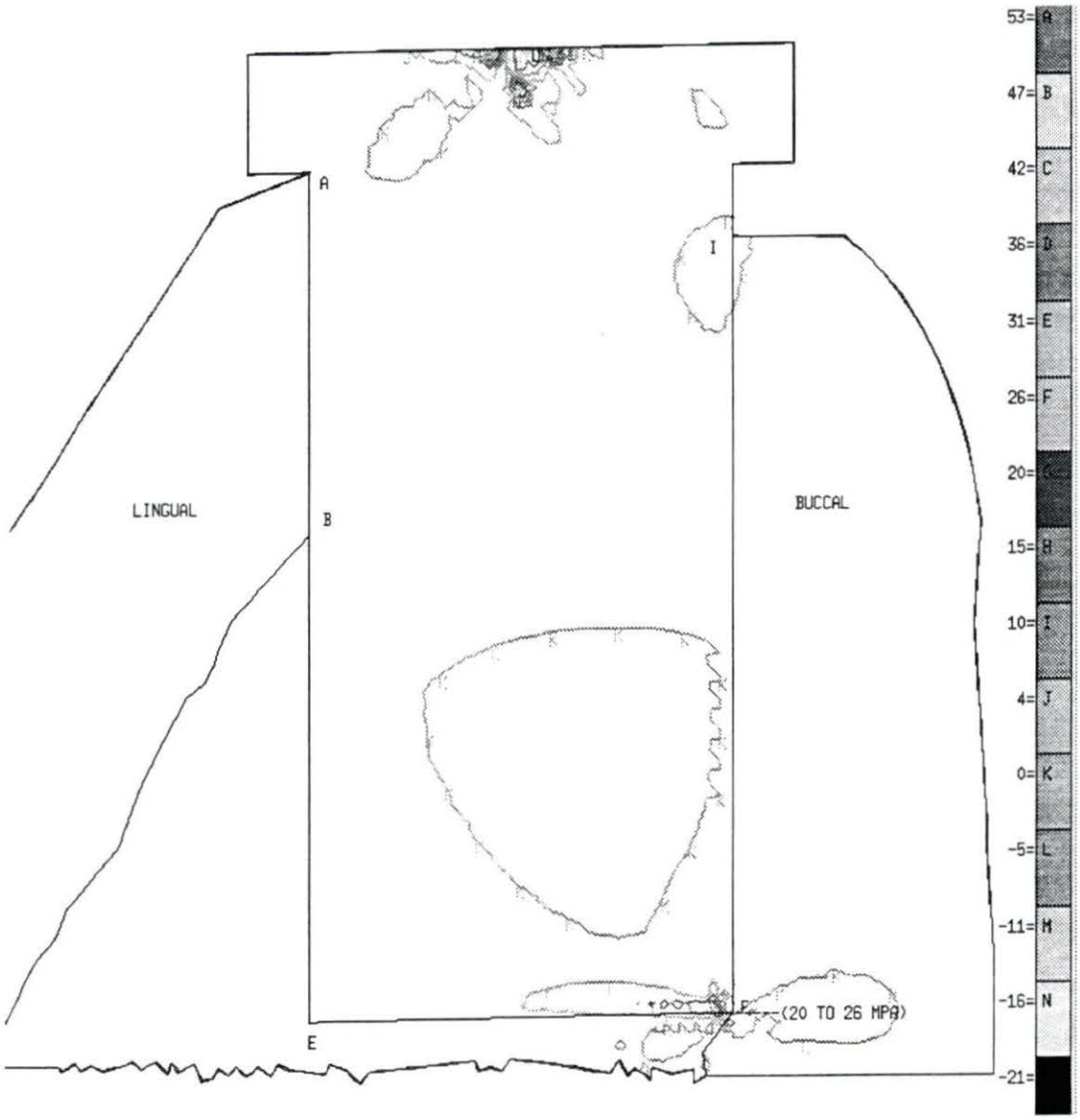

Figure 48. The maximum principal stress distribution predicted by FEA of the grooveless implant for an applied load of Fx = 8 N, Fy = -29 N

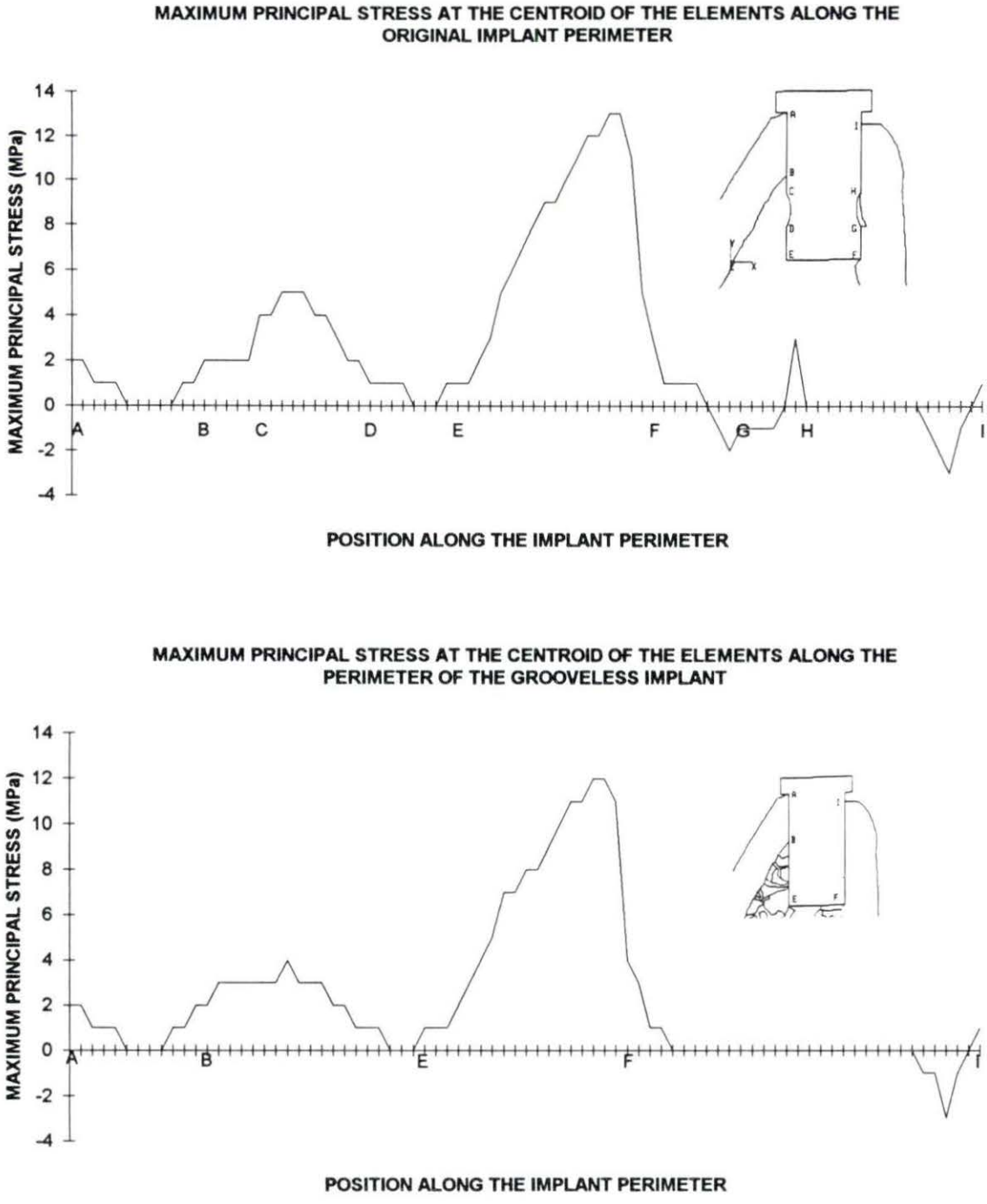

Figure 49. The magnitude of the principal stresses at the centroid of the elements located along the implant perimeter for both the original implant (top) and the grooveless implant (bottom) as predicted by FEA for a load of Fx = 8 N, Fy = -29 N

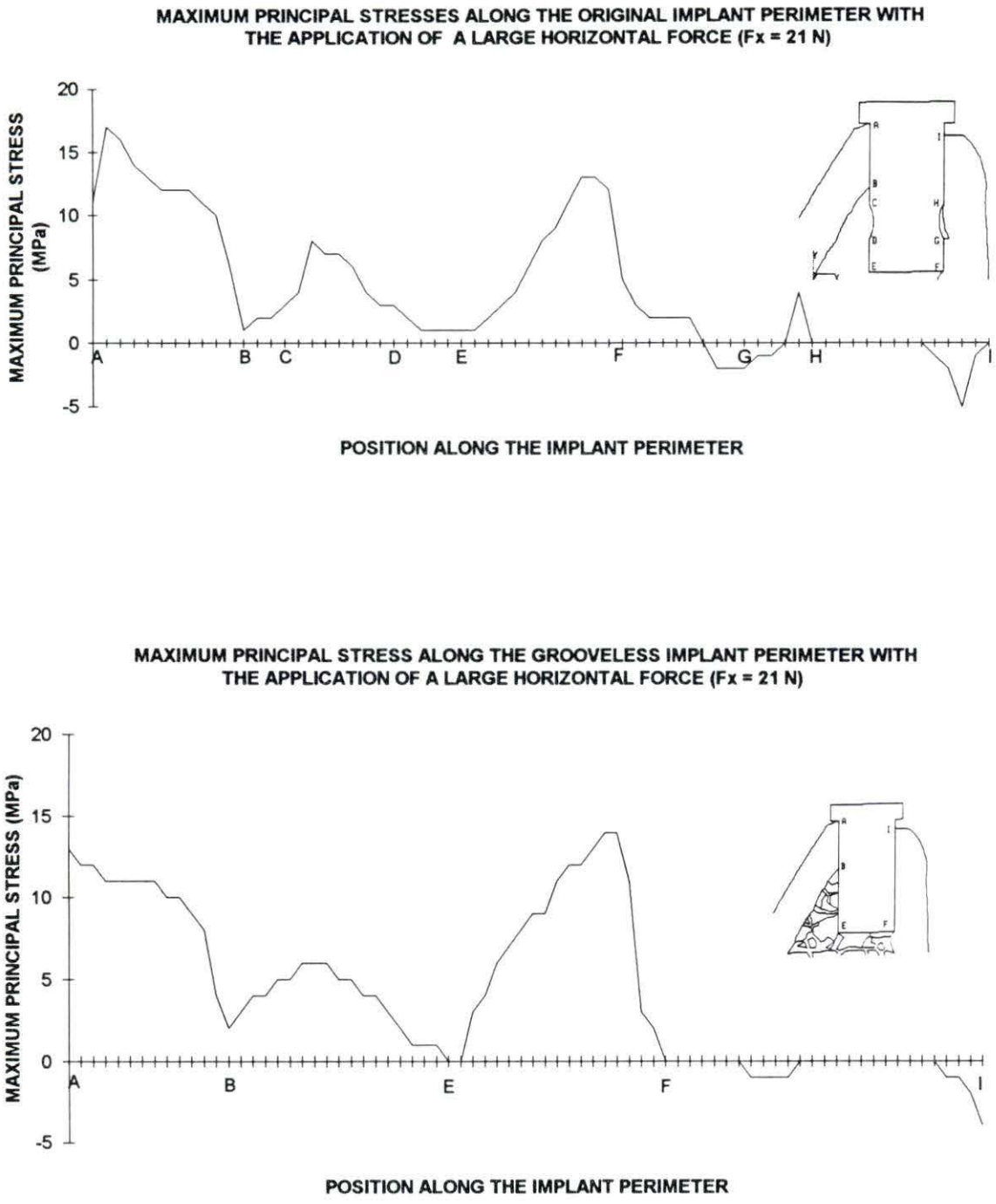

Figure 50. The top and bottom graphs illustrate the maximum principal stresses in the centroid of each of the perimeter elements of the original and pivoted implants, respectively, as predicted by FEA for large horizontal loading (Fx = 21 N, Fy = -21 N)

It is recommended that removal of the grooves from the original implant design be considered, to reduce the distribution and magnitude of the tensile stresses experienced by the implant, in response to anticipated physiological loading.

Principal strains Figure 51 contains two graphs which show the magnitude of the principal strains located at the nodes along the bone/implant interface for the original and the grooveless implant. The major difference between the two implants, in terms of the strains along the interface, is that removing the grooves reduces the level of strain in the bone along the buccal interface from a range of ~1000-2000 μE to a range of ~250-500 μE. This is because the buccal groove in the original implant was in contact with cancellous bone (E=360 MPa) but this same edge (now filled in with osteoceramic material) on the grooveless implant is assumed to be bonded to cortical bone (E=7.39 GPa) which is much stiffer. This level of strain could possibly lead to bone resorption along the buccal interface.

Long implant

The final design modification involved lengthening the implant by approximately 4 mm. The original implant design was 8 mm. This was chosen to accommodate the smallest anatomical measurements of the dogs that were used in a previous study (Niederauer, 1990).

Maximum principal stress Figure 52 illustrates the maximum principal stress distribution (only stresses ≥ 2.5 MPa are represented) and orientation experienced by the long implant in response to a stress of 30 N applied 15° from the vertical axis of the implant. The tensile stress distribution shown in Figure 52 is similar to that of the original implant subjected to the same loading (Figure 34). The stress concentration on the lingual side of the long implant is more widely distributed than that of the original implant, but the tensile stress concentration at the base of the long implant is more contained than that of the original implant. The magnitudes of the principal stresses at the centroid of the elements along the implant perimeter are presented in Figure 53 for both the original and the long implant. These graphs indicate that the long implant significantly reduces the stresses along the implant base (E-F). The magnitude of the stress concentration near point H is increased when the implant is lengthened.

Figure 54 contains two graphs which illustrate the magnitudes of the maximum principal stresses at the centroid of the edge elements, located along a path around the long and original implants, for a load of 30 N applied at an angle 135° to the positive x-axis

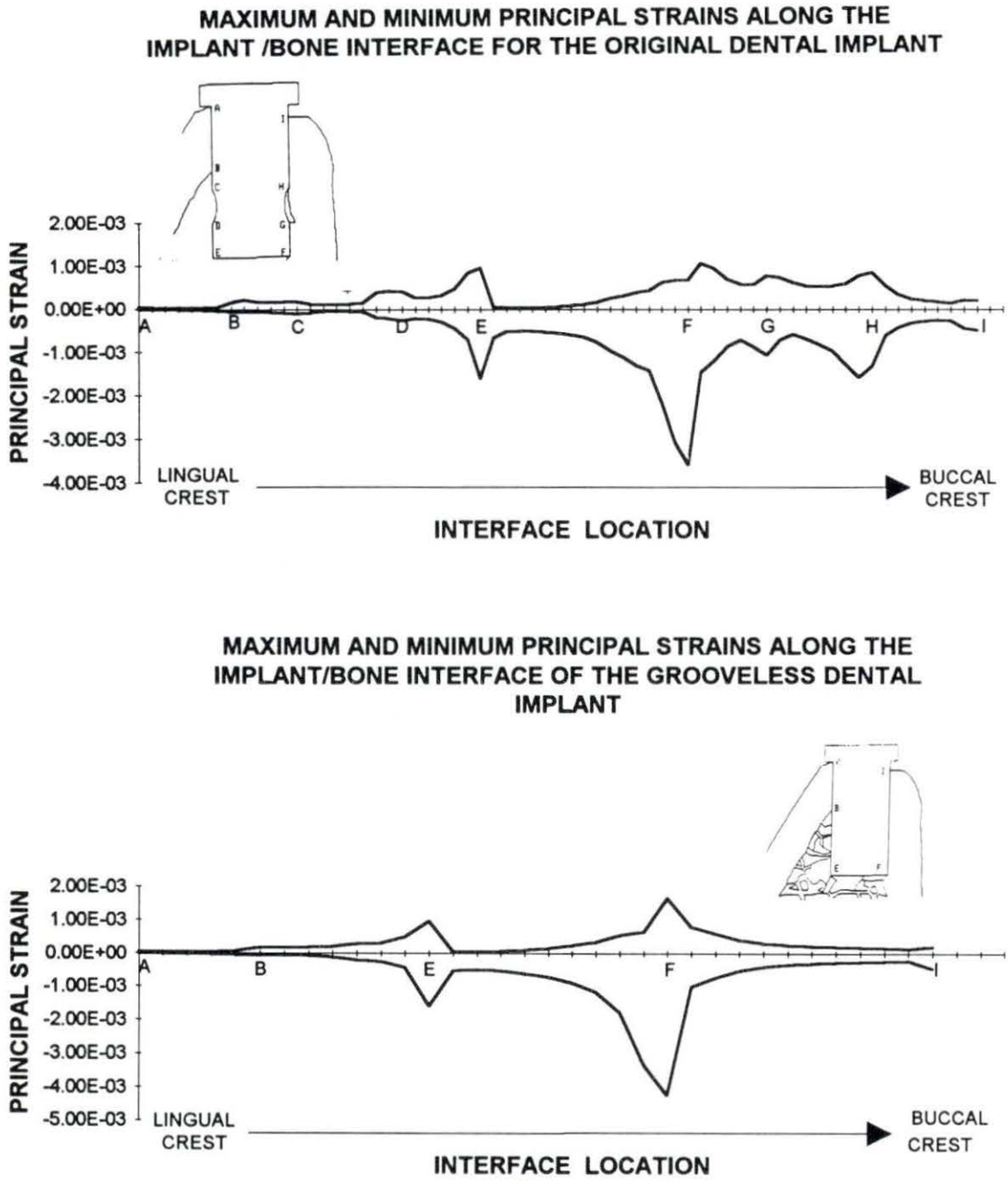

Figure 51. Two graphs which show the magnitude of the principal strains located at the nodes along the bone/implant interface for the original (top) and the grooveless implant (bottom) as predicted by FEA for a load of Fx = 8 N, Fy = -29 N

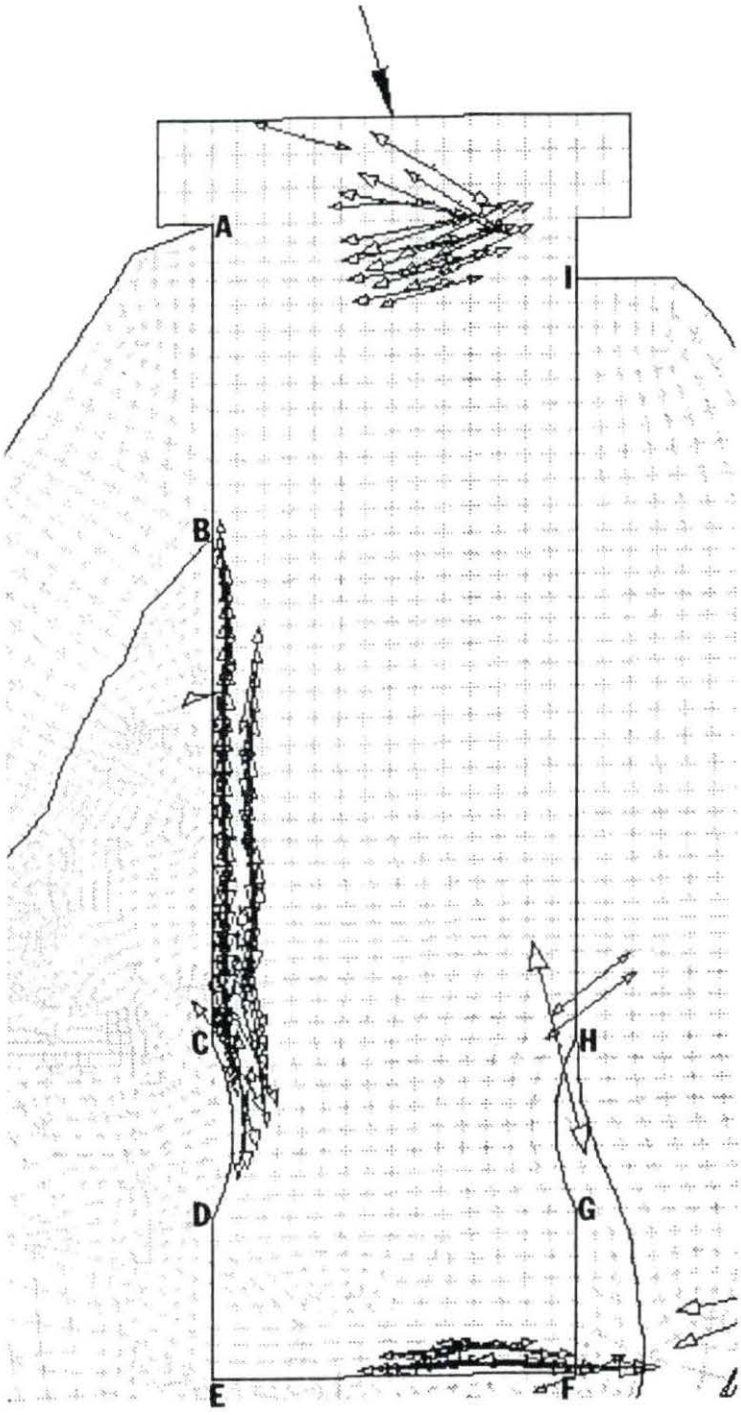

Figure 52. Tensor plot of the maximum principal stresses in the long implant for Fx= 8N, Fy= -29 N

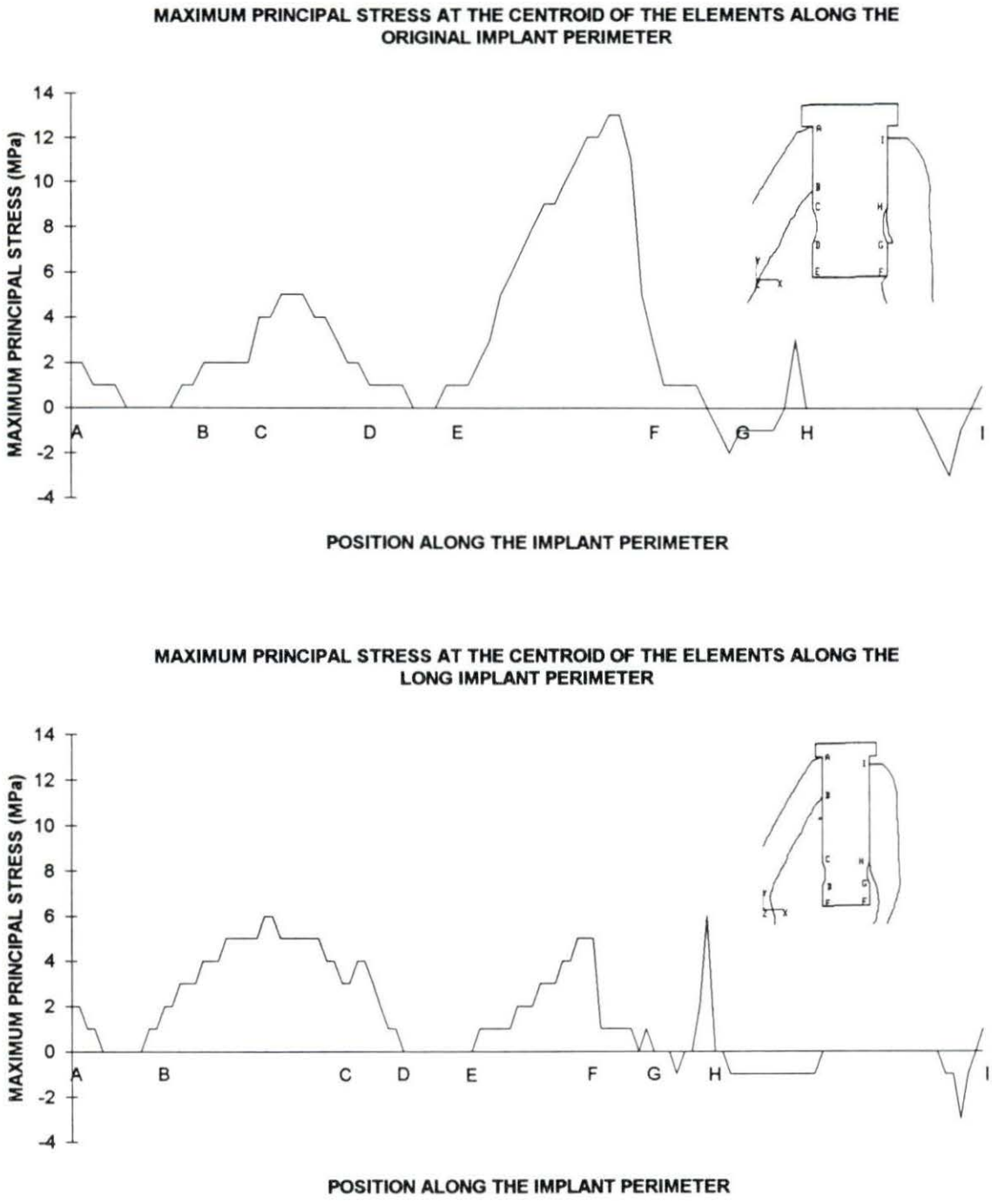

Figure 53. Magnitudes of the principal stresses at the centroids of the elements along the implant perimeter are presented for both the original and the long implant

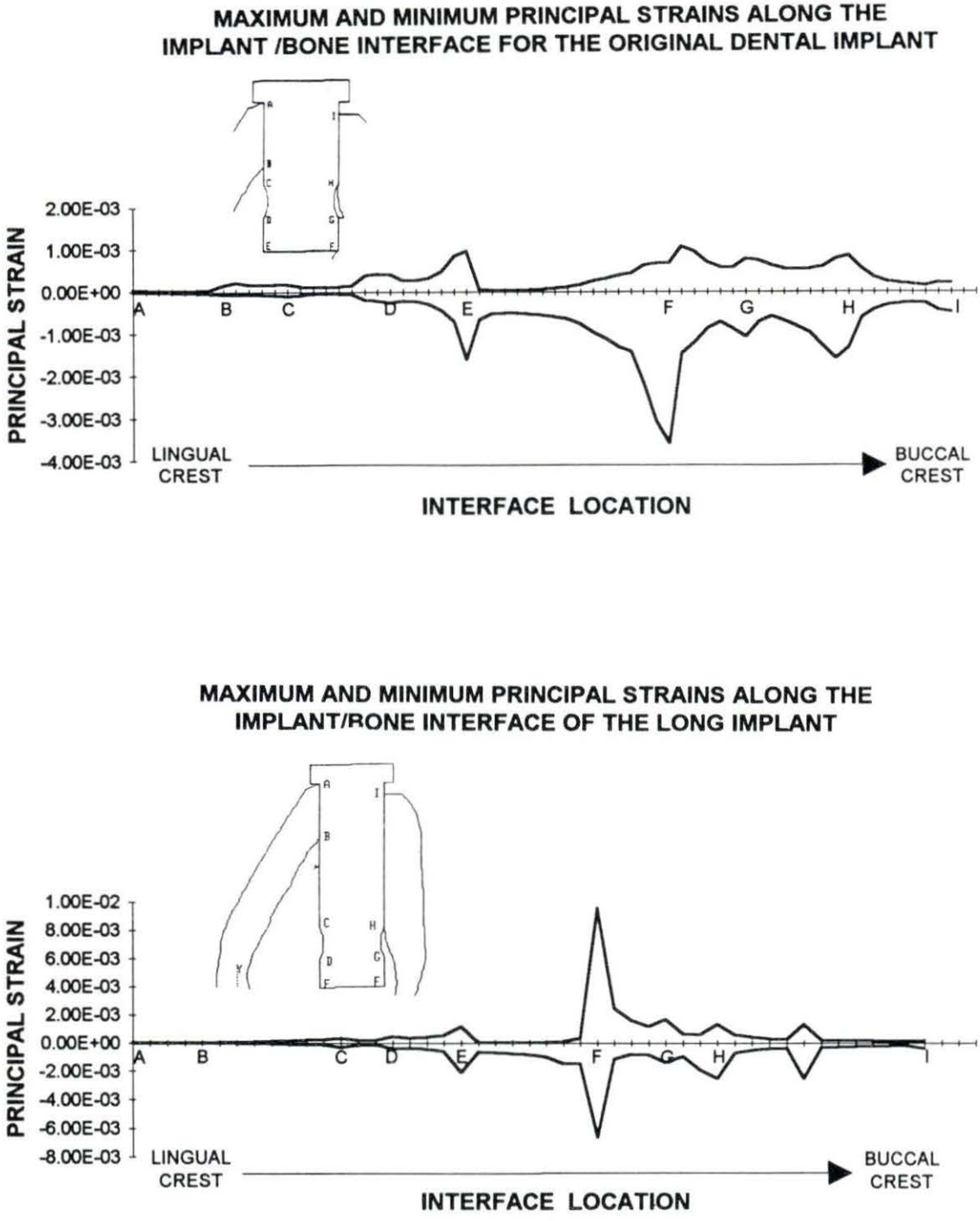

Figure 54. Two graphs which show the magnitude of the principal strains located at the nodes along the bone/implant interface for the original and the long implant

(Fx = 21 N, Fy = -21 N). Comparison of these two graphs indicate that, in general, lengthening the implant reduces the magnitude of the large tensile stresses in the osteoceramic that are observed with the application of large horizontal loads to the original implant.

If the lingual edge of the lengthened implant could be reinforced to accommodate the widespread tensile stresses shown in Figure 52 (B-D), then lengthening the implant may improve the lifetime of the osteoceramic dental implant. Simply adjusting the angle of implantation of the long implant, in a fashion similar to the pivoted implant (Figure 43), may also decrease the extent of tensile stress distribution along the lingual edge of the long implant.

Principal strain Figure 55 contains two graphs which show the magnitude of the principal strains located at the nodes along the bone/implant interface for the original and the long implant. These graphs show that the strains at the interface of both implants are very similar. The cancellous bone adjacent to the long implant at the buccal base corner, however, does exhibit extremely large strains of ~10,000 μE which is greater than the yield strain of cancellous bone (~7400 μE).

Investigation #3

Investigation #3 explored the effect of cancellous bone modeling on the magnitude and distribution of the stresses and strains in the long implant and the surrounding bone. Specifically, the long implant design was analyzed with three different finite element models which differed from one another only in how the cancellous bone was modeled. First, the principal stress results from the finite element analysis of the homogeneous model (Figure 31), the partially inhomogeneous model (Figure 32) and the strut model (Figure 33) of the long implant are compared. The principal strains in the bone surrounding the long implant, that are predicted by the finite element analysis of each finite element model, are then presented.

Maximum principal stress

Figure 56 is a tensor plot of the maximum principal stress results determined by finite element analysis of the homogeneous model of the long implant. Only those stresses that were ≥ 2.5 MPa were displayed. Figure 57 is a tensor plot of the maximum principal stresses (≥ 2.5 MPa) predicted to occur in the long implant via finite element analysis of

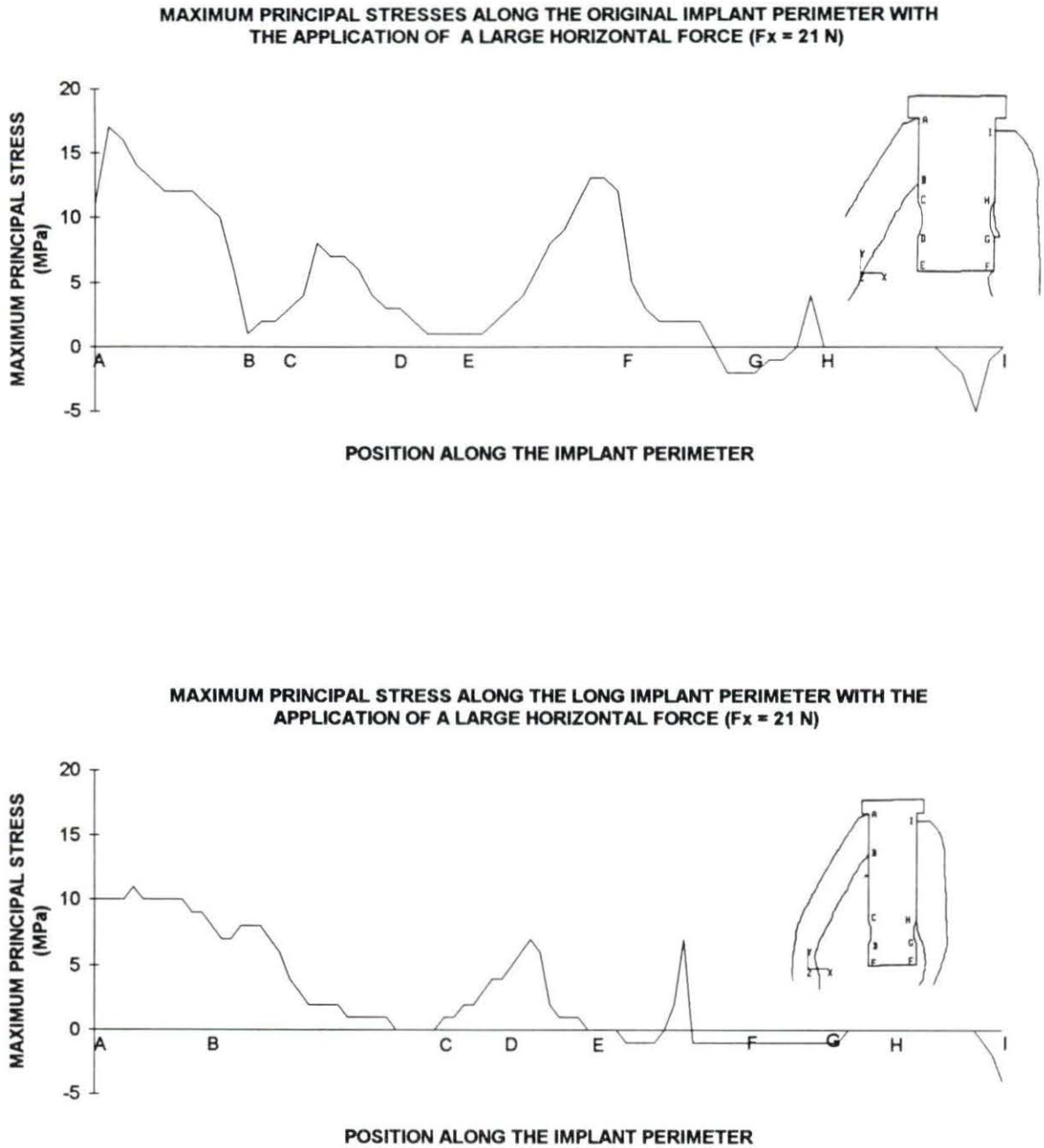

Figure 55. Maximum principal stress in the centroid of each of the perimeter elements of the original (top) and long (bottom) implants, as predicted by FEA for large horizontal loading (Fx = 21 N, Fy = -21 N)

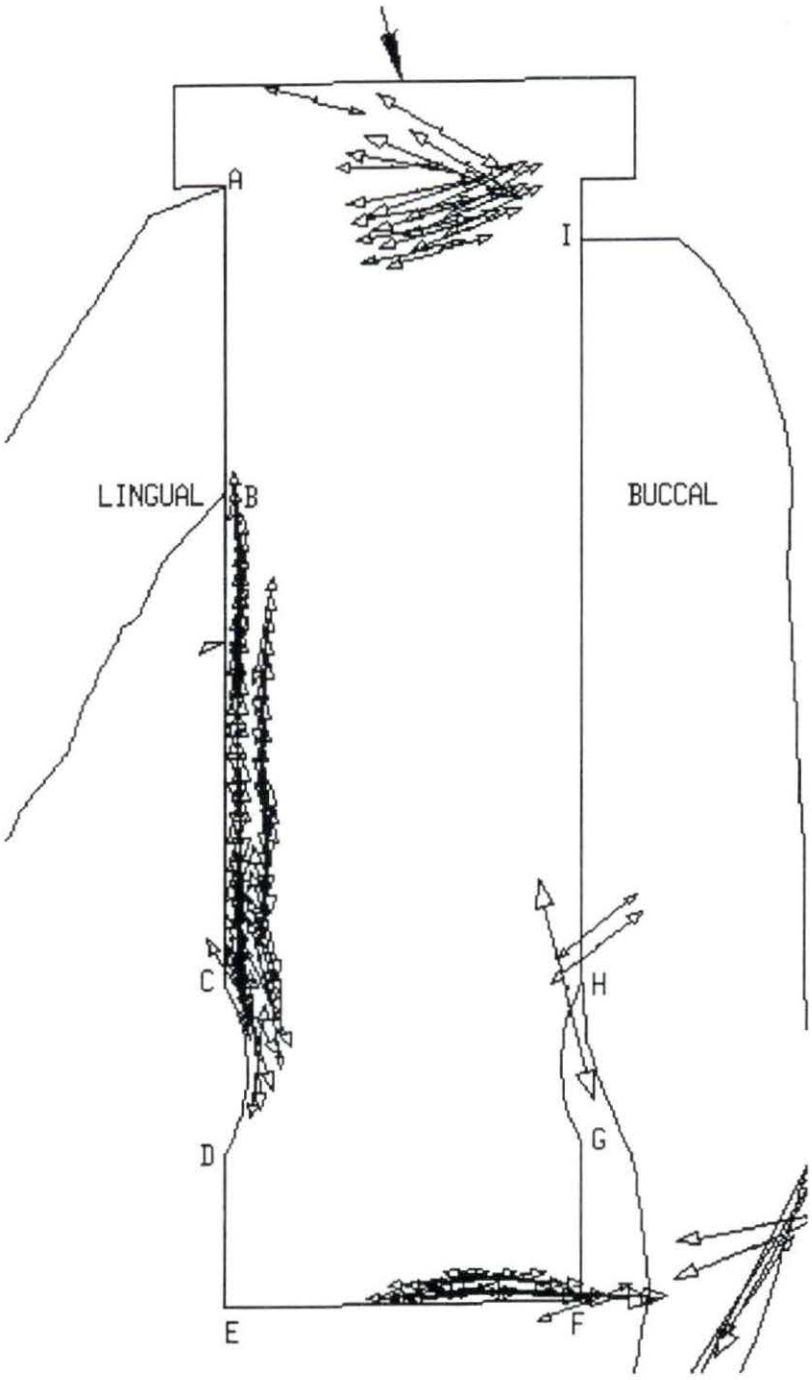

Figure 56. Tensor plot indicating the orientation and relative magnitude of the maximum principal stresses (≥ 2.5 MPa) in the implant as determined by finite element analysis of the homogeneous model of the long implant for an applied load of Fx = 8 N, Fy = -29 N

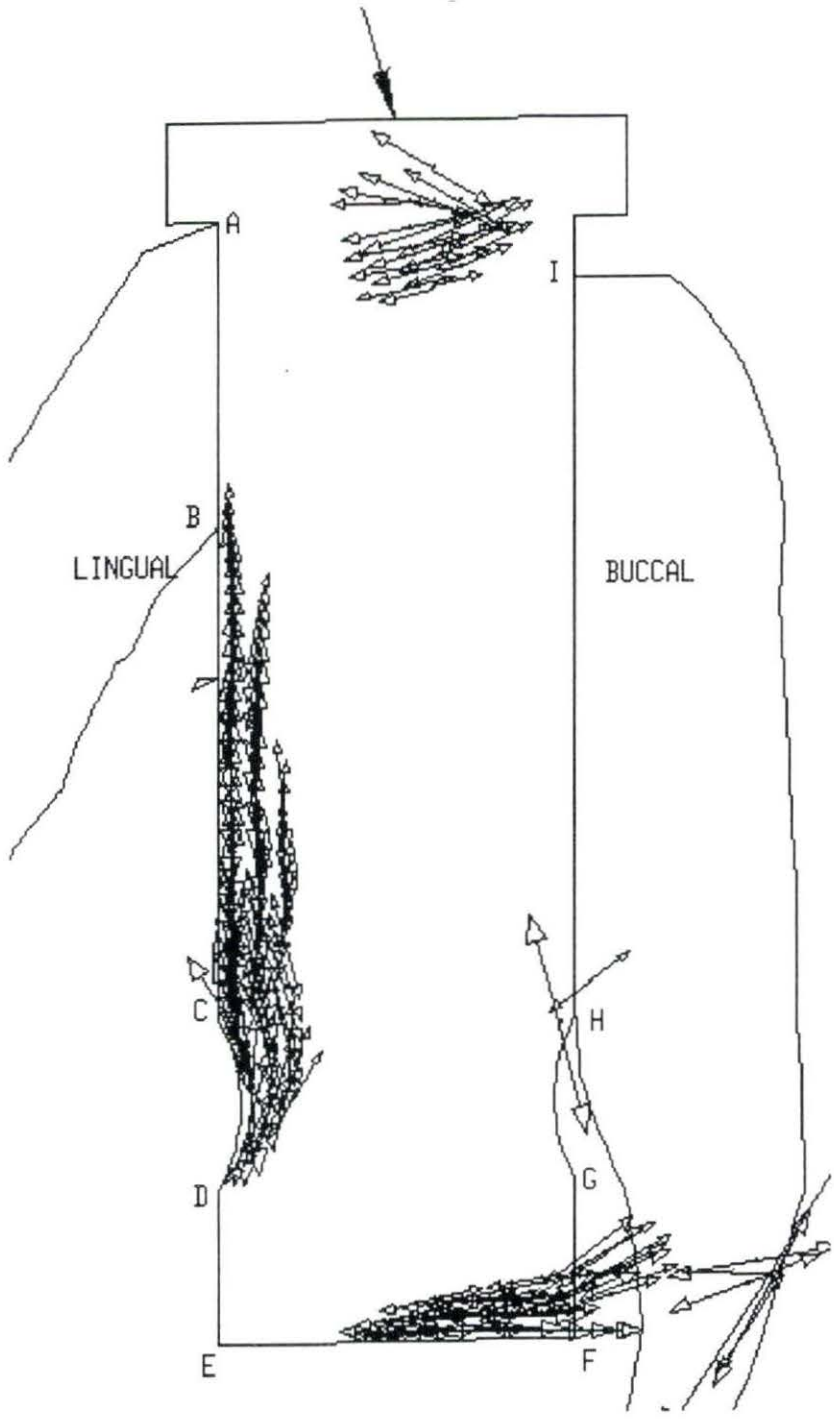

Figure 57. Tensor plot of the maximum principal stresses (≥ 2.5 MPa) predicted to occur in the long implant via finite element analysis of the partially inhomogeneous FEM for an applied load of Fx = 8 N, Fy = -29 N

the partially inhomogeneous FEM. Figure 58 is a tensor plot of the maximum principal stresses (≥2.5 MPa) as determined by finite element analysis of the strut model. All three tensor plots highlight two major areas of tensile stress concentration. These are located between points B and D on the lingual edge of the implant and along the buccal half of the implant base. The strut model predicts both of these distributions to be more widespread and larger in magnitude than those predicted by the partially inhomogeneous or homogeneous model. The homogeneous and partially homogeneous models also indicate some large stresses near point H, at the top of the buccal groove, that are not present in the strut model (Figure 58).

The magnitudes of the maximum principal stresses at the centroid of each of the elements along the long implant perimeter are presented in Figure 59 for each of the cancellous bone models. Note that the homogeneous and partially inhomogeneous model results demonstrate the same trends with only slight differences in stress magnitudes. The strut model finite element results, however, show significantly different trends and stress magnitudes. These differences occur where the strut model differs from the other models the most (E-H). These are areas where distinct trabeculae are modeled. These stress peaks are caused, in part, by the stress concentrations that arise due to the extreme difference in stiffness between the cancellous bone struts (7.39 GPa) and the intertrabecular spaces (1MPa). Stresses are preferentially transferred to the stiffer struts versus the highly compliant intertrabecular spaces. Figures 56 through 59 demonstrate that, for the loads applied to the implant in this analysis (Fx = 8 N, Fy = -29 N), modeling the cancellous bone as homogeneous or as partially inhomogeneous fails to locate the maximum tensile stresses in the implant.

It is possible that the modulus of elasticity of the trabecular struts is overestimated in this study. Measurements of the modulus of elasticity of trabecular bone material that have been presented in the literature range from 0.76 to 20 GPa (Rho et al., 1993). Even if the Young's modulus of the struts was assigned the lowest value in this range, there would still be quite a large difference between the stiffness of the struts and the intertrabecular spaces. This would still cause significant stress concentrations in the implant.

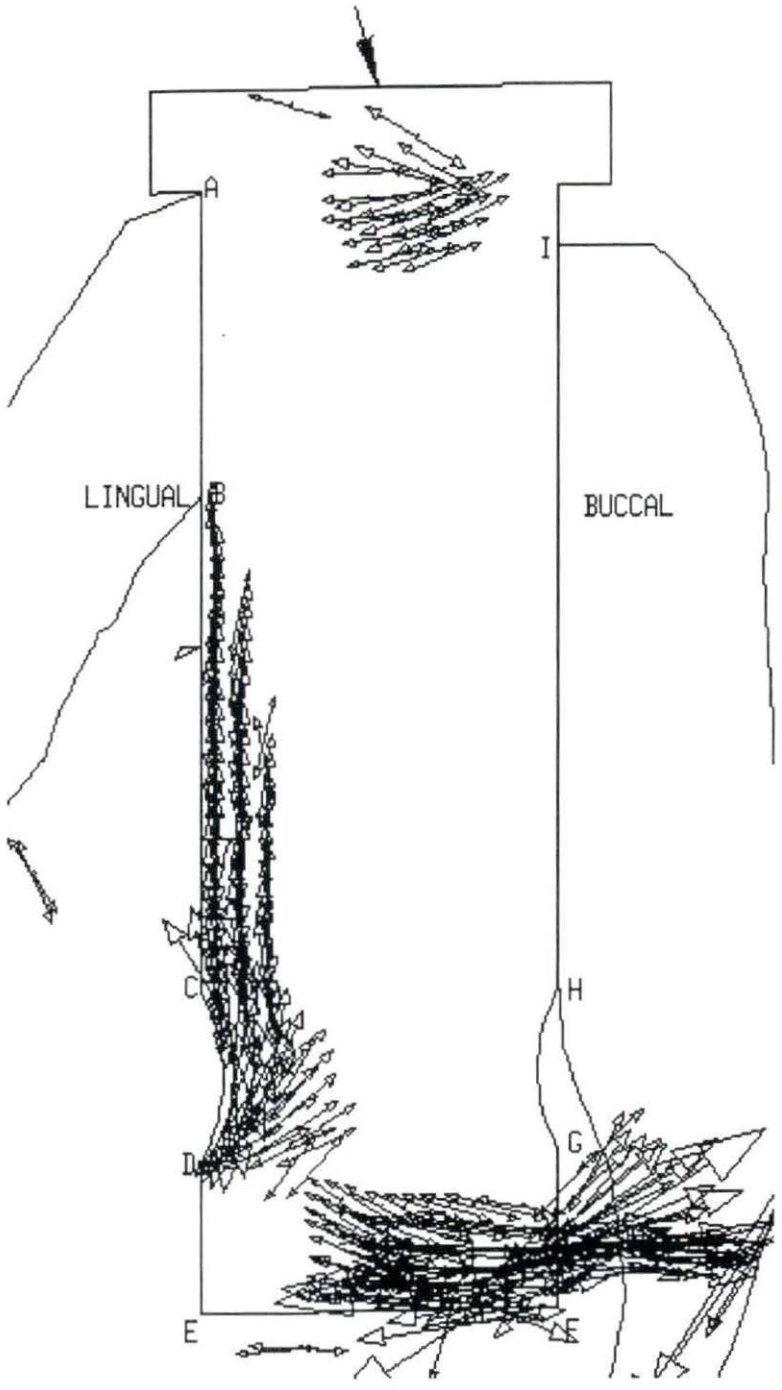

Figure 58. Tensor plot of the maximum principal stresses (≥2.5 MPa) as determined by finite element analysis of the strut model for an applied load of Fx = 8 N, Fy = -29 N

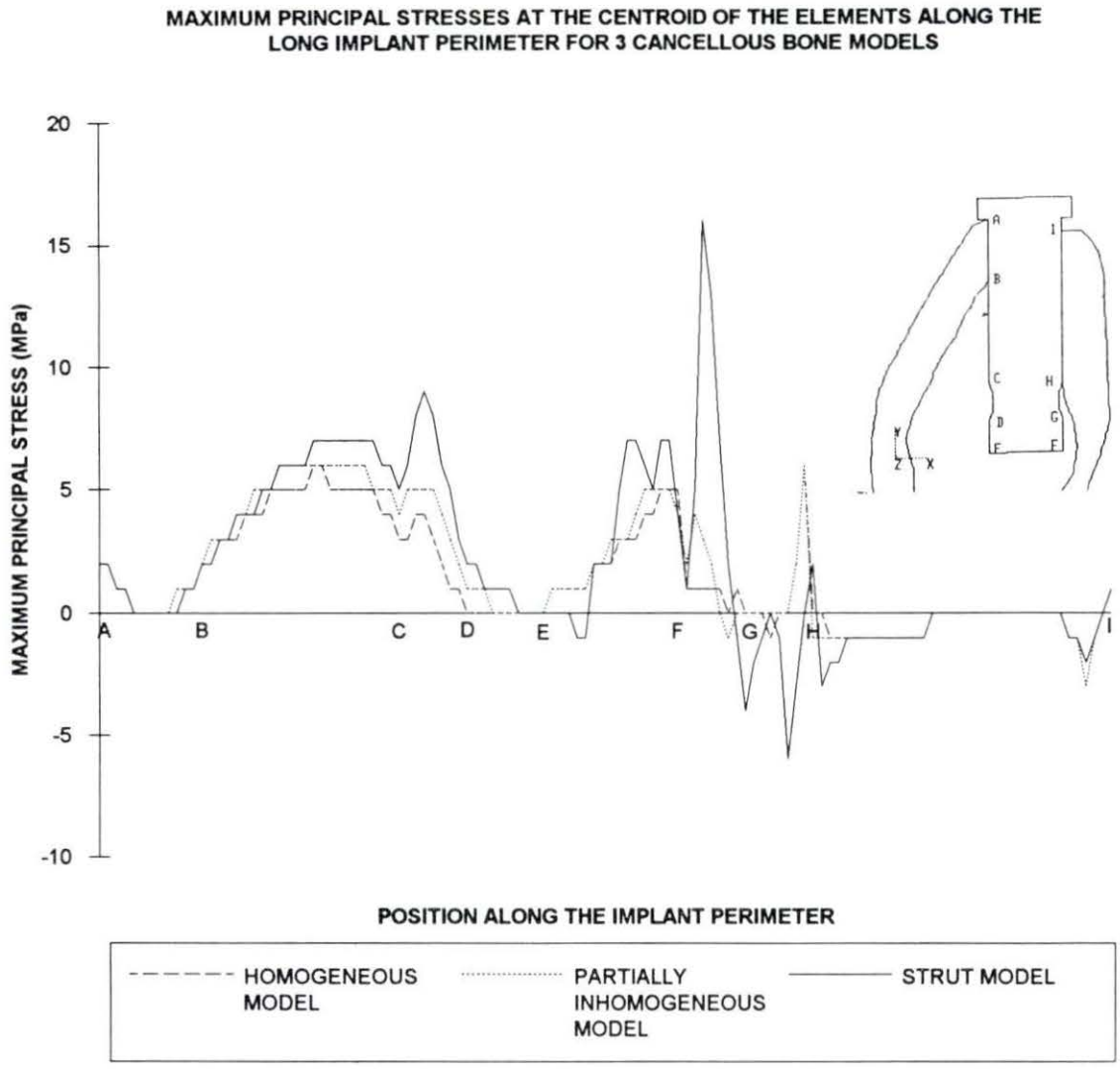

Figure 59. The magnitude of the maximum principal stresses at the centroid of the elements along the long implant perimeter as predicted by FEA of each of the cancellous bone models for an applied load of Fx = 8 N, Fy = -29 N

Minimum principal stress

Figure 60 illustrates the magnitudes of the minimum principal stresses at the centroid of each element along the long implant perimeter for each of the cancellous bone models. Again, FEA of the homogeneous and partially homogeneous models yields similar stress distributions and magnitudes. FEA of the strut model yields significantly different results. Stress peaks on Figure 60 are labeled 1 through 5, and coincide to the specific struts, also labeled 1 through 5, in Figure 61. Comparison of Figures 61 and 62 shows that the stress concentrations in the implant adjacent to bone struts that are detected by FEA of the strut model are not detected by FEA of the homogeneous model (Figure 62). Again, these stress concentrations are most likely due to the preferential transfer of stress from the implant to the stiffer bone struts, versus the more compliant intertrabecular spaces.

The literature contains only one study in which the individual struts of cancellous bone surrounding a dental implant are modeled in the creation of a finite element model (Lavernia et al., 1981). Their study concluded that modeling the individual struts yielded similar stress distributions, but significantly different stress magnitudes, in comparison to results obtained by FEA of homogeneously modeled cancellous bone. The reason that their study did not show that cancellous bone modeling affects stress distributions or trends may have been that their study used a very coarse mesh and assigned the same Young's modulus to the individual bone struts in their strut model and the cancellous bone area in their homogeneous model.

Principal strains

Figure 63 contains two graphs illustrating the principal strain magnitudes along the implant/bone interface for each FEM. The homogeneous and partially inhomogeneous FEM results are almost exactly the same along the entire interface. The strut model again predicts very different results, especially for points between E-H, which exhibit the most inhomogeneous structure. The strut model predicts areas of large maximum and minimum principal strain peaks along the implant base. Figures 64 and 65 illustrate strut model strain tensor plots of an enlarged area along the implant base. These Figures illustrate that the extremely large peak strains predicted by FEA of the strut model occur in areas occupied by extremely compliant intertrabecular space (E = 1 MPa). However, the strains predicted to occur in bone struts, which are believed to moderate the relative rates of bone resorption and deposition (Clift et al., 1992), are the strains of interests.

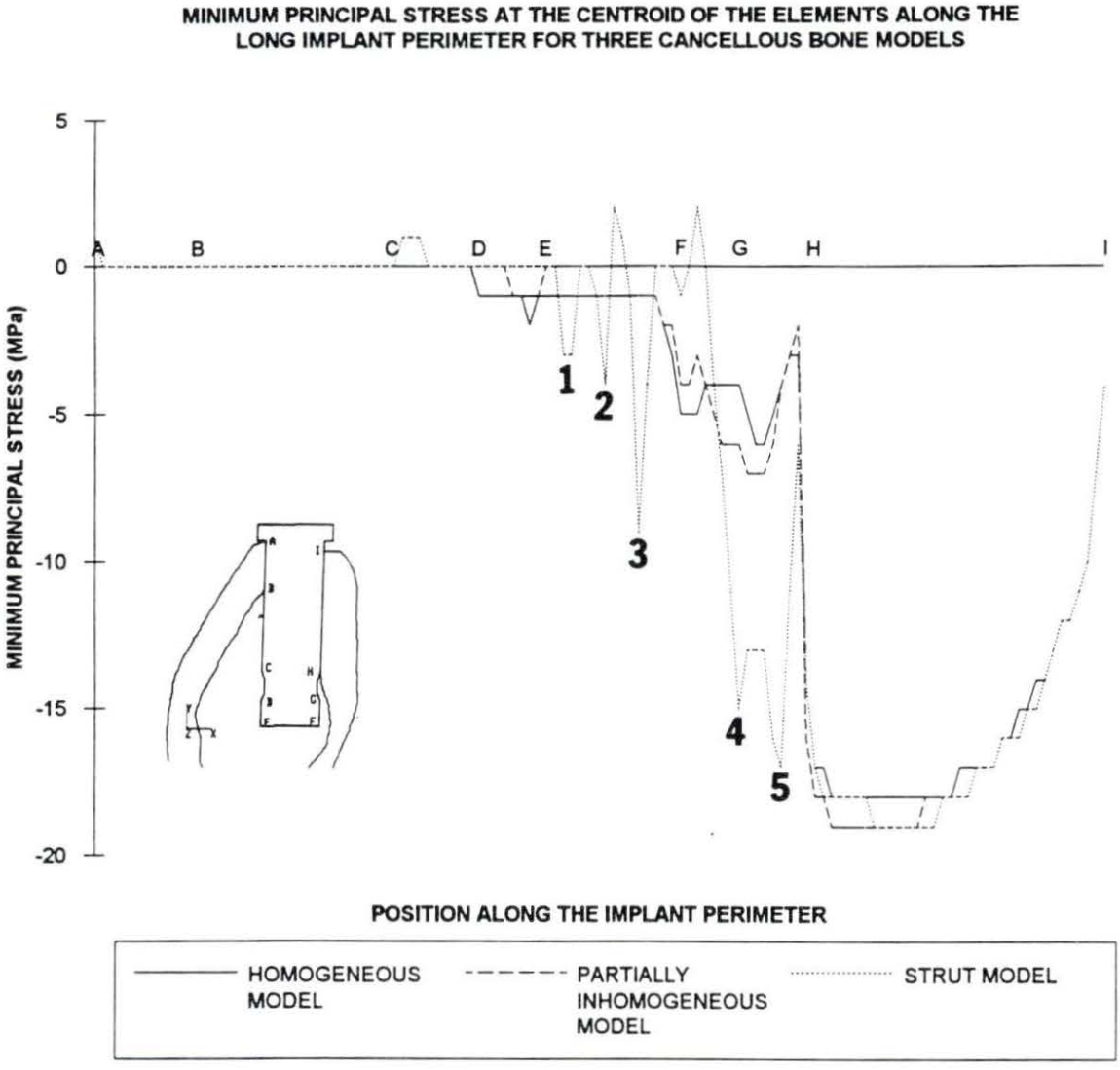

Figure 60. Minimum principal stress at the centroid of the elements along the long implant perimeter for three cancellous bone models

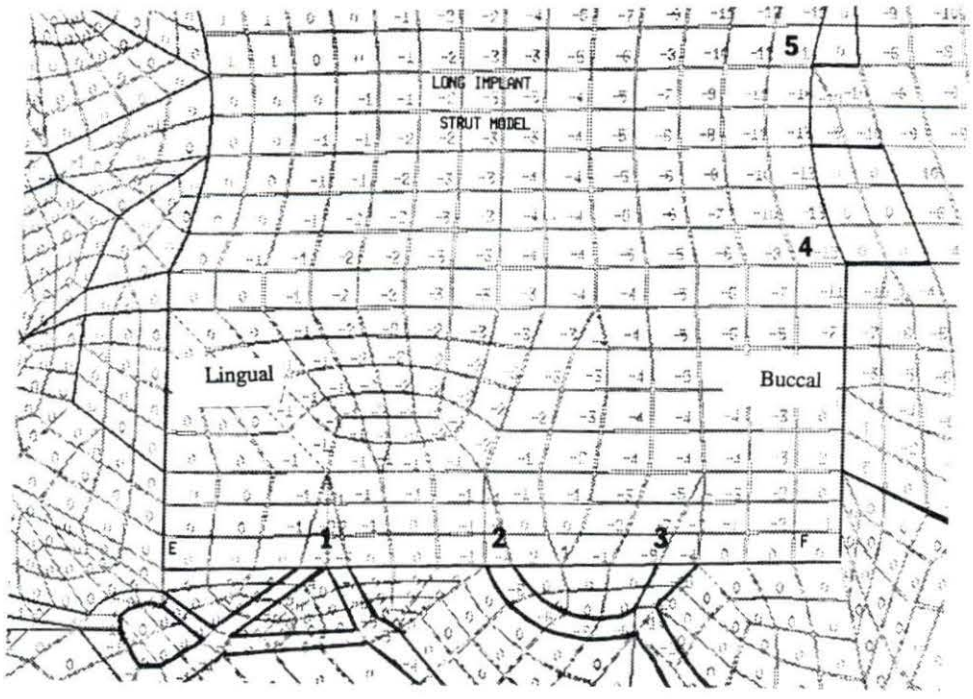

Figure 61. Minimum principal stress magnitudes at the centroid of the elements along the base of the long implant as determined by FEA of the strut model. Note the stress concentrations (1-5) in the implant adjacent to the cancellous bone struts

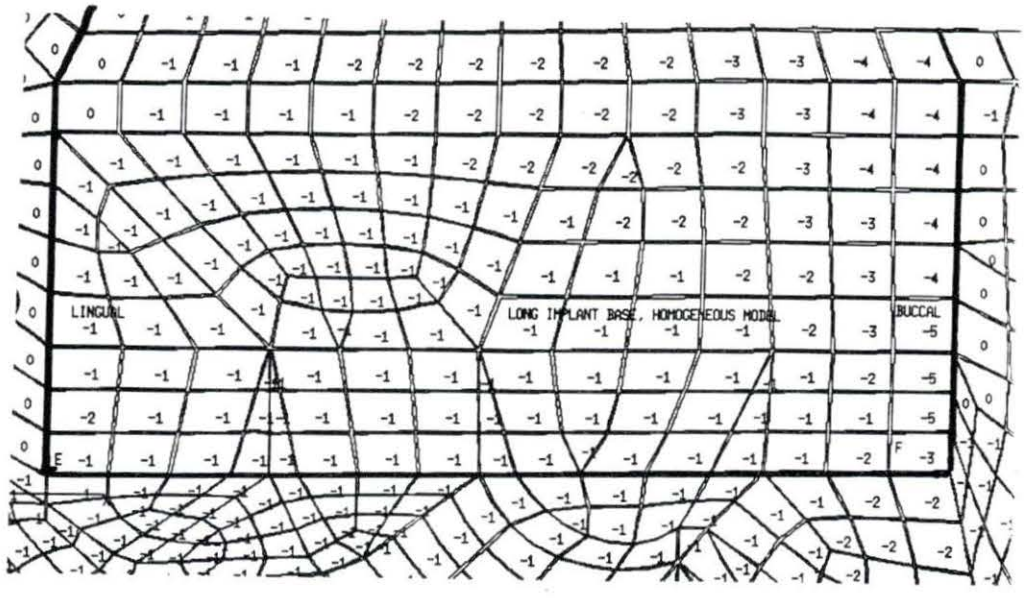

Figure 62. Minimum principal stress magnitudes at the centroid of the elements along the base of the long implant as determined by FEA of the homogeneous model

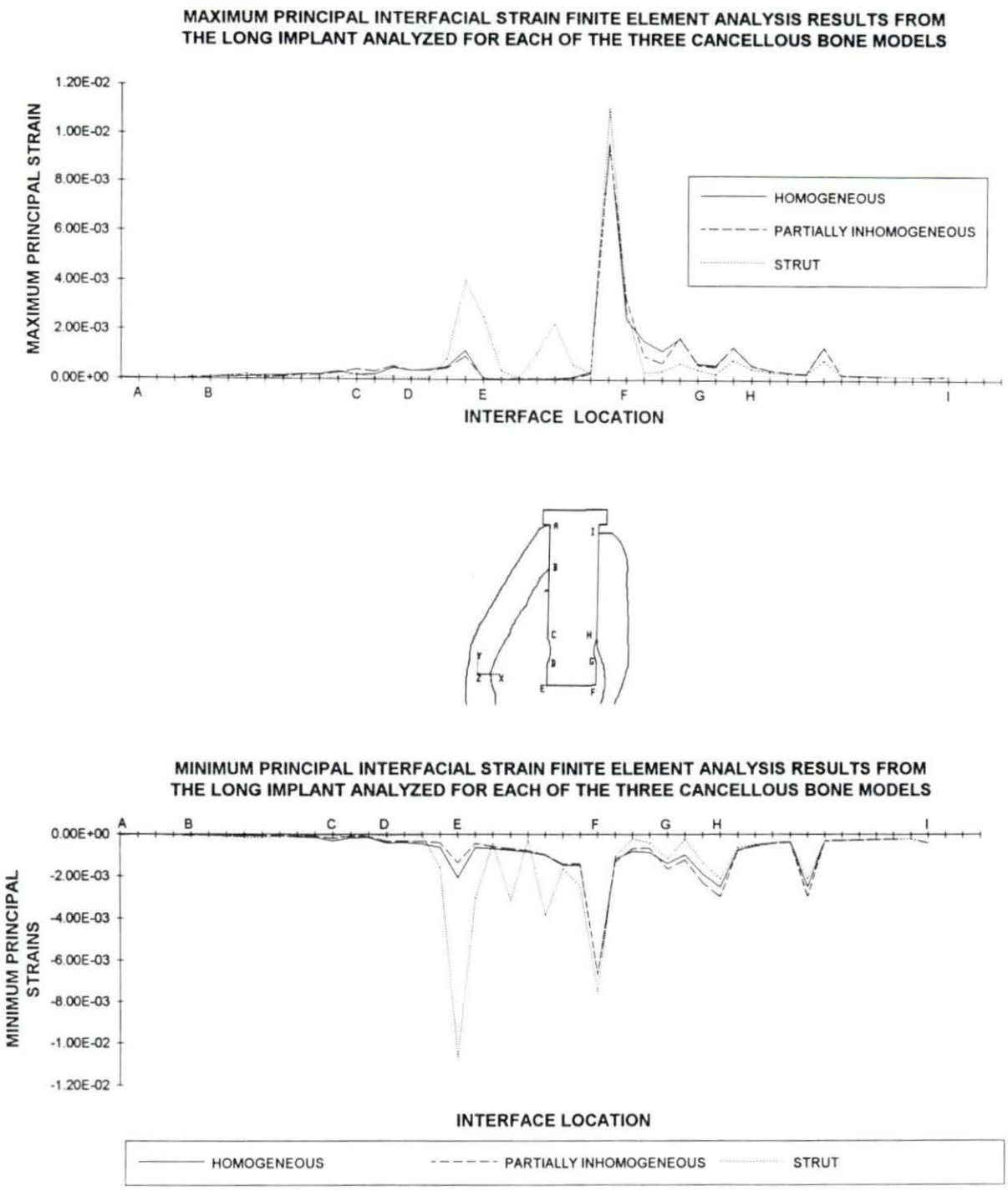

Figure 63. Two graphs illustrating the principal strain magnitudes along the implant/bone interface for each FEM

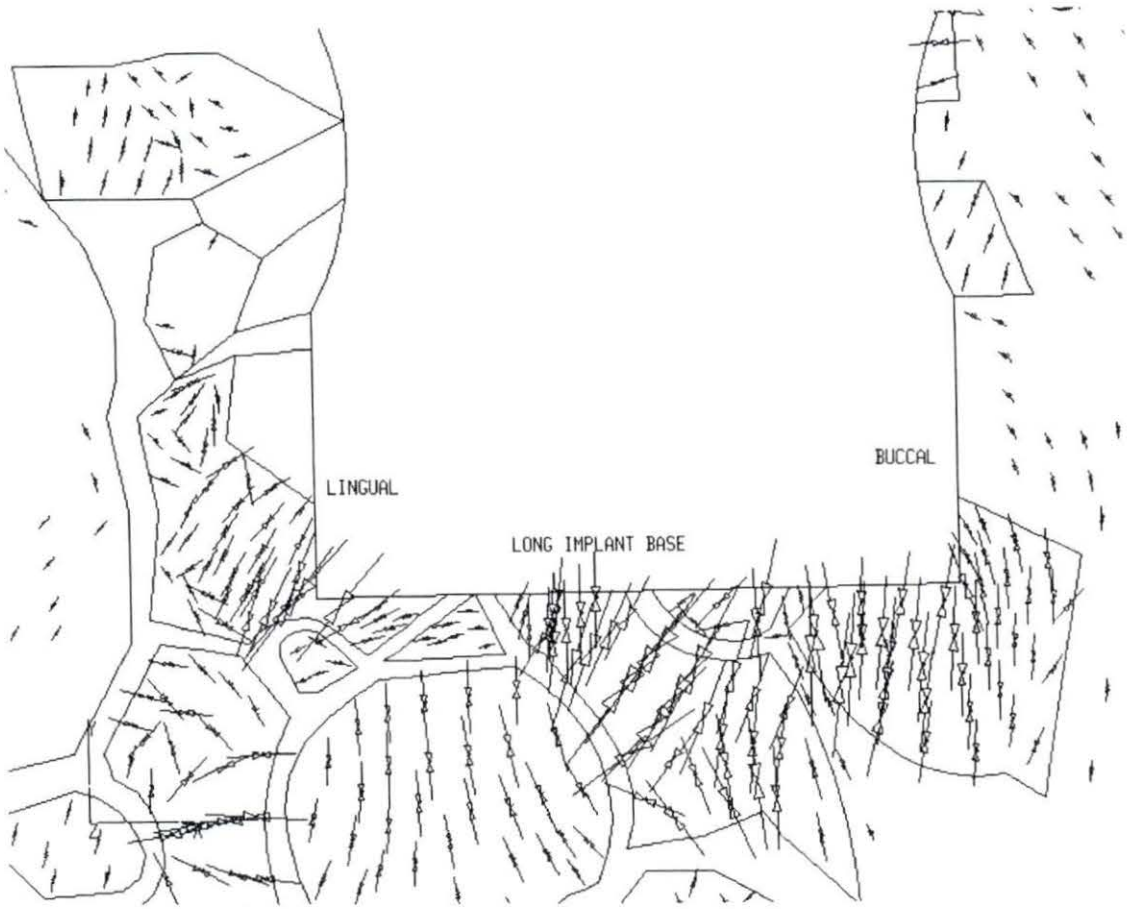

Figure 64. Tensor plot of the minimum principal strain along an enlarged area of the base of the long implant. The load applied to the strut model of the long implant is Fx = 8 N, Fy = -29 N

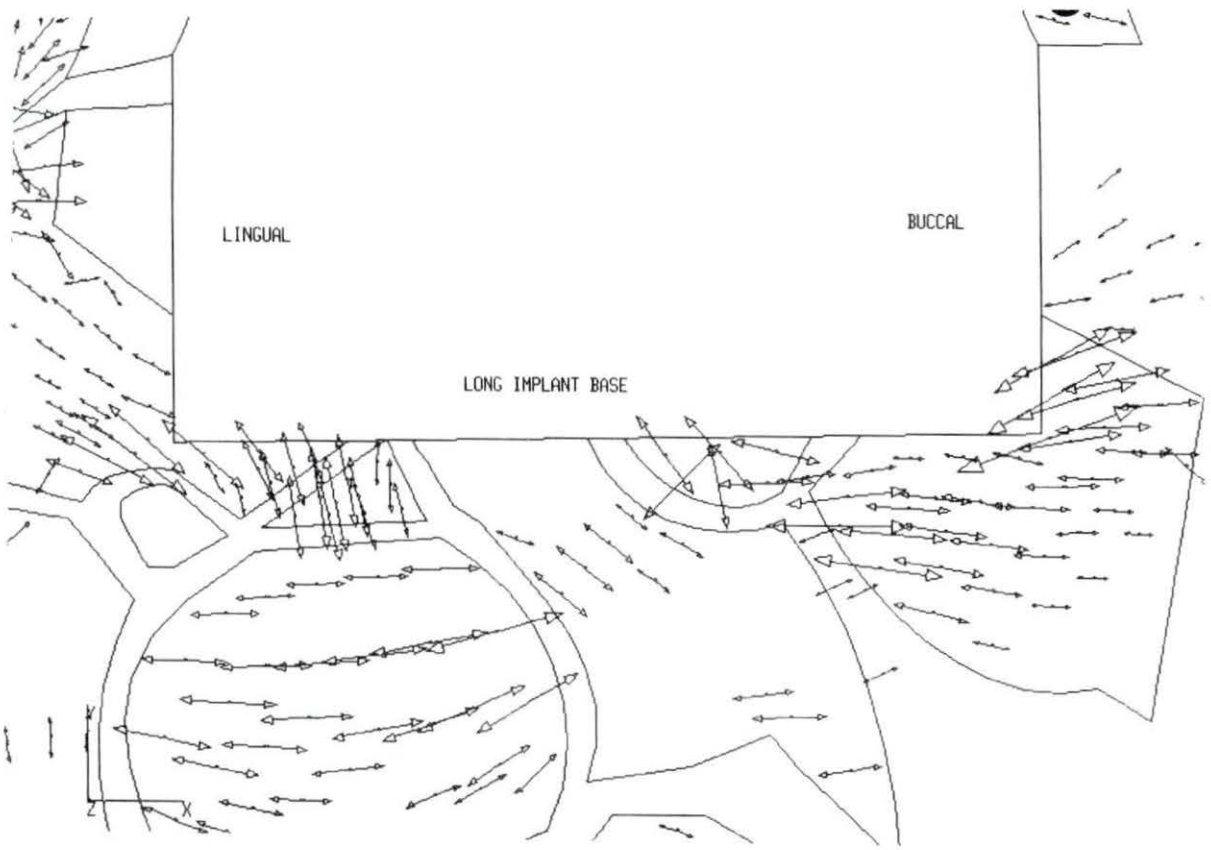

Figure 65. Tensor plot of the maximum principal strain along an enlarged area of the base of the long implant. The load applied to the strut model of the long implant is Fx = 8 N, Fy = -29 N

Figure 66 shows the particular elements (1-18) that were examined to determine how cancellous bone modeling affects the magnitude of strains in bone. These elements were chosen because they were located in areas occupied by bone struts in the original histological section. Each of these elements is located in exactly the same position in each of the three cancellous bone models, but they are assigned different material properties in each of the three finite element models. Figure 67 illustrates the maximum principal strains in each of these elements as predicted by FEA for each of the cancellous bone models. The homogeneous model and the partially inhomogeneous model indicate very similar strain magnitudes for almost all of the elements. This similarity was also noted in all of the finite element analyses that were performed in the other investigations which were concurrently run with each of the different cancellous bone models. Figure 59 also demonstrates the similarity in finite element maximum principal stress results when the cancellous bone is modeled as homogeneous or partially inhomogeneous. Throughout this study, it was found that modeling the cancellous bone as partially inhomogeneous, in an effort to account for the variation in cancellous bone density, did not yield results that were significantly different from those predicted by FEA when the bone was modeled as homogeneous. Hayes et al. (1982) reported that it was very important to take account of the variation in cancellous bone's apparent density for a finite element analysis of a human patella. It is possible that cancellous bone density is not as predominant of a factor in a finite element analysis of mandibular bone as that of patellar bone because the cortical bone shell of the mandible is much thicker and thus more dominant than that of the patella. Other possible reasons for the difference in the results between the two studies is that there was no implant included in the patellar study, the mesh was very coarse in the patellar study, and the geometry and entire biomechanical situation of the patella is totally different from that of the mandible.

The strut model maximum principal strain results illustrated in Figure 67 indicate that, in some elements, strain magnitudes are much smaller than those of the other models, but in other areas, the strains predicted from analysis of the strut model are much greater than those of the other models. Figure 68 illustrates the minimum principal strains in each of the selected elements as predicted by FEA for the three cancellous bone models. This graph shows that the strut model demonstrates the same trends in minimum principal strains as the other models but that its magnitudes are much less than those predicted by FEA of the homogeneous model and the partially homogeneous model.

Ideally, all finite element models would model every strut of cancellous bone in three dimensions, but in reality, this cannot be done and possibly should not be done. If one is

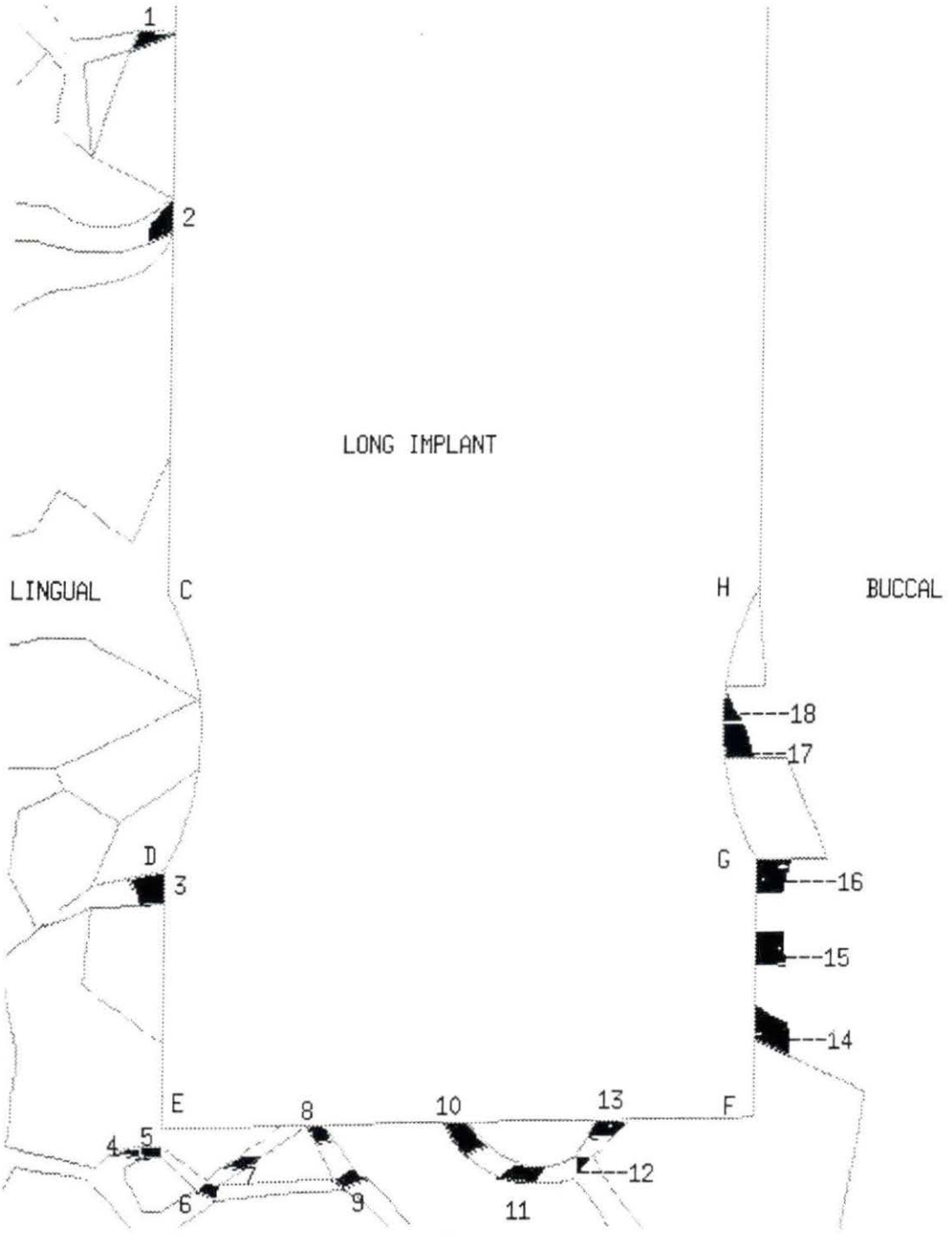

Figure 66. Elements evaluated from the long implant to determine the effect of cancellous bone modeling on the magnitudes of strain in bone for a load of Fx = 8 N, Fy = -29 N

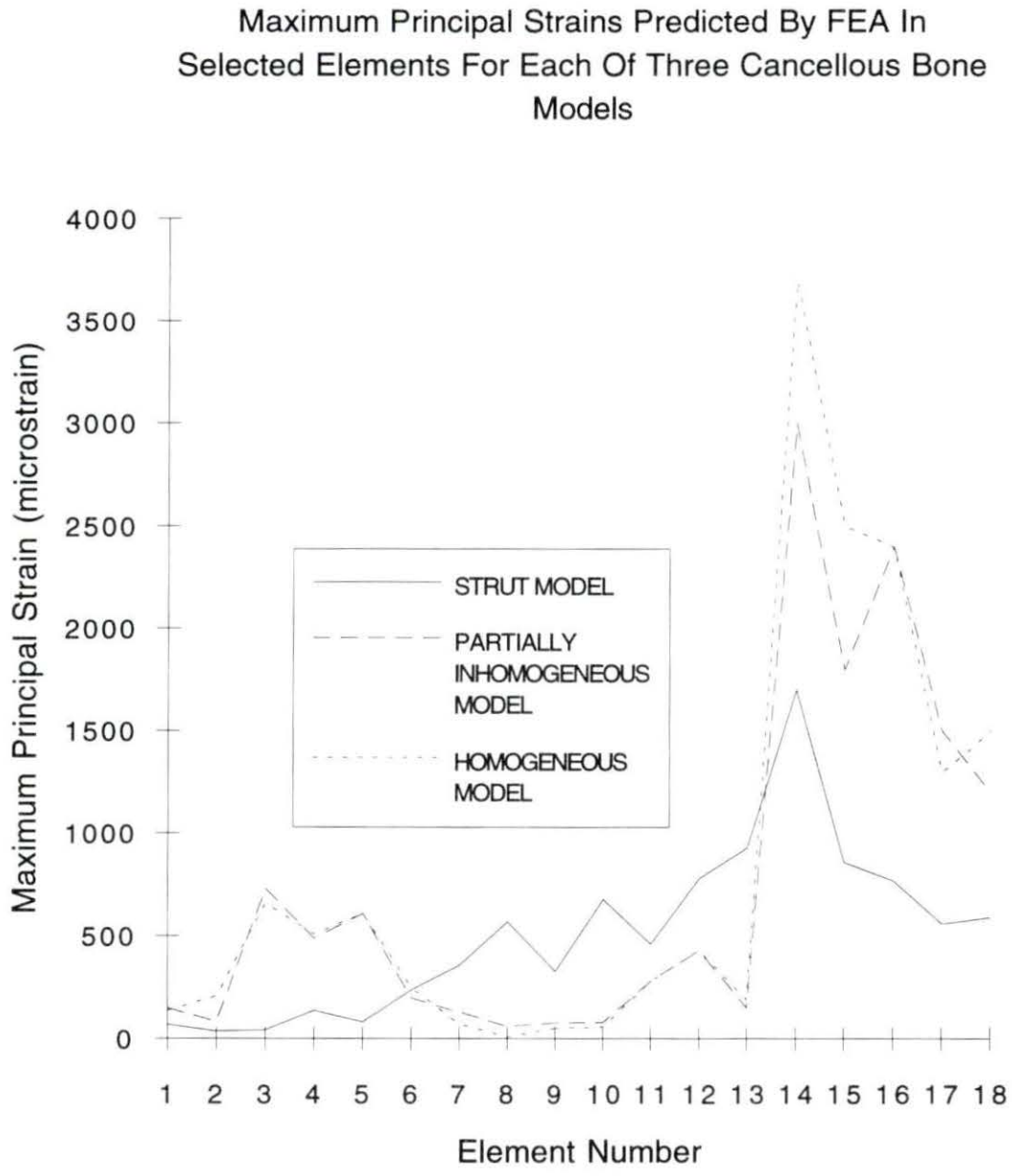

Figure 67. Graph illustrating the maximum principal strains in each of the elements defined in Figure 63 as predicted by FEA for each of the cancellous bone models

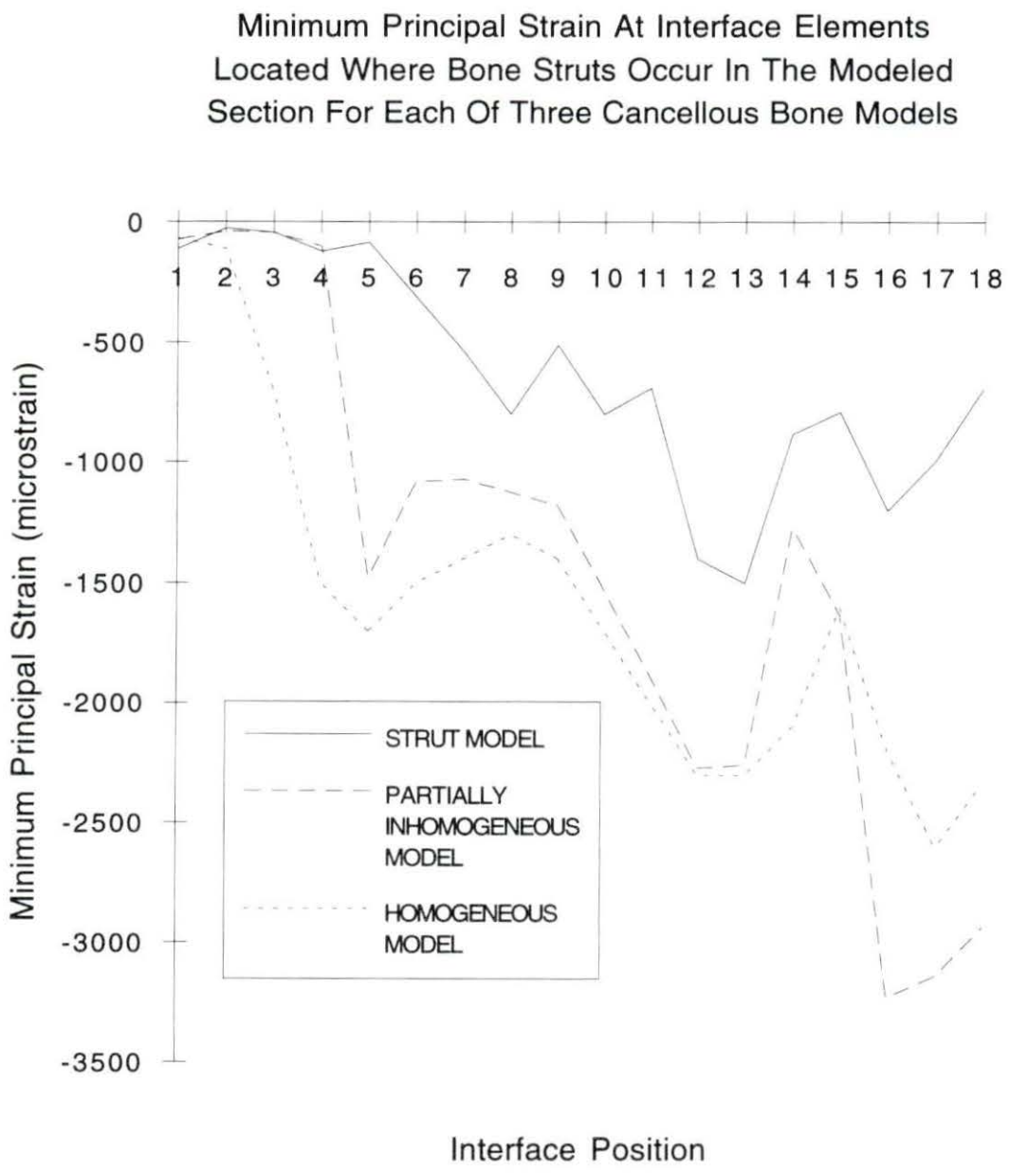

Figure 68. Graph illustrating the minimum principal strains in each of the elements defined in Figure 66, as predicted by FEA for each of the cancellous bone models

using finite element analysis to do implant parameter studies, it is quite difficult to separate the effects of a design modification from the effects of the difference in the bone architecture and density adjacent to the implant. This is why all the analyses regarding implant modifications, in the present study, were based on homogeneous finite element models. Additionally, there is substantial variability in the cancellous bone structure and density between individuals. There is also extensive variability in the cancellous bone of a single person, due to the changing nature of the tissue adjacent to an implant caused by the healing process.

It is important, however, to try to understand how modeling cancellous bone as homogeneous may affect finite element results. This study found that when cancellous bone was modeled as homogeneous, most major trends in stress and strain distribution were detected, but some critical distributions were not. Stress and strain magnitudes predicted by FEA of a homogeneous model differed from those of an inhomogeneous model, which presumably represented *in vivo* conditions more accurately. Therefore, when modeling cancellous bone adjacent to an implant as homogeneous, it is important to remember that, particularly if the bone adjacent to the implant is sparse, some trends in stress and strain distributions may go undetected and that the magnitudes of the results should not be taken as reference data. For implant parameter studies, this study indicates that homogeneous modeling of cancellous bone is adequate.

CONCLUSIONS

This study used finite element stress analysis of a 2-D finite element model of an osteoceramic dental implant placed in a canine mandible to approximate the stresses and strains experienced by the implant and surrounding bone in response to estimated physiological loading. Three distinct, but related, investigations were conducted.

Investigation #1 predicted that the original osteoceramic dental implant would fracture due to the tensile stresses it would most likely experience in response to anticipated physiological loading. This investigation also demonstrated that horizontal loading contributed significantly to bending in the implant, resulting in extremely large tensile stresses in both the implant and the crestal cortical bone.

Investigation #2 found that the angle of implantation of a ceramic implant is very critical in determining the tensile stresses that the implant will experience *in vivo*. Pivoting the implant was found to completely remove two large areas of tensile stress concentration, but it introduced a new, but smaller, area of tensile stresses. Removal of the grooves in the original implant design reduced the tensile stress magnitudes throughout the implant. Lengthening the original implant significantly reduced the stresses along the implant base but increased the distribution of tensile stresses along the lingual implant edge. Pivoting the long implant and/or reinforcing its lingual edge was recommended to minimize the risk of fracture. It was concluded that all three design modifications in combination with prestressing may lower the risk of implant fracture by reducing the magnitude and/or extent of tensile stress distributions in the original implant. The most significant finding in this investigation was the importance of proper implant placement, as demonstrated by the pivoted implant analysis. It is recommended that the implant be placed as symmetrically as possible relative to the cortical bone of the mandible.

Investigation #3 demonstrated that it didn't matter whether the variation in apparent density within a cancellous bone area was taken into account when determining the modulus of elasticity of a section of cancellous bone to be used in a finite element model. Finite element analysis results were fairly similar whether a single modulus of elasticity was assigned based upon the determination of a single apparent density or several values were assigned to the cancellous bone of the FEM to account for the variation in apparent density. Modeling the individual struts of trabecular bone and intertrabecular spaces versus modeling cancellous bone as homogeneous was found to make a difference in the results determined

by FEA of the respective models. It was concluded that, when modeling cancellous bone adjacent to an implant as homogeneous, it is important to remember, particularly if the bone adjacent to the implant is sparse, that some trends in stress and strain distributions may go undetected and that the magnitudes of the results should not be taken as reference data. For implant parameter studies, it was concluded that homogeneous modeling of cancellous bone was adequate.

REFERENCES

Aksaci, D. 1981. Evaluation of a fluorapatite-spinel ceramic as a bone implant. M.S. Thesis. Iowa State University, Ames, IA.

Albrektsson, T., G. Zarb, P. Worthington, and R. Eriksson. 1986. The long-term efficacy of currently used dental implants: a review and proposed criteria of success. Int. J. Oral and Maxillofac. Implants. 1: 11-25.

Albrektsson, T. and U. Lekholm. 1989. Osseointegration-Current state of the art. Dent. Clin. North Am. 33:1-15.

Albrektsson, T. and L. Sennerby. 1991. State of the art in oral implants. J. Clin. Periodontol. 18: 474-481

Ashman, R. B. 1992. Personal communication.

Ashman, R. B., and J. Y. Rho. 1988. Elastic moduli of trabecular bone material. J. Biomech. 21:177.

Ashman, R. B., G. Rosinia, S. C. Cowin, M. G. Fontenot and J. C. Rice. 1985. The bone tissue of the canine mandible is elastically isotropic. J. Biomech. 18: 717-721.

Ashman, R. B., S. C. Cowin, W. C. Van Buskirk and J. C. Rice. 1984. A continuous wave technique for the measurement of the elastic properties of cortical bone. J. Biomech. 17: 349-361.

Ashman and Van Buskirk. 1987. The elastic properties of a human mandible. Adv. Dent. Res. 1(1): 64-67.

Atmaram, G.H. 1979. Stress analysis of single-tooth implants: Effect of elastic parameters and geometry of implant. Biomat. Med. Dev. Art. Organs 7(1): 99-104.

Austriaccio, N. R., J. L. Williams and D. S. Drummond. 1991. Trabecular bone densitometry using interactive image analysis. J. Biomed. Eng. 13: 486-488.

Banks, W. J. 1986. Applied Veterinary Histology. 2nd ed. Williams and Wilkins, Baltimore, Maryland.

Bauer, G. 1990. Biochemical aspects of osseo-integration. Pages 81-98 in G. Heimke. Osse-Integrated Implants. Vol. 1. CRC Press, Inc., Boca Raton, Florida.

Bensusan, J. S., D. T. Davy, K. G. Heiple and P. J. Verdin. 1983. Tensile, conpressive and torsional testing of cancellous bone. Trans. 29th Orthop. Res. Soc. 8: 132.

Beaupre, G. S., T. E. Orr and D. R. Carter. 1990. An approach for time dependent bone modeling and remodeling-theoretical development. J. Orthop. Res. 8: 651-661.

Bickford, W. B. 1990. A first course in the finite element method. Irwin Pub., Homewood, IL

Bidez, M. W., B. J. Stephens and J. E. Lemons. 1988. A comparison of interfacial assumptions in a three dimensional stress analysis of a CP-Ti dental implant system. Transactins Third World Biomaterials Congress, Kyoto. Paper 2C2-44: 117.

Bidez, M. W., Y. Chen, S. W. McLoughlin and C. E. English. 1992. Finite element analysis (FEA) studies in 2.5-mm round bar design: the effects of bar length and material composition on bar failure. J. Oral Implantol. 18(2): 122-128.

Bonfield, W. and M. D. Grynpas. 1977. Anisotropy of Young's modulus of bone. Nature. 270: 453-454.

Borchers, L. and P. Reichart. 1983. Three-dimensional stress distribution around a dental implant at different stages of interface development. J. Dent. Res. 62(2): 155-159.

Borchers, R. E. 1991. Multiaxial failure criteria for trabecular bone. M.S. Thesis, Massachusetts Institute of Technology, Cambridge, MA.

Bourne, G. H. 1956. The Biochemistry and Physiology of Bone. Vol. 1. Academic Press, New York, NY.

Branemark, P. I. 1977. Osseointegrated implants in the treatment of the edentulous jaw: experience from a 10-year period. Scand. J. Plast. Reconstr. Surg. 16 (Suppl.).

Branemark, P. I., G. A. Zarb, T. Albrektsson. 1985. Tissue-integrated prostheses. Quintessence, Chicago, IL.

Brown, T. D. and A. B. Ferguson. 1980. Mechanical property distributions in the cancellous bone of the human proximal femur. Acta. Orthop. Scand. 51: 429-437.

Brown, T. D., D. P. Pedersen, M. L. Gray, R. A. Brand and C. T. Rubin. 1990. Toward an identification of mechanical parameters initiating periosteal remodeling: A combined experimental and analytical approach.

Bruneel, N. and J.A. Helsen. 1988. In-vitro simulation of biocompatibility of Ti-Al-V. J. Biomed. Mater. Res. 22: 203-214.

Brunski, J. B. 1988. Biomechanics of oral implants: future research directions. J. Dent. Ed. 52(12): 775-787.

Brunski, J. B. 1992. Biomechanical factors affecting the bone-implant interface. Clin. Mater. 10: 153-201.

Brunski, J. B. 1993. Personal communication.

Brunski, J. B. and J. A. Hipp. 1984. *In vivo* forces on endosteal implants: A measurement system and biomechanical considerations. J. Prosth. Dent. 51: 82.

Buch, J. D., J. G. Crose and C. O. Bechtal. 1974. Biomechanical and biomaterial considerations of natural teeth, tooth replacements, and skeletal fixation. Biomat. Med. Dev. Artif. Organ. 2(2): 171-186.

Bundy, K. 1989. Bone prostheses and implants. Pages 159-184 in S. C. Cowin, ed. Bone Mechanics. CRC Press, Boca Raton, FL.

Burr, D. B. and T. Stafford. 1990. Validity of the bulk-staining technique to separate artifactual from *in vivo* microdamage. Clin. Orthop. 260: 305-308.

Burr, D. B., R. B. Martin, M. B. Schaffler and E. L. Radin. 1985. Bone remodeling in response to *in vivo* fatigue microdamage. J. Biomech. 18: 189-200.

Burstein, A. H., J. D. Currey, V. H. Frankel, K. G. Heiple, P. Lunseth and J. C. Vessely. 1972a. Bone strength: the effect of screw holes. J. Bone Jt. Surg. 54: 1143-1156.

Burstein, A. H., J. M. Zika, K. G. Heiple and L. Klein. 1975. Contribution of collagen and mineral to the elastic-plastic properties of bone. J. Bone Jt. Surg. 57: 956-961.

Buser, D., Schank, R. K. and Steinmann, S. 1991. Influence of surface characteristics on bone integration of titanium implants-a histomorphometric in miniature pigs. J. Biomed. Mater. Res. 25: 889-902.

Caler, W. E. and D. R. Carter. 1989. Bone creep-fatigue damage accumulation. J. Biomech. 22: 625-635.

Carter, D. R. and W. C. Hayes. 1976a. Fatigue life of compact bone. I. Effects of stress amplitude, temperature and density. J. Biomech. 9: 27:34.

Carter, D. R. and W. C. Hayes. 1976b. Bone compressive strength: the influence of density and strain rate. Science. 194: 1174.

Carter, D. R. and W. C. Hayes. 1977a. Compact bone fatigue damage. I. Residual strength and stiffness. J. Biomech. 10: 325-327.

Carter, D. R. and W. C. Hayes, 1977b. Compact bone fatigue damage. II. A microscopic examination. Clin. Orthop. 127: 265-274.

Carter, D. R. and W. C. Hayes. 1977c. The compressive behavior of bone as a two-phase porous structure. J. Bone Jt. Surg. 59: 954-962.

Carter, D. R., W. E. Caler, D. M. Spengler and V. H. Frankel. 1981. Fatigue behavior of adult cortical bone-the influence of mean strain and strain range. Acta Orthop. Scand. 52: 481.

Carter, D. R. and W. E. Caler. 1983. Cycle-dependent and time-dependent bone fracture with repeated loading. J. Biomech. Eng. 105: 166-170.

Carter, D. R. and W. E. Caler. 1985. A cumulative damage model for bone fracture. J. Orthop. Res. 3: 84-90.

Carter, D. R., G. H. Schwab and D. M. Spengler. 1980. Tensile fracture of cancellous bone. Acta. Orthop. Scand. 51: 733-741.

Carter, D. R. and D. M. Spengler. 1978. Mechanical properties and composition of cortical bone. Clin. Orthop. 135: 192.

Carter, D. R. and T. M. Wright. 1986. Yield characteristics of cortical bone. Pages 10-35 in Functional behavior of orthopedic biomaterials. Volume I: Fundamentals. CRC Press, Boca Raton, FL.

Cezayirlioglu, H., E. Bahniuk, D. T. Davy and K. G. Heiple. 1985. Anisotropic yield behavior of bone under combine axial loading and torque. J. Biomech. 18: 61-69.

Choi, K., J. L. Kuhn, M. J. Ciarelli and S. A. Goldstein. 1989. The elastic modulus of trabecular, subchondral, and cortical bone tissue. Trans. 35th orthop.Res. Soc. 14: 102.

Choi, K. 1990. The elastic moduli of human subchondral, trabecular, and cortical bone tissue and the size-dependency of cortical bone modulus. J. Biomechanics 23: 1103-1113.

Choi, K. and S. A. Goldstein. 1991. The fatigue properties of bone tissueson a microstructural level. Trans. 37th orthop. Res. Soc. 16: 485.

Clift, S. E., J. Fisher and C. J. Watson. 1992. Finite element stress and strain analysis of the bone surrounding a dental implant: effect ofvariations in bone modulus. Proc. Instn. Mech. Engrs. 206: 237-241.

Cook, S. D., J. J. Klawitter and A. M. Weinstein. 1981. A model for the implant-bone interface characteristics of porous dental implants. J. Dent. Res. 61(8): 1006-1009.

Cook, S. D., J. J. Klawitter and A. M. Weinstein. 1982. The influence of implant geometry on the stress distribution around dental implants. J. Biomed. Mater. Res. 16: 369-379.

Cowin, S. C. 1985. The relationship between the elasticity tensor and the fabric tensor. Mech. Mater. 4: 137.

Cowin, S. C. 1986. Wolff's law of trabecular architecture at remodeling equilibrium. J. Biomech. Engr. 108: 111.

Cowin, S., W. Buskirk and R. Ashman. 1987. Properties of bone. Pages 2.1-2.27 in R. Skalak and S. Chien, eds. Handbook of Bioengineering. McGraw-Hill , New York, NY.

Cowin, S. C. 1989. The mechanical properties of cancellous bone. Pages 129-155 in Cowin, S. C., ed. Bone mechanics. CRC Press, Boca Raton, FL.

Cowin, S.C. 1991. Candidates for the mechanosensory system in bone. J. Biomech. Engr. 113: 191-197.

Craig, R. G. 1986. Dental mechanics. in D. H. Norrie, ed. Finite Element Handbook. McGraw-Hill, New York, NY.

Crowninshield, R. and M. Pope. 1974. The response of compact bone in tension at various strain rates. Ann. Biomed. Eng. 2: 217-225.

Currey, J. D. 1969a. The mechanical consequences in the variation of the mineral content of bone. J. Biomechanics 2: 1-11.

Currey, J. D. 1969b. The relationship between the stiffness and mineral content of bone. J. Biomechanics 2: 477-480.

Currey, J. D. 1970. The mechanical properties of bone. Clin. Orthop. 73: 210.

Currey, J. D. 1984. The Mechanical Adaptation of Bones. Princeton University Press, Princeton, NJ.

Currey, J. D. 1990. Physical characteristics affecting the tensile failure properties of compact bone. J. Biomechanics 22: 837-844.

Cutright, D., S. Bhaskar, M. Brady L. Getter and W. Posey. 1972. Reaction of bone to tricalcium phosphate ceramic pellets. Oral Surg. 33 (5) : 850-856.

Davies, J. E., S. F. Tarrant and T. Matsuda. 1987. Interaction between primary bone cell cultures and biomaterials Part 1: Methos; The *in vitro* and *in vivo* stages. Pages 579-584 in A. Pizzoferrato, P. G. Marchette, A. Ravaglioli and A. J. C. Lee, eds. Biomaterials and clinical applications. Elsevier Science Publishers, B. V., Amsterdam.

de Groot, K. 1981. Pages 199-222 in D.F. Williams, ed. Biocompatibility of clinical implant materials. CRC Press, Inc., Boca Raton, FL.

de Groot, K. 1983. Bioceramics of calcium phosphate. CRC Press, Boca Raton, FL.

de Lange, G. L., S. de Putter, R. de Vos, R. de Laat and K. de Groot. 1986. Permucosal dental implants. The relationship between bone anchorage and the quality of surrounding gingival tissues. Pages 519-524 in P. Christel, ed. Biological and biomechanical performance of biomaterials. Elsevier Scientific Publishing Company, New York, NY.

Denissen, H. W. and K. de Groot. 1979. Immediate dental root implants from synthetic dense calcium hydroxyapatite. J. Prosthet. Dent. 42: 551.

Denissen, H. W., W. Kalk, H. M. de Nieuport, J. C. Maltha and A. van de Hooff. 1990. Mandibular bone response to plasma-sprayed coatings of hydroxyapatite. Int. J. Prosthodont. 3: 53-58.

de Putter, C. 1984. Permucosal dental implants of dense hydroxylapatite. Ph. D. Dissertation. Free University Press, Amsterdam.

de Putter, C., K. deGroot and S. Sillevis. 1983. Transmucosal implants of dense hydroxyl apatite. J. Prosthet. Dent. 49: 87.

d'Hoedt, B., D. Lukas, L. Muhlbradt, F. Scholz, W. Sculte, F. Quante and A. Topkaya. Periotest methods-development and clinidal trial. (English abstract). Dtsdh-Zahnarztl-Z. 40(2): 113-125.

Ducheyne, P., L. Heymans, M. Martens, E. Aernoudt, P. d. e. Meester and J. C. Mulier. 1977. The mechanical behavior of intracondylar cancellous bone of the femur at different loading rates. J. Biomech. 10: 747-762.

Ducheyne, P. and McGuckin, Jr., J. F. 1990. Composite bioactive ceramic-metal materials. Pages 175-193 in Yamamuro, T., L. Hench and J. Wilson, eds. Handbook of Bioactive Ceramics. Volume II: Calcium Phosphate and Hydroxylapatite Ceramics. CRC Press, Boca Raton, FL.

Elias, J. J. and J. B. Brunski. 1991. Finite element analysis of load distribution among dental implants. 1991 Advances in Biengineering, BED-Vol. 20: 155-158.

English, C. 1990. An overview of implant hardware. JADA. 121: 360-354.

Eurell, J. C. and L. E. Kazarian. 1982. The scanning electron microscopy of compressed vertebral bodies. Spine. 7: 123-128.

Evans, F. G. 1973. Mechanical Properties of Bone. Charles C. Thomas, Springfield, IL.

Farah, J. W., R. G. Craig and R. A. Yapp. 1973. Stress distribution caused by blade-type dental implants. Implantologist. 1(4): 77-86.

Ferraro, J. W. 1979. Experimental evaluation of ceramic calcium phosphate as a subsitute for bone grafts. Plast. Reconstr. Surg. 63: 634.

Fitzgerald, R. W. 1982. Mechanics of Materials. 2nd ed. Addison-Wesley Publishing, Reading, MA.

Fondrk, M., E. Bahniuk, D. T. Davy and C. Michaels. 1988. Some viscoplastic characteristics of bovine and human cortical bone. J. Biomech. 21: 623-630.

French, A. A., C. Q. Bowles, P. L. Parham, J. D. Eick, W. J. Killoy and C. M. Cobb. 1989. Comparison of peri-implant stresses transmitted by four commercially available osseointegrated implants. Int. J. Period. Rest. Dent. 9: 221-230.

Frost, H. M. 1960. Presence of microscopic cracks *in vivo* in bone. Henry Ford Hosp. Bull. 8: 25-35.

Frost, H. M. 1964. The laws of bone structure. Charles C. Thomas, Springfield, IL.

Frost, H. M. 1973. Bone modeling and skeletal modeling errors. Charles C. Thomas, Springfield, IL.

Frost, H. M. 1988. Structural adaptations to mechanical usage: A three-way rule for l amellar bone remodeling. Comp. Vet. Orthop. Trauma. 1: 7-17.

Frost, H. M. 1990. Skeletal structural adaptations to mechanical usage: 1. Redefining Wolff's law: The bone modeling problem. Anat. Rec. 226: 403-413.

Fyhrie, D. P. and D. R. Carter. 1986. A unifying theory relating stress to trabecular bone morphology. J. Orthop. Res. 4: 304-317.

Galante, J., W. Rostoker and R. D. Ray. 1970. Physical properties of trabecular bone. Calcif. Tissue Res. 5: 236-246.

Gibson, L. J. 1985. The mechanical behavior of cancellous bone. J. Biomech. 20: 1135.

Gibson, L. J. and M. F. Ashby. 1988. Cellular Solids: Structure and Properties. Pergamon Press, Elmsford, New York.

Goldstein, S. A. 1987. The mechanical properties of trabecular bone: dependence on anatomic location and function. J. Biomechanics 20: 1055-1061.

Goldstein, S. A., D. L. Wilson, D. A. Sonstegard and L.S. Matthews. 1983. The mechanical properties of human tibial trabecular bone as a function of metaphyseal location. J. Biomech. 16: 965-969.

Goldstein, S. A., S. J. Hollister, J. L. Kuhn and N. Kikuchi. 1990. The mechanical and remodeling properties of trabecular bone. Pages 61-81 in Mow, V. C., A. Ratcliff and S. L. Y. Woo., eds. Biomechanics of diarthrodial joints, Volume II. Springer-Verlag, New York.

Gong, J. K., J. S. Arnold and S. H. Kohn. 1964. Composition of trabecular and cortical bone. Anat. Rec. 149: 325.

Goodship, A. E., L. E. Lanyon and H. McFie. 1979. Functional adaptation of bone to increased stress. J. Bone Jt. Surg. 61-A: 539-546.

Graf, H. 1969. Bruxism. Dental Clinics North America 13: 659-665.

Graves, A.M. 1988. Evaluation of a bioactive ceramic as an endosseous tooth root implanted in sheep. M.S. Thesis. Iowa State University, Ames, IA.

Halawa, M., A. J. C. Lee, R. S. M. Ling and S. S. Vangala. 1978. The shear strength of trabecular bone from the femur and some factors affecting the shear strength of the cement-bone interface. Arch. Orthop. Traum. Surg. 61A: 539-546.

Hammner, J., O. Reed and A. Hand. 1970. Clinical radiographic and histologic electron microscopic observations of plastic tooth implantation in baboons. Oral Surg., Oral Med., Oral Pathol. 30: 555.

Hart, R. T. 1989. The finite element method. Pages 54-73 in Cowin, S. C., ed. Bone mechanics. CRC Press, Inc., Boca Raton, FL.

Hart, R. T. and D. T. Davy. 1989. Theories of bone modeling and remodeling. Pages 253-274 in Cowin, S. C., ed. Bone mechanics. CRC Press, Inc., Boca Raton, FL.

Hart, R. T., V. V. Hennebel, N. Throngpreda, W. C. Buskirk and R. C. Anderson. 1992. Modeling the biomechanics of the mandible: A three-dimensional finite element study. J. Biomech. 25: 261-266.

Hayes, W. C. and D. R. Carter. 1976. Post-yield behavior of subchondral trabecular bone. J. Biomed. Mat. Res. (Symp.) 7: 537-544.

Hayes, W. C. and B. D. Snyder. 1981. Toward a quantification of Wolff's Law in trabecular bone. Pages 43-68 in Symp. on the Mechanical Properties of Bone. Cowin, S. C., Ed., American Society of Mechanical Engineers, Boulder.

Hayes, W. C., B. D. Snyder and B. M. Levine. 1981. Stress-morphology relationships in trabecular bone of the patella. Pages 107-127 in Simon, B. R., ed. Proceedings from the International Conference on Finite Elements in Biomechanics. University of Arizona.

Healy, K. E. and P. Ducheyne. 1992. The mechanisms of passive dissolution of titanium in a model physiological environment. J. Biomed. Mater. Res. Symp. 26: 319-338.

Heimke, G. 1990. Osseo-integrated implants. Vol. I. CRC Press, Inc., Boca Raton FL.

Hench, L. L. and E. C. Etheridge. 1982. Biomaterials-an interfacial approach. Academic Press, New York, NY.

Hipp, J. A., J. B. Brunski, M. S. Shephard and G. V. B Cochran. Finite element models for implants in bone: interfacial assumptions. Pages 447-452 in Schneider, E. and S. A. Perren, eds. Biomechanics: Current interdisciplinary research. Martinus Nijhoff, Dordrecht, The Netherlands.

Hodgskinson, R. and J. D. Currey. 1989. Hardness, an indicator of the mechanical competence of cancellous bone. J. Orthop. Res. 7: 754-758.

Howie, D. W., B. Vernon-Roberts, R. Oakeshott and B. Manthey. 1988. A rat model of resorption of bone at the cement-bone interface in the presence of polyethylene wear particles. J. Bone Joint Surg. 70(A): 257-263.

Huiskies, R. 1983. Principles and methods of solid biomechanics. Pages 89-97 in G. W. Hastings and P. Ducheyne, eds. Functional Behavior of Orthopedic Biomaterials. Volume I: Fundamentals. CRC Press Inc., Boca Raton, FL.

Huiskies, R. 1984. Design, fixation and stress analysis of permanent orthopedic implants: the hip joint. Pages 121-162 in Ducheyne, P. and G. W. Hastings,.eds. Functional

behavior of orthopedic biomaterials. Vol. II.-Applications. CRC Press Inc., Boca Raton, FL.

Huiskies, R. and D. Nunamaker. 1984. Local stresses and bone adaptation around orthopedic implants. Calcif. Tissue Int. 36(suppl.): 110-117.

Huiskies, R. 1986. Biomechanics of bone implant interactions. Pages 245-262 in Schmid-Schoenbum, G. W. Frontiers of biomechanics. Springer-Verlag, New York, NY.

Huiskies, R., H. Weinans, H. Grootanboer, M. Dalstra, B. Fudala and T. Sloof. 1987. Adaptive remodeling theory applied to prosthetic design analysis. J. Biomech. 20(11-12): 1135-1150.

Hulbert, S. F., J. C. Bokros, L. L. Hench, J. Wilson, and G. Heimke. 1987. Ceramics in clinical applications, past, present, and future. Pages 3-27 in P. Vinvenzini, ed. High tech ceramics. Elsevier Science Publishers, B. V., Amsterdam.

Hvid, I. and S. L. Hansen. 1985. Trabecular bone strength patterns at the proximal tibial epiphysis. J. Orthop. Res. 3: 464-472.

Hylander, W. L. 1981. Patterns of stress and strain in the Macaque mandible. Pages 1-35 in Carlson, D. S., ed. Craniofacial biology. Ann Arbor: Center for Human Growth and Development. .

Imamura, K., H. Ozawa, T. Hiraide, N. Takahashi, Y. Shibaski, T. Fukuhara and T. Suda. 1990. Continuously applied compressive pressure induces bone resorption by a mechanism involving prostaglandin E_2 synthesis. J. Cell Physiol. 144: 222-228.

Ismail, Y. H., L. N. Pahountis, and J. F. Fleming. 1987. Comparison of two-dimensional and three-dimensional finite element analysis of a blade implant. Int. J. Oral Implant. 4: 25.

Janikowski, T. and T.D. McGee. 1969. Artificial teeth for permanent implantation. Proc. Iowa Acad. Sci. 76: 113-118.

Jarcho, M., R. L. Salisbury, M. B. Thomas, and R. H. Doremus. 1979. Preparation and thermal properties of dense polycrystalline oxyhydroxyapatite. J. Am. Ceram. Soc. 62: 455-460.

Jee, W. S. S. and X. J. Li. 1990. Adaptation of cancellous bone to overloading in the adult rat: a single photon absorptiometry and histomorphometry study. Anat. Rec. 227: 418-426.

Jensen, N. C., L. P. Madsen and F. Linde. 1991. Topographical distribution of trabecular bone strength in the human os calcanei. J. Biomechanics 24: 49-55.

Junqueria, L. C. and J. Carneiro. 1983. Basic Histology. 3rd ed. Lange Medical Publications, Los Altos, Ca.

Kaplan, S. J., W. C. Hayes, J. L. Stone and G. S. Beaupre. 1985. Technical note: tensile strength of bovine cancellous bone. J. Biomech. 18: 723-727.

Karagianes, M. T., R. E. Westerman and J. J. Rasmussen. 1974. Development and evaluation of porous ceramic and titanium alloy dental anchors implanted in miniature swine. J. Biomed. Mater. Res. Symp. 5(2): 391.

Katz, J. L. 1980. Anisotropy of Young's modulus of bone. Nature (London). 283: 106.

Keaveny, T. M. and W. C. Hayes. 1993a. Mechanical properties of cortical and trabecular bone. Pages 285-344. in B. K. Hall, ed. Bone. Volume 7: Bone Growth-B. CRC Press, Boca Raton, FA.

Keaveny, T. M. and W. C. Hayes. 1993b. A 20-year perspective on the mechanical properties of trabecular bone. J. Biomech. Eng. 115: 534-542.

Keller, T. S., Z. Mao, and D. M. Spengler. 1990. Young's modulus, bending strength, and tissue physical properties of human compact bone. J. Orthop. Res. 8: 592-603.

Kerr, J. P. 1992. Unpublished format transformation computer code.

Kertesz, P. 1993. A colour atlas of veterinary dentistry and oral surgery. Wolfe Pub., Aylesbury, England.

Kingery, W. D., H. K. Bowen and D. R. Uhlman. 1976. Introduction to ceramics. 2nd edition. John Wiley and Sons, New York, NY.

Kitoh, M., T. Suetsugu, Y. Murakami, and T. Tabata. 1978. A biomathematical study on implant design and stress distribution. Bull. Tokyo Med. Dent. Univ. 25: 269-276.

Klawitter, J. J., A. M. Weinstein, F. W. Cooke, L. J. Peterson, B. M. Pennel and R. V. McKinney, Jr. 1977. An evaluation of porous alumina ceramic dental implants. J. Dent. Res. 56: 768-776.

Knoell, A. C. 1977. A mathematical model of an *in vitro* human mandible. J. Biomechanics 10: 159-166.

Ko, C. C., D. H. Kohn and S. J. Hollister. 1992. Micromechanics of implant/tissue mechanics. J. Oral Implant. 18: 220-230.

Kohn, D. H. 1992. Overview of factors important in implant design. J. Oral Implantol. 18(3): 204-219.

Kohn, D. H. and P. Ducheyne. 1990. A parametric study of the factors affecting the fatigue strength of porous coated Ti-6Al-4V implant alloy. J. Biomed. Mater. Res. 24: 1483-1501.

Ku, J. L., S. A. Goldstein, K. W. Choi, M. London, M. Feldkamp and L. S. Matthews. 1987. The mechanical properties of a single trabeculae. Trans. 33rd Orthop. Res. Soc. 12: 48.

Kuhn, J. L., S. A. Goldstein, M. J. Ciarelli and L. S. Matthew. 1989. The limitations of canine trabecular bone as a model for humans: A biomechanical study. J. Biomech. 22:95-107.

Lang, S. B. 1970. Ultrasonic method for measuring elastic coefficients of bone and results on fresh and dried bovine bones. IEEE Trans. Biomed. Eng. 17: 101.

Lanyon, L. E. and C. T. Rubin. 1985. Static versus dynamic loads as an influence on bone remodeling. J. Biomech. 17: 897-890.

Lanyon, L.E., A. E. Goodship, C. J. Pye and J. H. MacFie. 1982. Mechanically adaptive bone remodeling. J. Biomech. 15: 141-154.

Lanyon, L.E., I. L. Paul, C. T. Rubin, E. L. Thrasher, R. DeLaura, R. M. Rose and E. L. Radin. 1981. *In vivo* strain measurements from bone and prosthesis following total hip replacement. J. Bone Jt. Surg. 63: 989-1001.

Lanyon, L.E., W. G. Hampson, A. E. Goodship and J. S. Shah. 1975. Bone deformation recorded *in vivo* from strain gages attached to human tibial shaft. Acta. Orthop. Scand. 46: 256-268.

Lavernia, C. J., S. D. Cook and A. M. Weinstein. 1981. An analysis of stresses in a dental implant system. J. Biomech. 14(8): 555-560.

Lavernia, C. J., S. D. Cook, A. M. Weinstein and J. J. Klawitter. 1982. The influence of the bone-implant interface stiffness on stress profiles surrounding Al2O3 and carbon dental implants. Ann. Biomed. Eng. 10: 129-138.

Linde, F., I. Hvid and B. Pongsoipetch. 1989. Energy absorptive properties of human trabecular bone specimans during axial compression. J. Orthop. Res. 7: 432-439.

Linkow, R. I., A. W. Rinaldi, W. W. Weiss, Jr. and G. H. Smith. 1990. Factors influencing long-term implant success. J. Prosthetic Dent. 63: 64-70.

Listgarten, M. A., Buser, D. and Steinemann, S. G. 1992. Light and transmission electron-microscopy of the intact interface between non-submerged titanium coated epoxy resin implants and bone or gingiva. J. Dent. Res. 71: 364-371.

Listgarten, M. A. and C. H. Lai. 1975. Ultrastructure of the intact interface between an endosseous epoxy resin dental implant and the host tissues. J. Biol. Buccal. 3: 13.

Luthy, H., J. R. Strub and P. Scharer. 1987. Analysis of plasma flame-sprayed coatings on endosseous oral titanium implants exfoliated in man: preliminary results. Int. J. Oral Maxillofac. Implants. 2: 197-202.

Maloney, W. J., M. Jasty, J. J. Callaghan, J. O. Galante and W. H. Harris. 1990. Femoral osteolysis in association with stable cementless femoral components. Trans. Soc. for Biomater. 16:177.

Martini, F. 1989. Fundamentals of anatomy and physiology. Prentice Hall, Englewood, CA.

Marquis, P. 1993. Dental implants. J. Dentistry. 21(1): 5-30.

Martin, R. B. 1990. Effects of simulated weightlessness on bone properties in rats. J. Biomechanics 23: 1021-1029.

Martin, R. B. 1991. Determinants of the mechanical properties of bones. J. Biomechanics 24(Suppl. 1): 79-88.

Martin, R. B. and D. B. Burr. 1989. The Structure, Function, and Adaptation of Compact Bone. Raven Press, New York.

Martin, R. B. and J. Ishida. 1989. The relative effects of collagen fiber orientation, porosity, density, and mineralization on bone strength. J. Biomech. 22: 419-426.

Martini, F. 1989. Fundamentals of anatomy and physiology. Prentice Hall, Englewood Cliffs, NJ.

Matsushita, Y., M. Kitoh, K. Mizuta, H. Ikeda and T. Suetsugu. 1990. Two-dimensional FEM analysis of hydroxyapatite implants: Diameter effects on stress distribution. J. Oral Implant. 16: 6-11.

McElhaney, J. H. 1966. Dynamic response of bone and muscle tissue. J. Appl. Physiol. 21: 1231.

McGee, T. D. and J. Wood. 1974. Calcium phosphate magnesium aluminate osteoceramics. Biomed. Mater. Symp. 5: 137.

McKellop, H., I. Clarke, K. Markolf and H. Amstutz. 1981. Friction and wear properties of polymer, metal and ceramic prosthetic joint materials evaluated on a multichannel screening device. J. Biomed. Mater. Res. 15: 619-653.

McKinney, R. V., D. E. Steflik, D. L. Koth and B. B. Singh. 1988. The scientific basis for dental implant therapy. J. Dent. Educ. 52(12): 696-705.

McLean, F. C. and R. U. Marshall 1968. Bone, Fundamentals of the Physiology of Skeletal Tissue. The University of Chicago Press, Chicago, IL.

Meade, J. B. 1989. The adaptation of bone to mechanical stress: Experimentation and current concepts. in S. C. Cowin, ed. Bone Mechanics. CRC Press, Inc., Boca Raton, FL.

Meffert, R. M. 1988. The soft tissue interface in dental implantology. Int. J. Oral Implantol. 5(1): 55-58.

Meijer, H. J. A., F. J. M. Starmans, F. Bosman and W. H. A. Steen. 1993. A comparison of three finite element models of an edentulous mandible provided with implants. J. Oral Rehab. 20: 147-157.

Melvin, J. W., J. H. McElhaney and V. L. Roberts. 1970. Development of a mechanical model of the human head. Determination of tissue properties and synthetic substitute materials. Soc. Automotive Engineers Trans. 79: 700-703.

Mente, P. L. and J. L. Lewis. 1987. Young's modulus of trabecular bone tissue. Trans. Orthop. Res. Soc. 12: 49.

Michel, M. C., P. K. Zysset and W. C. Hayes. 1991. Fatigue behavior of trabecular bone. Trans. 37th Orthop. Res. Soc. 16: 156.

Mihalko, W. M., T. C. May, J. F. Kay and W. R. Krause. 1992. Finite element analysis of interface geometry effects on the crestal bone surrounding a dental implant. Implant. Dent. 1: 212-217.

Mosekilde, L. and L. Mosekilde. 1988. Iliac crest trabecular bone volume as predictor for vertebral compressive strength, ash density and trabecular bone volume in normal individuals. Bone. 9: 195-199.

Mosekilde, L., A. Viidik and L. Mosekilde. 1985. Correlations between the compressive strength of iliac and vertebral trabecular bone in normal individuals. Bone. 6: 291-295.

Natiella, J. R. 1986. Special aspects of dental implants. Pages 461-470 in A. von Recum, ed., Handbook of Biomaterial Evaluation. Macmillen , New York, NY.

Natiella, J. R., J. E. Armitage and M. A. Meenaghan. 1974. Tissue response to dental implants protruding through mucous membrane. Oral Sci. Rev. 5: 85-105.

Neil, J. L., T. C. Demos, J. L. Stone and W. C. Hayes. 1983. Tensile and compressive properties of vertebral trabecular bone. Trans. 29th Orthop. Res. Soc. 8: 344.

Nentwig, G. H. 1985. Single tooth replacement by a ceramic implant Munich type. J. Oral Implantol. 12(1): 84-90.

Niederauer, G. G. 1990. Ceramic tooth root implants in dogs: Design and clinical evaluation. M. S. Thesis, Iowa State University, Ames, IA.

Niznick, G. A. 1985. Implant prosthodontics, a team approach. J. Oral Implantology 12(1): 1-24.

Nunamaker, D. M., D. M. Butterweck and M. T. Provost. 1990. Fatigue fractures in thoroughbred racehorses: relationships with age, peak bone strain, and training. J. Orthop. Res. 8: 604-622.

Ochoa, J. A., A. P. Sanders, D. A. Heck and B. M. Hillberry. 1991. Stiffening of the femoral head due to intertrabecular fluid and intraosseous pressure. J. Biomech. Eng. 113: 259-262.

O'Connor, J. A., L. E. Lanyon and H. MacFie. 1982. The influence of strain rate on adaptive bone remodeling. J. Biomech. 15: 767-781.

Osborn, J. W. and F. A. Baragar. 1985. Predicted pattern of human muscle activity during clenching derived from a computer assisted model. J. Biomech. 18: 599-612.

Park, J. B. 1979. Biomaterials. Plenum Press, New York, NY.

Parr, G. R., D. E. Steflik, A. L. Sisk and A. Aguero. 1988. Clinical and histological observations of failed two-stage titanium alloy basket implants. Int. J. Oral Maxillofac. Implants. 3: 49-56.

Paydar, N., H. U. Sksy, C. L. Poyrez and W. E. Roberts. 1991. Finite element model of a human mandible for investigating joint reactions and bone stresses during mastication. 1991 Advances in Bioengineering, ASME, BED-Vol. 20: 163-166.

Perren, S. M. and A. Boitzy. 1978. Cellular differentiation and bone biomechanics during the consolidation of a fracture. Anat. Clin. 1: 13-28.

Pilliar, R. M., H. U. Cameron and I. MacNab. 1975. Porous surface layered prosthetic devices. Biomed Eng. 10: 126-131.

Pilliar, R. M., D. A. Deporter, P. A. Watson and N. Valiquette. 1991. Dental implant design-Effect on bone remodeling. J. Biomed. Mat. Res. 25: 467-483.

Pilliero, S. J., P. Schnitman and P. Pentel. 1973. Histopathology of oral endosteal metallic implants in dogs. J. Dent. Res. 52: 1117.

Pope, M. H., and J. C. Outwater. 1974. Mechanical properties of bone as a function of position and orientation. J. Biomech. 7: 61-66.

Privitzer, E., O. Widera and J. A. Tesk. 1975. Some factors affecting dental implant design. J. Biomed. Mater. Res. Symp. 6: 251-255.

Pugh, J. W., R. M. Rose and E. L. Radin. 1973. Elastic and viscoelastic properties of trabecular bone. J. Biomech. 6: 657-670.

Rangert, B., T. Jemt and L. Raneus. 1989. Forces and moments on Branemark implants. J. Dent. Res. 68(255): 587.

Rees, J. S. and P. H. Jacobsen. 1992. Stresses generated by luting resins during cementation of composite and ceramic inlays. J. Oral Rehabil. 19(2): 115-122.

Reilly, D. T. and A. H. Burstein. 1975. The elastic and ultimate properties of compact bone tissue. J. Biomechanics 8: 393-405.

Reilly, D. T., A. H. Burstein and V. H. Frankel. 1974. The elastic modulus for bone. J. Biomech. 7: 271-275.

Rho, J. Y., R. B. Ashman and C. H. Turner. 1993. Young's modulus of trabecular and cortical bone material: Ultrasonic and microtensile measurements. J. Biomechanics. 26(2): 111-119.

Rice, J. C., S. C. Cowin and J. A. Bowman. 1988. On the dependence of the elasticity and strength of cancellous bone on apparent density. J. Biomech. 21: 155-168.

Richter, E.J. 1989. Basic biomechanics of dental implants in prosthetic dentistry. J. Prosthet. Dent. 61: 602-609.

Riegar, M. R., M. Mayberry and M. O. Brose. 1990. Finite element analysis of six endosseous implants. J. Prosthet. Dent. 63: 671-676.

Roberts, W. E. 1988. Bone tissue interface. J. Dent. Edu. 52: 804-809.

Roberts, W. E., P. K. Turley, N. Brezniak and P. J. Fielder. 1987. Bone physiology and metabolism. Calif. Dent. Assoc. J. 10: 54-61.

Robertson, D. M. and D. C. Smith. 1978. Compressive strength of mandibular bone as a function of microstructure and strain rate. J. Biomech. 11: 455-471.

Rubin, C. and L. Lanyon. 1982. Limb mechanics as a function of speed and gait: A study of functional strains in the radius and tibia of horse and dog. J. Exper. Biol. 101: 187-211.

Rubin, C. T. and L. Lanyon. 1985. Regulation of bone mass by mechanical loading: The effect of peak strain magnitude. Calc. Tissue Int. 37: 441-447.

Rubin, C. T. and L. E. Lanyon. 1987. Osteoregulatory nature of mechanical stimuli: funcion as a determinant for adaptive remodeling of bone. J. Orthop. Res. 5: 300-310.

Rubin, C. T. and K. J. McLeod. 1990. Biologic modulation of mechanical influences in bone remodeling. Pages 97-118 in Mow, V. C., A. Ratcliff and S. L. Y. Woo., eds. Biomechanics of diarthrodial joints, Volume II. Springer-Verlag, New York.

Saha, S. and P. H. Gorman. 1981. Strength of human cancellous bone in shear and its relationship to bone mineral content. Trans. Orthop. Res. Soc. 217.

Schaffler, M. B., E. L. Radin and D. B. Burr. 1989. Mechanical and morphological effects of strain rate on fatigue of compact bone. Bone 10: 207-214.

Schnitman, P. A. 1993. Implant dentistry: Where are we now? JADA. 124: 39-47.

Schroeder, A., E. Van der Zypen and H. Stitch. 1981. The reactions of bone connective tissue and epithelium to endosteal implants with titanium sprayed surfaces. J. Maxillo-Facial Surg. 9: 15-25.

Siegele, D. and U. Soltész. 1989. Numerical investigations of the influence of implant shape on stress distribution in the jaw bone. Int. J. Oral Maxillofac. Implants 4: 333-340.

Skalak, R. 1988. Stress transfer at the implant interface. J. Oral Implant. 13: 581-593.

Smith, D. M., M. R. A. Khairi, J. Norton and C. C. Johnson, Jr. 1976. Age and activity effects on rate of bone mineral loss. J. Clin. Invest. 58: 716-721.

Soltesz, U. and D. Siegale. 1982. Principal characteristics of the stress distribution in the jaw caused by dental implants. Pages 439-444 in Huiskies, R., D. van Campen and J. de Wijn, eds. Biomechanics: Principles and applications. M Nijhoff Pub., The Hague, The Netherlands.

Soltesz, U., D. Siegale, J. Riedmuller and P. Shultz. 1982. Stress concentration and bone resorption in the jaw of dental implants with shoulders. Pagess 115-122 in Lee, A. J. C, T. Albrektsson and P. Branemark, eds. Clinical applications of biomaterials. John Wiley, Chichester.

Spector, M. 1988. Current concepts in bony ingrowth and remodeling. Pages 69-86 in Fitzgerald, R., ed. Non-cemented total hip arthroplasty. Raven Press, New York, NY.

Steflik, D. E., P. J. Hanes and A. L. Sisk. 1992. Transmission electron-microscope and high-voltage electron microscopic observations of the bone and osteocyte activity adjacent to unloaded dental implants placed in dogs. J. Periodont. 63: 443-452.

Stillman, N. and C. W. Douglass. 1993. The developing market for dental implants. JADA. 124: 51-56.

Stone, J. L., G. S. Beaupre and W. C. Hayes. 1983. Multiaxial strength characteristics of trabecular bone. J. Biomech. 16: 743-752.

Ten Cate, A. R. 1985. The gingival junction. Pages 143-153 in P. I. Branemark, ed. Tissue integrated prosthesis: Osseointegrations in clinical dentistry. Quintessence Publishing Company, Chicago, IL.

Tesk, J. A. and O. Widera. 1973. Stress distribution in bone arising from loading on endosteal dental implants. J. Biomed. Mater. Res. Symp. 7: 251-261.

Tholen, M. 1982. Veterinary endodontics (letter). J. Am. Vet. Med. Assoc. 180(1): 4.

Throckmorton, G. S. and L. S. Throckmorton. 1985. Quantitative calculation of temporomandibular joint reaction forces. I. The importance of the jaw muscle forces. J. Biomech. 18: 445-452.

Townsend, P. R., P. Raux, R. M. Rose, R. E. Miegal and E. L. Radin. 1975. The distribution and anisotopy of stiffness of cancellous bone in the human patella. J. Biomech. 8: 363-367.

Tsai, S. W. and E. M. Wu. 1971. A general theory of strength for anisotropic materials.. J. Compos. Mater. 5: 58.

Turner, C. H. 1989. Yield behavior of bovine cancellous bone. J. Biomech. Eng. 111: 256-260.

Turner, C. H., S. C. Cowin, J. Y. Rho, R. B. Ashman and J. C. Rice. 1990. The fabric dependence of the orthotropic elastic constants of cancellous bone. J. Biomech. 23: 549-561.

Turner, C H. 1991. Homeostatic control of bone structure: an application of feedback theory. Bone. 12: 203-217.

Turner, C. H. 1992. Personal communication.

Tweden, K. S. 1987. A comparison of four endosseous dental implants: Single crystal sapphire,; pyrolytic carbon; an alloy of titanium, aluminum, and vanadium; and a biologically active ceramic. Ph. D. Dissertation. Iowa State University, Ames, Iowa.

van Mullem, P. J. and J. C. Maltha. 1984. Histology of bone. Pages 53-75 in K. de Groot, ed. Bioceramics of calcium phosphates. CRC Press, Boca Raton, FL.

Weibel, E. R. 1979. Stereological methods. Vol. 1: Practical methods of biological morphometry. Academic Press, London.

Whedon, G. D. and R. P. Heaney. 1993. Effects of physical inactivity, paralysis, and weightlessness on bone growth. Pages 57-79 in B. K. Hall, ed. Bone. Volume 7: Bone Growth-B. CRC Press, Boca Raton, FL.

Wiggs, R. B. 1989. Canine oral anatomy and physiology. The Compendium/Small Animal. 11(12): 1475-1482.

Williams, D. F. 1981. Biocompatibility of clinical implant materials. Vol. 1. CRC Press, Boca Raton, FL.

Williams, K. R., C. J. Watson, W. M. Murphy, J. Scott, M. Gregory and D. Sinobad. 1990. Finite element analysis of fixed prostheses attached to osseointegrated implants. Quintessence Int. 21: 563-570.

Wolff, J. 1892. Das Gesetz der Transformation der Knochen. Hirschwald, Berlin.

Worthington, P. 1988. Current implant usage. J. Dent. Educ (Special Issue). 52: 692-695.

Wright, T. M. and W. C. Hayes. 1976a. The fracture mechanics of fatigue crack propagation in compact bone. J. Biomed. Mater. Res. Symp. 7: 637-648.

Wright, T. M. and W. C. Hayes. 1976b. Tensile testing of bone over a wide range of strain rates: effects of strain rate, micro-structure and density. Med. Biol. Eng. Comput. 14: 671-680.

Yoon, H.S. and J. L. Katz. 1976. Ultrasonic wave propagation in human cortical bone--II. Measurements of elastic properties and microhardness. J. Biomech. 9: 459-464.

Yoon, H. S. and J. L. Katz. 1979. Temperature dependence of the ultrasonic velocities in bone. IEEE Ultrasonics Symp. Proc. 395.

Yukna, R. A. 1991. Clinical comparison of hydroxyapatite-coated titanium dental implants placed in fresh extraction sockets and healed sites. J. Periodont. 62: 468-472.

Zarb, G. A. 1983. Proceedings of the Toronto Conference on Osseointegration in Clinical Dentistry. J. Prosthet. Dent. 50: 1-3.

Zienkiewicz, O. C. and R. Taylor. 1988. The finite element method. 4th Ed. McGraw-Hill, London.

ACKNOWLEDGEMENTS

I would like to thank my major professor, Dr. Thomas McGee, for his encouragement, enthusiasm and guidance throughout this project. I would also like to thank the other members of my committee, Dr. Thomas Rogge, Dr. Stanley Wagner and Dr. Loren Zachary for their time and advice. Special thanks are extended to Dr. Gabrielle Niederauer for her suggestions, encouragement,and the use of her retrieved bone/implant specimens. The important contributions made to this project by John Kerr, Rich Thielman, Jim Wellman and Margie Carter are also acknowledged and very much appreciated.

I especially want to thank my wonderful parents, Eugene and Marianne Smyth. They have always encouraged me on every endeavor, and their love, strength and dreams are with me always....

Finally, I would like to thank my utterly fantastic children: Brian Bernard, Erin Cathleen and Michael Eugene. Their sacrifices, hard work, and most importantly, their laughter and hugs kept me going and going and going...

APPENDIX A. IMAGE ANALYSIS OUTPUT

The following is an example of the image analysis output indicating the x and y coordinates of the implant/bone cross-section used to develop the various finite element models in this study:

10	253
11	253
12	253
13	253
14	253
639	258
637	259
638	259
635	260
636	260
632	261
633	261
634	261
629	262
630	262
631	262
626	263
627	263
628	263
624	264
625	264
622	265
623	265
621	266
619	267
620	267
618	268
616	269
617	269
615	270
614	271
614	272
613	273
613	274
612	275
612	276
611	277
611	278
610	279
610	280
609	281
609	282
608	283
608	284
608	285
608	286

APPENDIX B. FORMAT CONVERSION CODE

The following is the C program developed by Kerr (1992) that was used to transform the image analysis output (Appendix A) into a format acceptable to the finite element pre-processing program, PATRAN:

```
#include <stdio.h>
void rd_file();
FILE *np;
FILE *fp;
char outfl[12], flname[12];
float ZCOOR;
main()

{
        printf("\n\n\n Enter filename to write to:        ");
        scanf("%s", outfl);
        fp = fopen(outfl, "a");
        printf("\n\n\n filename to read ->");
        scanf("%s", flname);
        printf("\n\n\n Enter ZCOOR:     ");

        scanf("%f", &ZCOOR);
        if ((np = fopen(flname, "r")) == NULL)
                printf("\n\n\n File does not exist.");
        else
                rd_file();
}

void rd_file()
{

        unsigned int  ON, tmp, ZR, num;
        float xpos, ypos;
                ON =1;
                ZR =0;
                tmp =31;
                num =1;

        while (!feof(np)){
                fscanf(np, "%f\t", &xpos);
                fscanf(np, "%f\n", &ypos);
                        xpos = xpos - 100;
                        ypos = 512 - ypos;
                        fprintf(fp, "%u%8u", tmp, num);
                fprintf(fp,"%8u%8u%8u%8u%8u%8u%8u\n",ZR, ON, ZR, ZR, ZR);
                fprintf(fp, "%16.9E\%16.9E\%16.9E\n", xpos, ypos, ZCOOR);
                        num + = 1;
        }
}
```

APPENDIX C. NEUTRAL FILE FORMAT

The following is an example of the format used to input the data obtained from image analysis (Appendix A) and transformed by the computer program in Appendix C to PATRAN:

```
31       1       0       1       0       0       0 4197316       0
-9.000000000E+01 2.590000000E+02 4.000000000E+00
31       2       0       1       0       0       01074790400       0
-8.900000000E+01 2.590000000E+02 4.000000000E+00
31       3       0       1       0       0       01074790400       0
-8.800000000E+01 2.590000000E+02 4.000000000E+00
31       4       0       1       0       0       01074790400       0
-8.700000000E+01 2.590000000E+02 4.000000000E+00
31       5       0       1       0       0       01074790400       0
-8.600000000E+01 2.590000000E+02 4.000000000E+00
31       6       0       1       0       0       01074790400       0
 5.390000000E+02 2.540000000E+02 4.000000000E+00
31       7       0       1       0       0       01074790400       0
 5.370000000E+02 2.530000000E+02 4.000000000E+00
31       8       0       1       0       0       01074790400       0
 5.380000000E+02 2.530000000E+02 4.000000000E+00
31       9       0       1       0       0       01074790400       0
 5.350000000E+02 2.520000000E+02 4.000000000E+00
31      10       0       1       0       0       01074790400       0
 5.360000000E+02 2.520000000E+02 4.000000000E+00
31      11       0       1       0       0       01074790400       0
 5.320000000E+02 2.510000000E+02 4.000000000E+00
31      12       0       1       0       0       01074790400       0
 5.330000000E+02 2.510000000E+02 4.000000000E+00
31      13       0       1       0       0       01074790400       0
 5.340000000E+02 2.510000000E+02 4.000000000E+00
31      14       0       1       0       0       01074790400       0
 5.290000000E+02 2.500000000E+02 4.000000000E+00
31      15       0       1       0       0       01074790400       0
 5.300000000E+02 2.500000000E+02 4.000000000E+00
31      16       0       1       0       0       01074790400       0
 5.310000000E+02 2.500000000E+02 4.000000000E+00
31      17       0       1       0       0       01074790400       0
 5.260000000E+02 2.490000000E+02 4.000000000E+00
31      18       0       1       0       0       01074790400       0
 5.270000000E+02 2.490000000E+02 4.000000000E+00
31      19       0       1       0       0       01074790400       0
 5.280000000E+02 2.490000000E+02 4.000000000E+00
31      20       0       1       0       0       01074790400       0
 5.240000000E+02 2.480000000E+02 4.000000000E+00
```